SAND2020-7662PE

Nonlinear Dynamic Analysis of a Finger-Like Mechanism for Morphing Wings

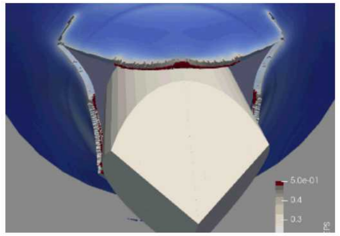

Students:

Aabhas Singh & Kayla Wielgus

Mentors:

Robert Kuether, Ignazio Dimino, Matthew Allen

Sandia National Laboratories is a multimission laboratory managed and operated by National Technology & Engineering Solutions of Sandia, LLC, a wholly owned subsidiary of Honeywell International Inc., for the U.S. Department of Energy's National Nuclear Security Administration under contract DE-NA0003525.

Fuel Cost if NOMAD was in Albuquerque

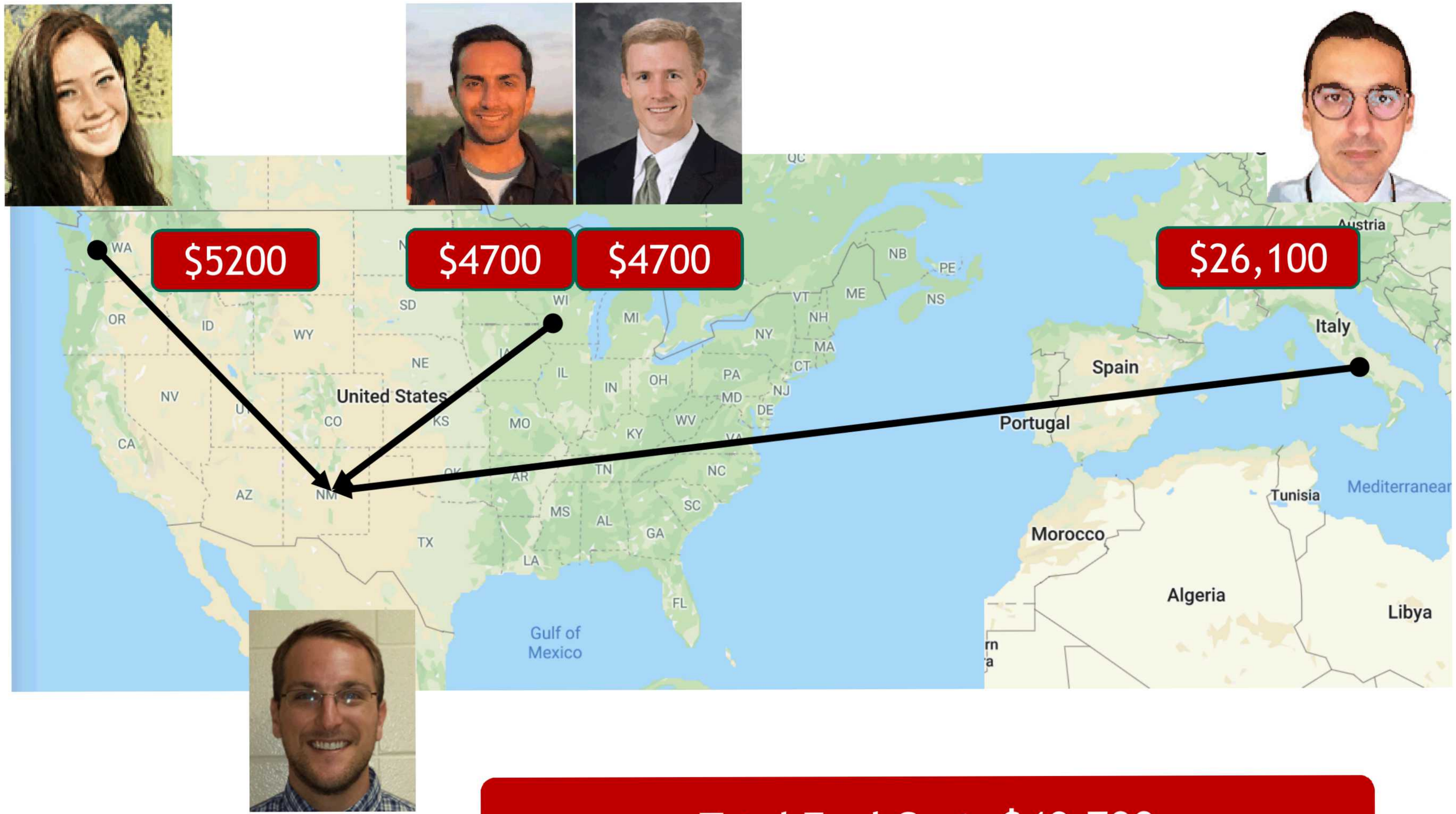

Jet Fuel Avg. 2019 PPG	$1.88
Aircraft Avg. MPGGE	0.43

https://www.eia.gov/
https://afdc.energy.gov/data/10311
Maps.google.com

Total Fuel Cost: $40,700

Hinged Wings – A Compromise

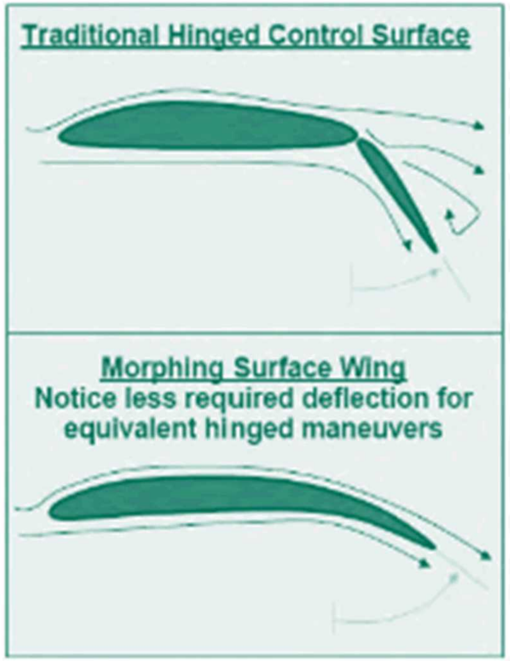

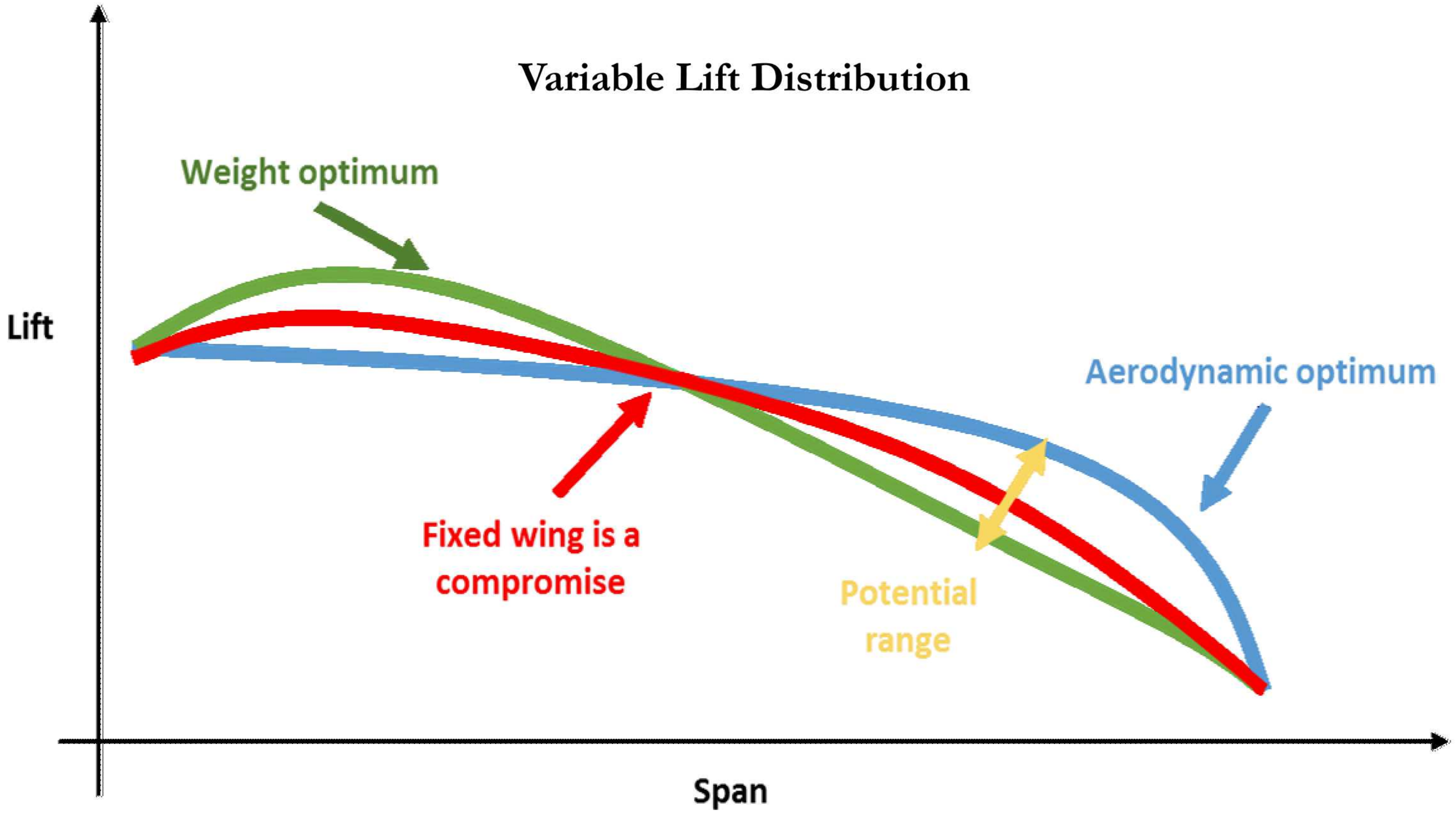

Morphing Wings – Nature Motivated

Nature inspires

Actual A/C devices

Morphing Wings – Not just a Concept

They are flexible, shape-changing and bio-inspired high-lift devices:

- ✓ Reduced fuel consumption
- ✓ Reduced airframe noise

https://www.youtube.com/watch?v=bC5BUuDFhmg

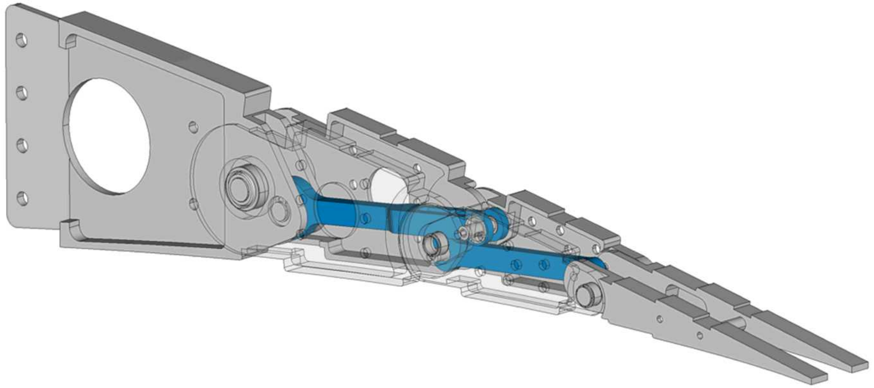

Kinematic Systems

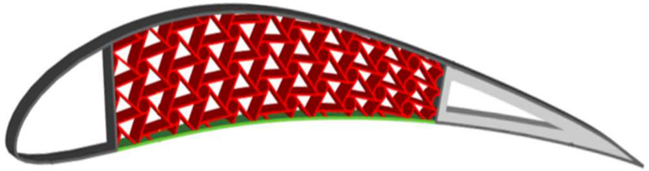

Compliant

Kinematic Finger Like Mechanisms

Finger – Like Mechanisms consists of different blocks (connected by hinges and links) moving with a pre-defined mechanical law and driven by load-bearing actuators

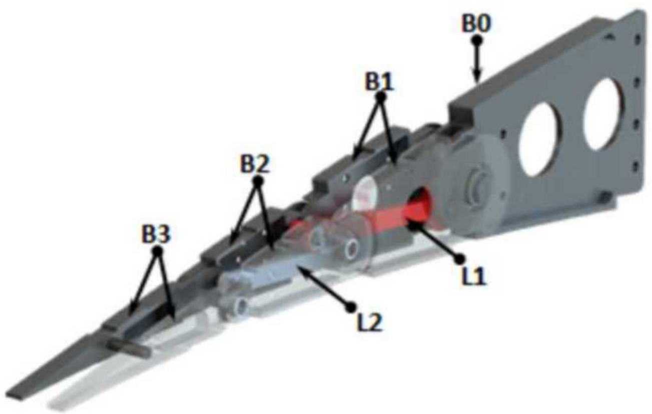

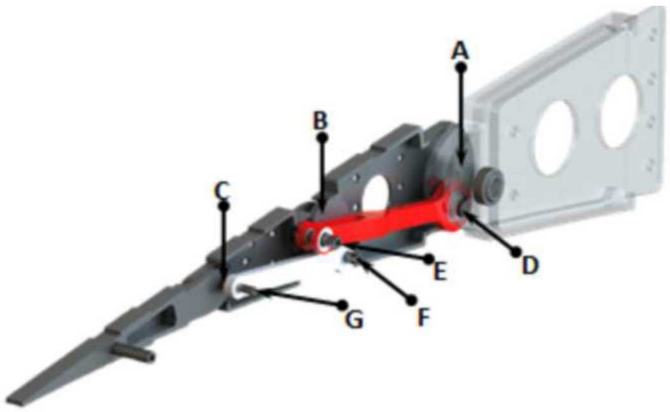

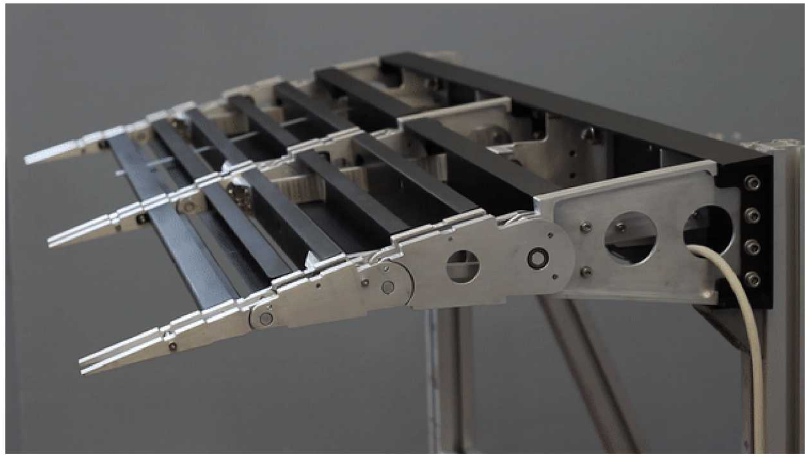

Several connected components exhibit frictional nonlinearity at the interfaces

Importance of Modeling Frictional Interfaces

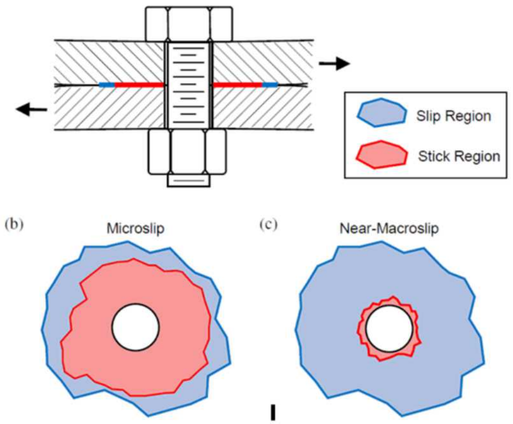

Well tightened bolts still exhibit regions of slip at the edge of contact

- Microslip/Macroslip
- Introduces hysteresis and amplitude dependent behavior

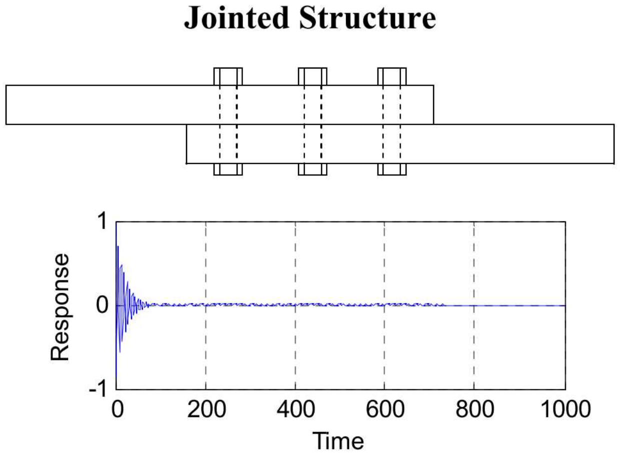

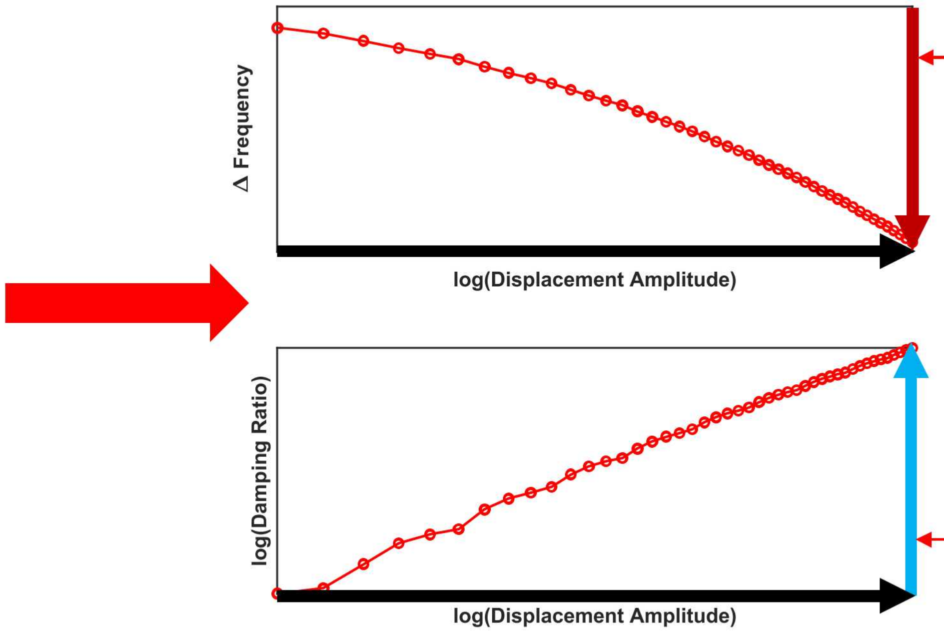

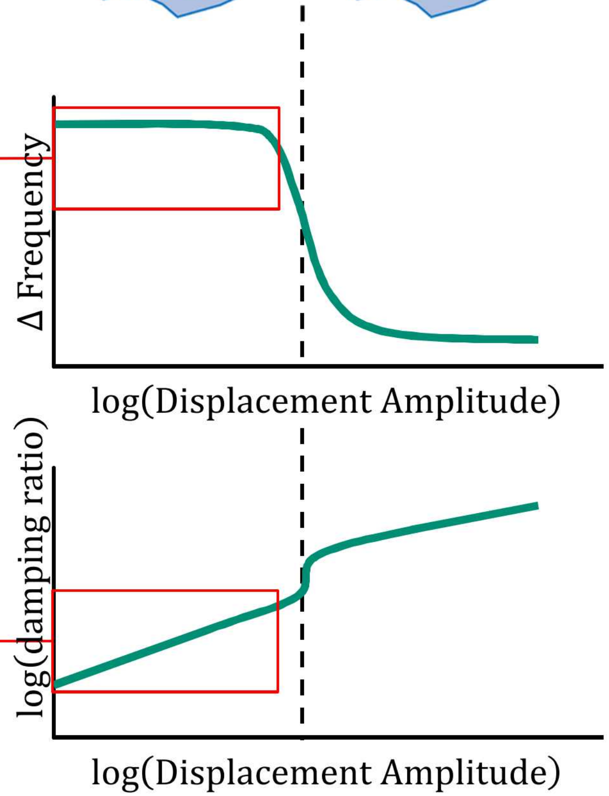

Project Objective

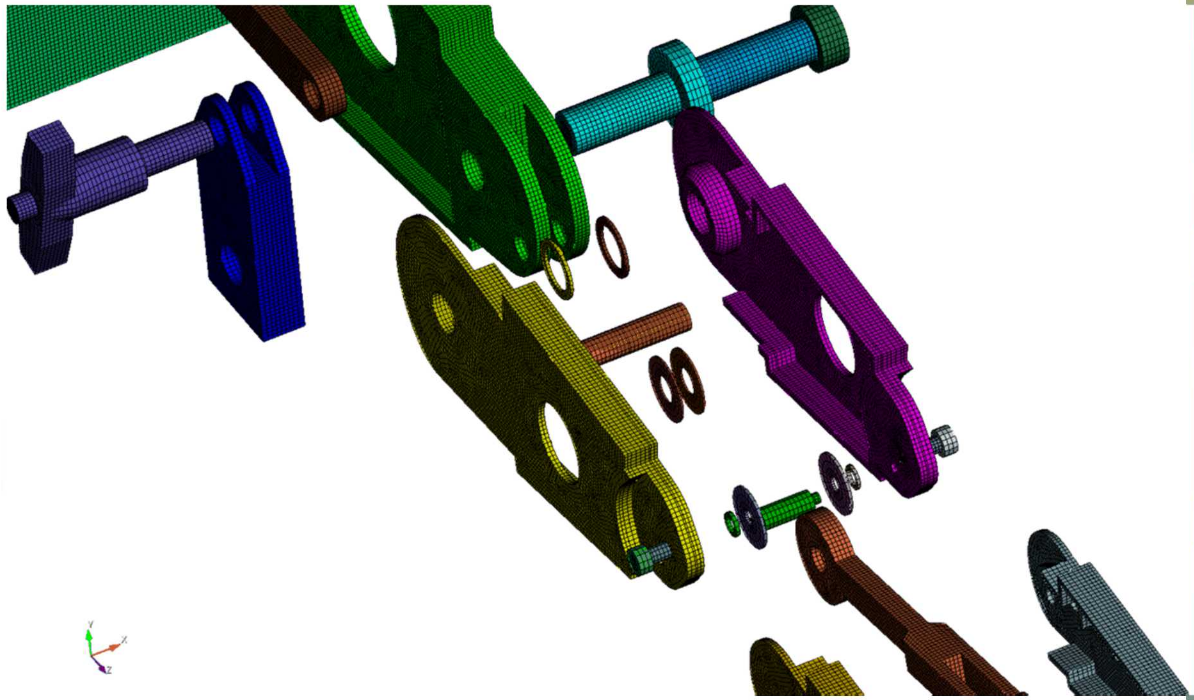

Develop a nonlinear finite element model of an industrial structure to better understand the nonlinear damping and frequency behavior

Full – Order Modeling with Quasi-Static Modal Analysis

The Quasi-Static Modal Analysis Process

QSMA of a Full-Order Model

SM

Nonlinear Preload Analysis

$$Kx + f_{NL}(x,\theta) = f_{pre}$$

SD

Linearized Modal Analysis

$$\left(K + \frac{df_{nl}(x,\theta)}{dx}\bigg|_{x=x_{pre}} - \omega_r^2 M\right)\phi_r = 0$$

SM

Modal Force Application

$$Kx + f_{nl}(x,\theta) = f_{pre} + M\phi_r\alpha$$

R. M. Lacayo and M. S. Allen, "Updating Structural Models Containing Nonlinear Iwan Joints Using Quasi-Static Modal Analysis," *Mechanical Systems and Signal Processing*, vol 118, pp. 133-157, 2019

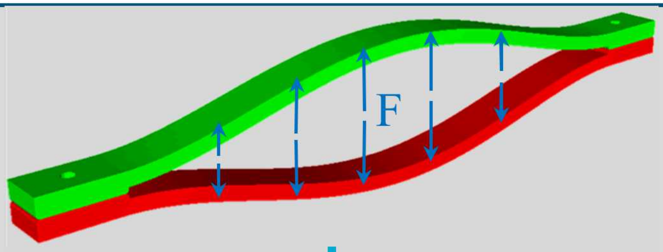

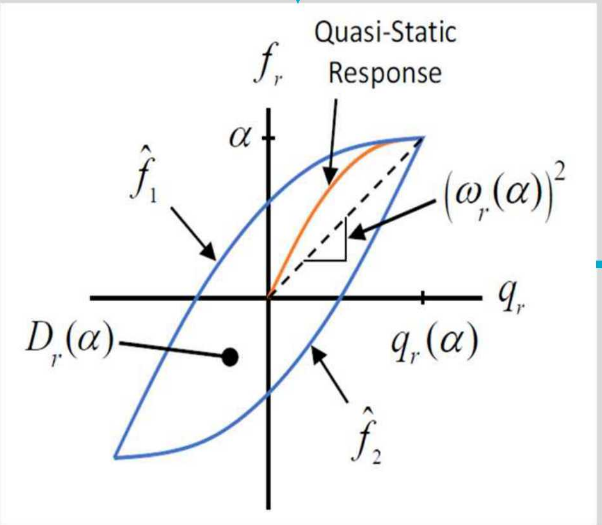

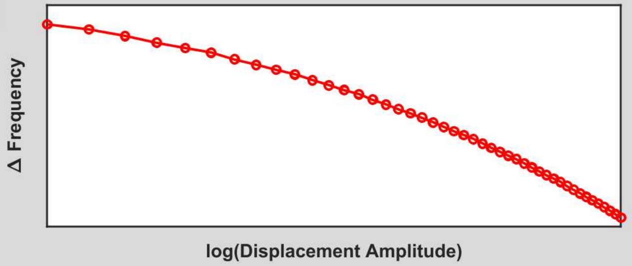

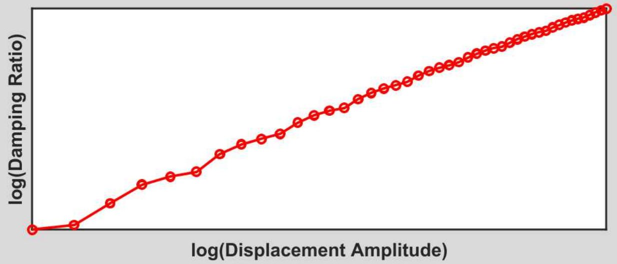

Dynamic analysis of a structure is computationally expensive so we use a static analysis

- ~10x increase in speed for a quasi-static case (seconds) vs. static response case (hours)
- Dynamic simulation could take upwards of weeks

Application to the Morphing Wing

Gravity Load – Test Condition

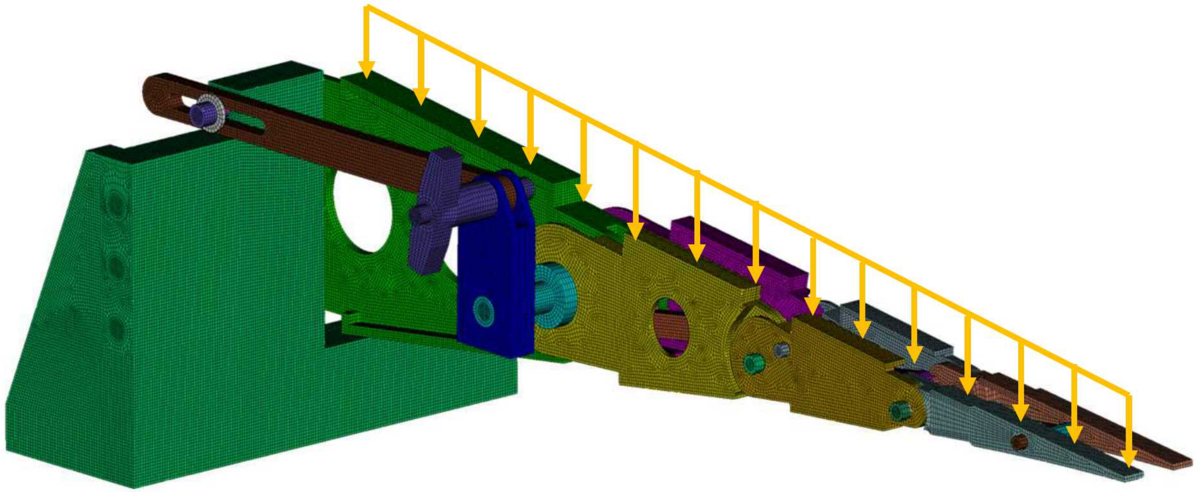

Tip Load – Representative Operative Condition

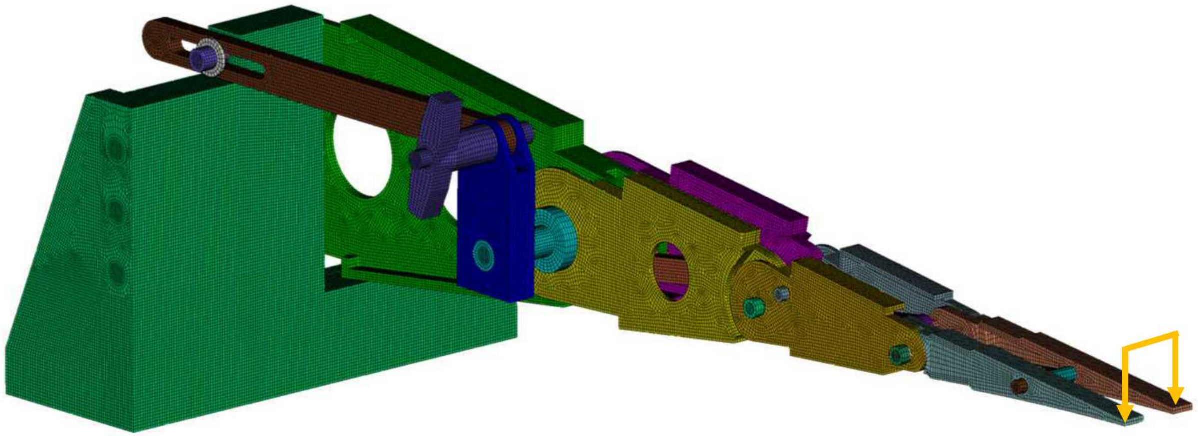

Apply QSMA to get frequency and damping curves for these two preload methods

Apply Preload on the Structure

Nonlinear Preload Analysis
$Kx + f_{NL}(x,\theta) = f_{pre}$

SM

Gravity Load

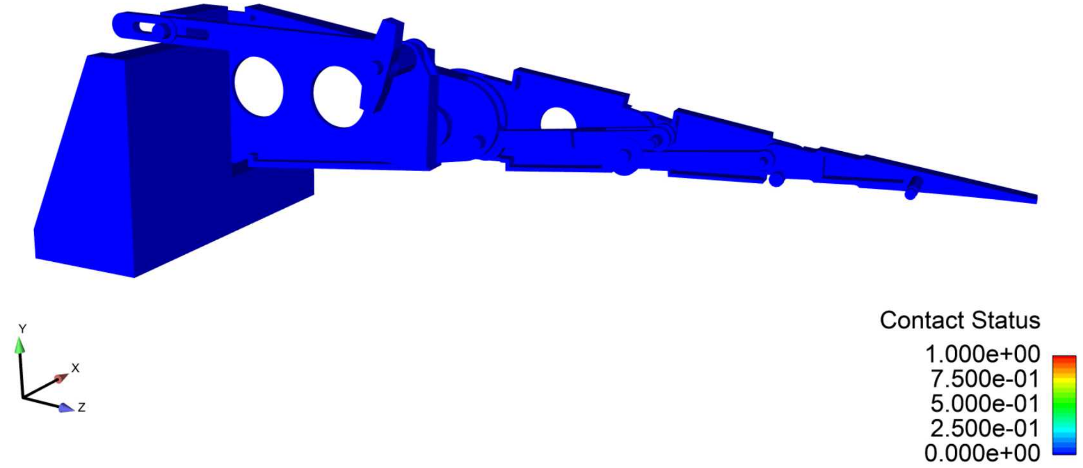

Tip Load

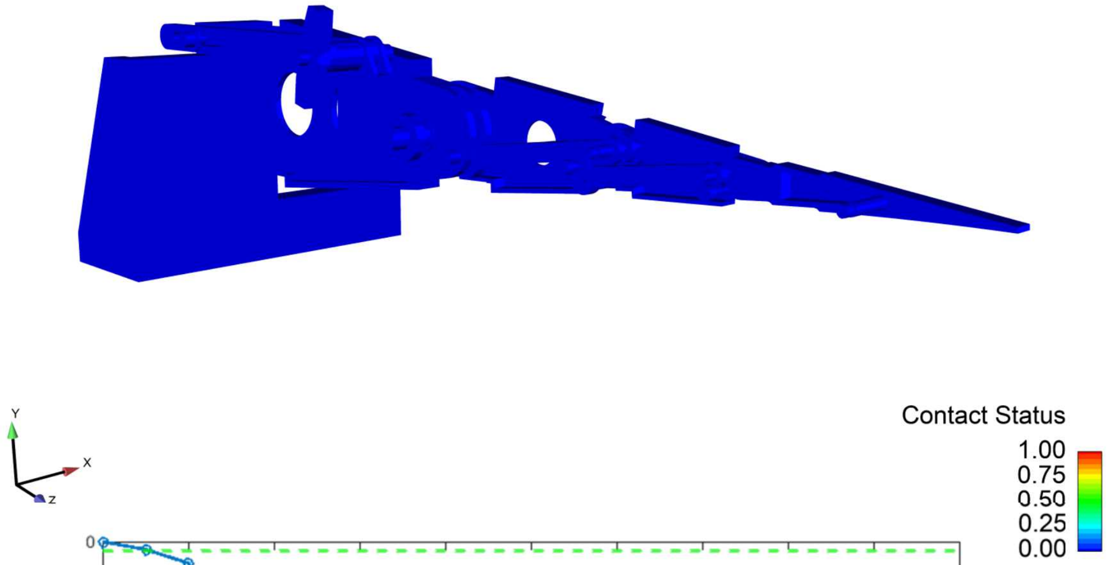

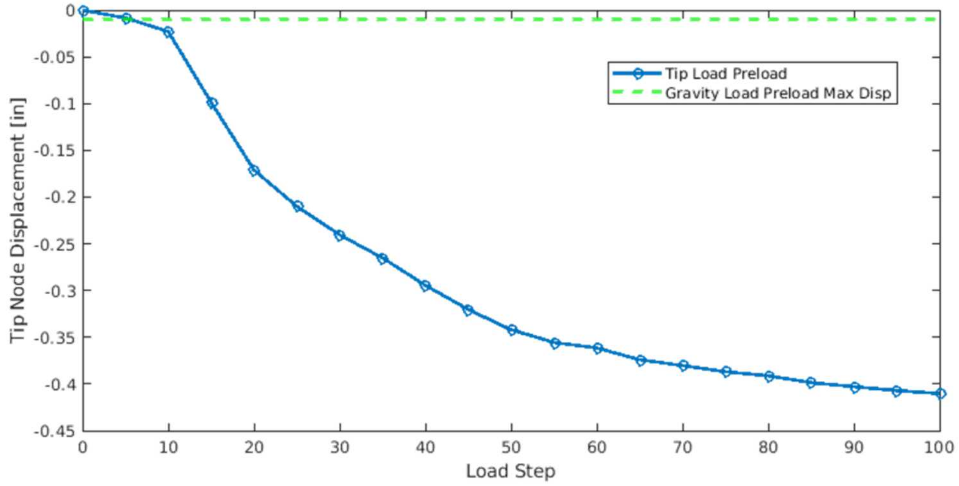

Mode Of Interest

SD

Linearized Modal Analysis

$$\left(K + \frac{df_{nl}(x,\theta)}{dx}\bigg|_{x=x_{pre}} - \omega_r^2 M\right)\phi_r = 0$$

164.5 Hz

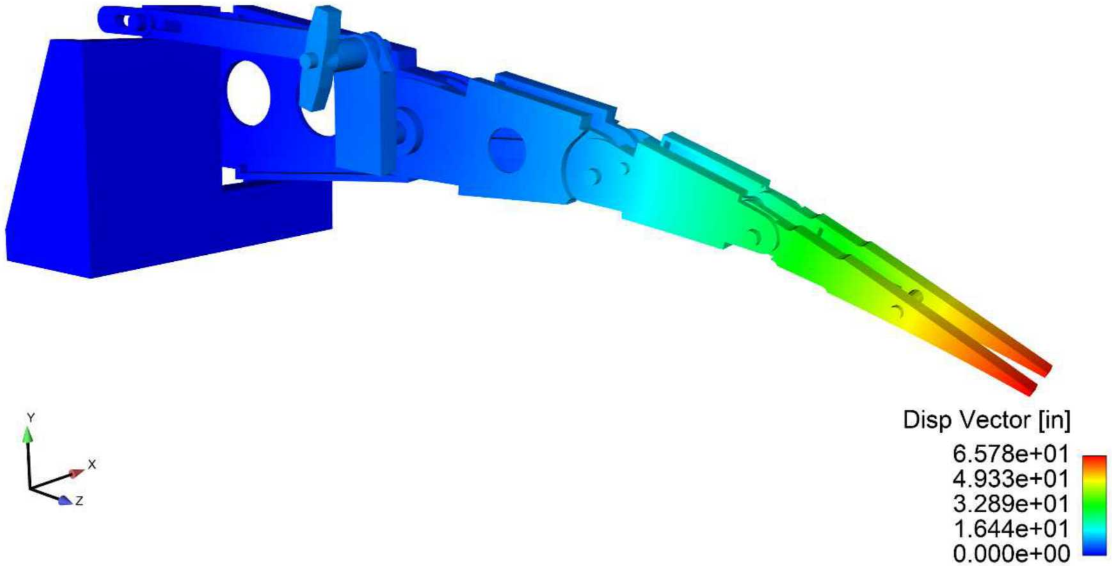

Gravity Load

166.1 Hz

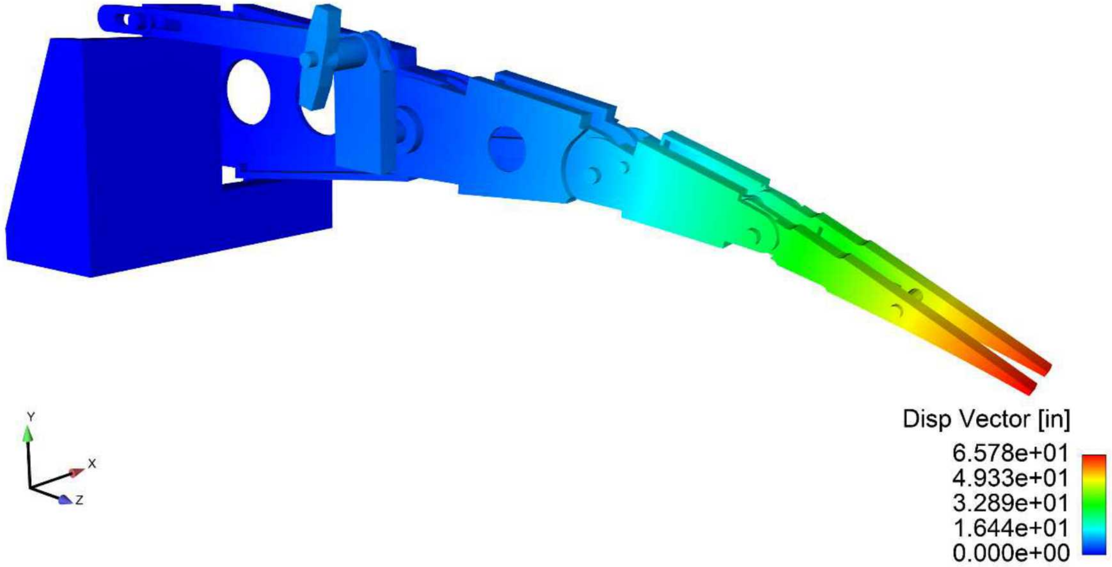

Tip Load

Gravity Load Vs. Tip Load QSMA

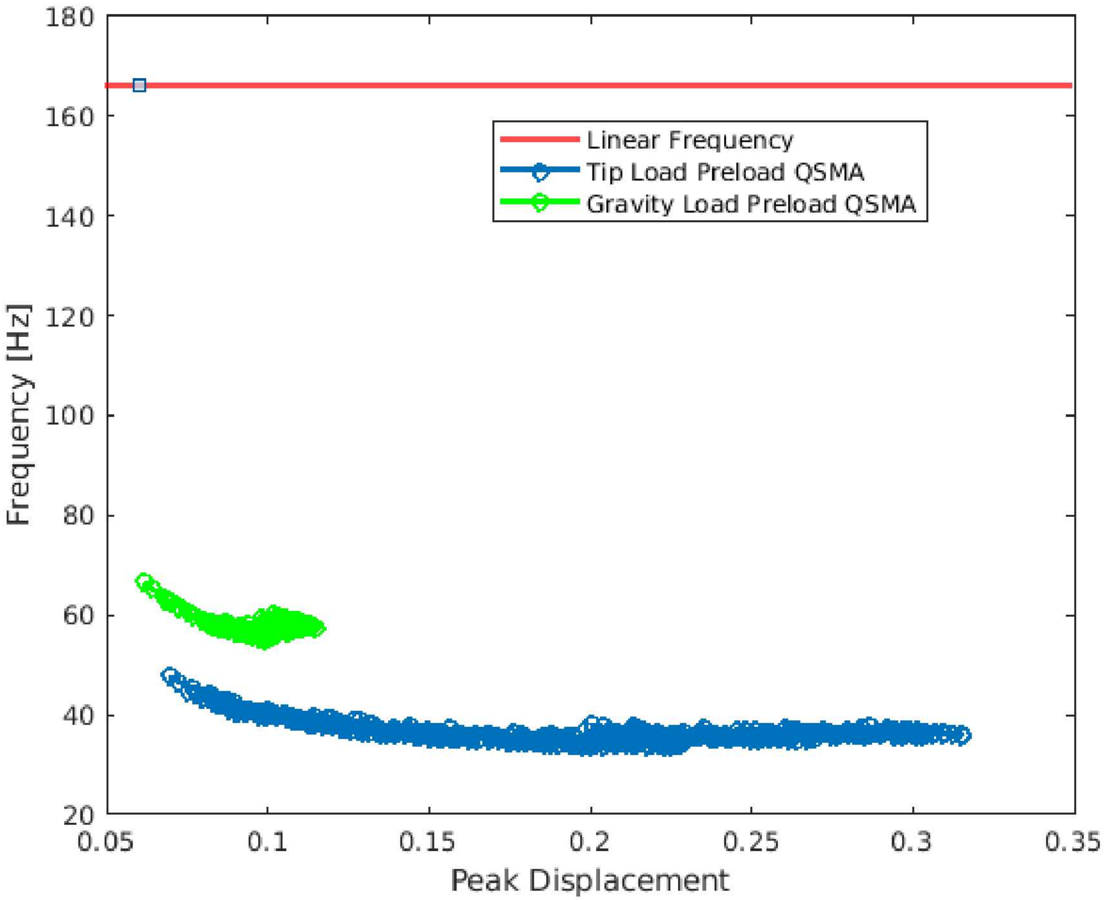

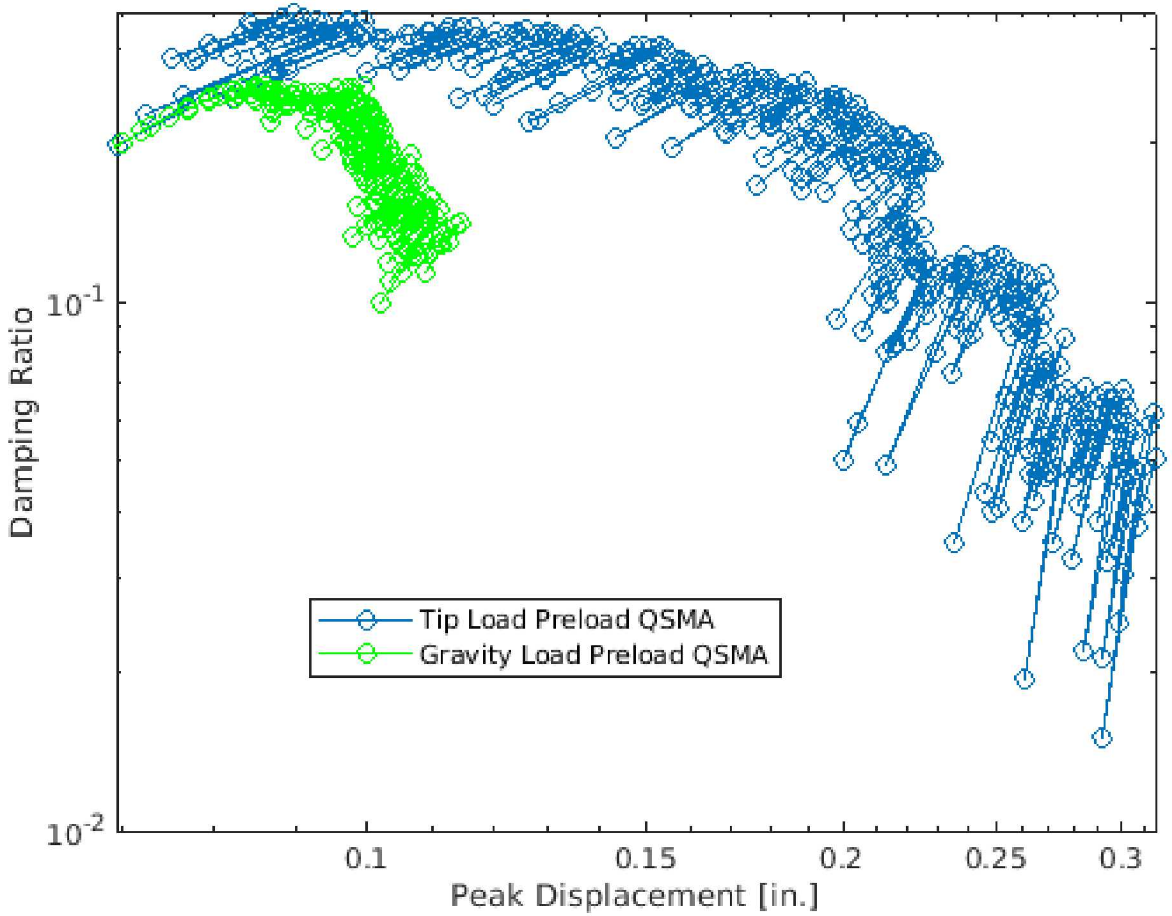

Interface Reduction using Multi-Point-Constraints

Modeling through Whole Joint Models

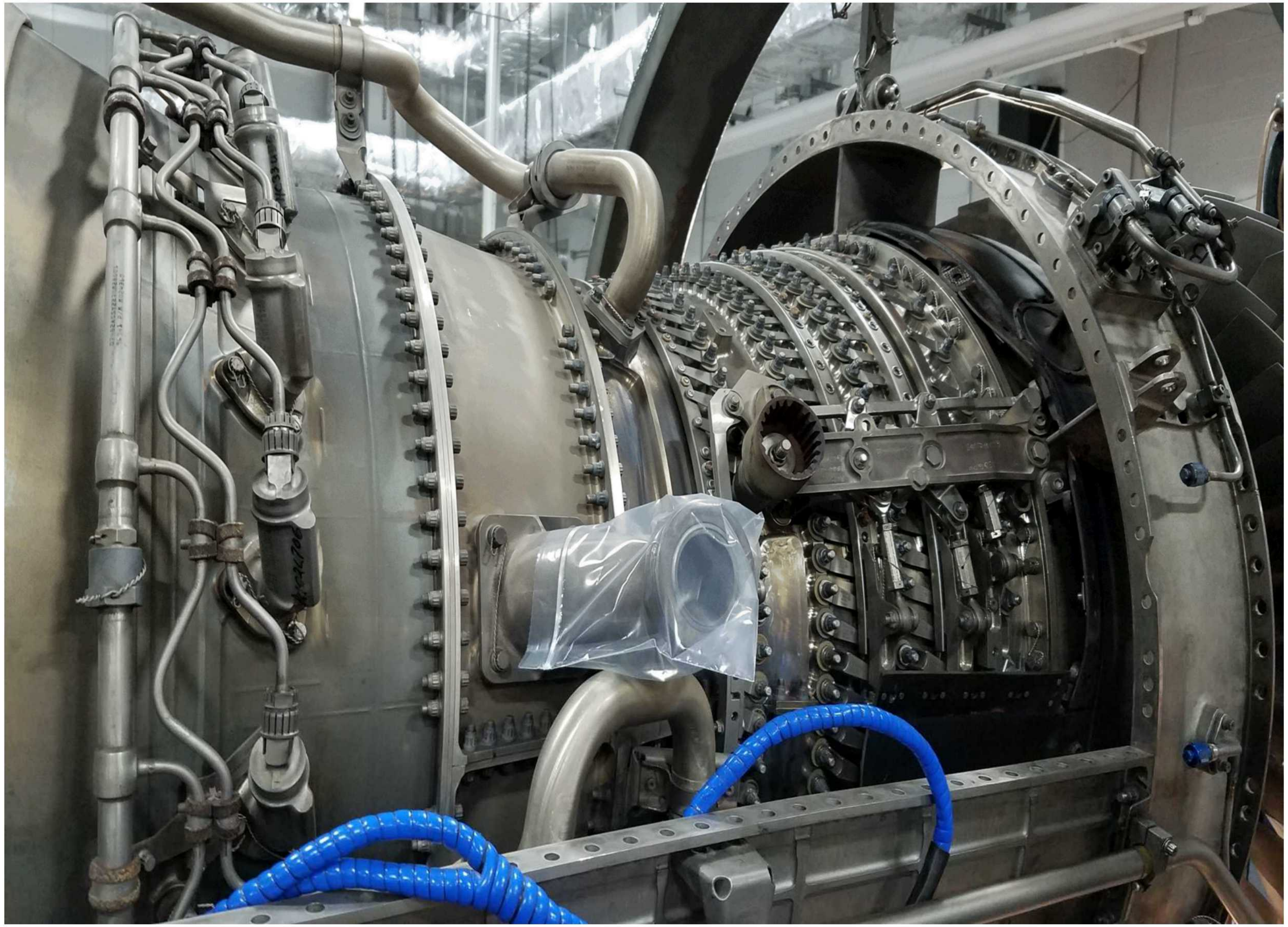

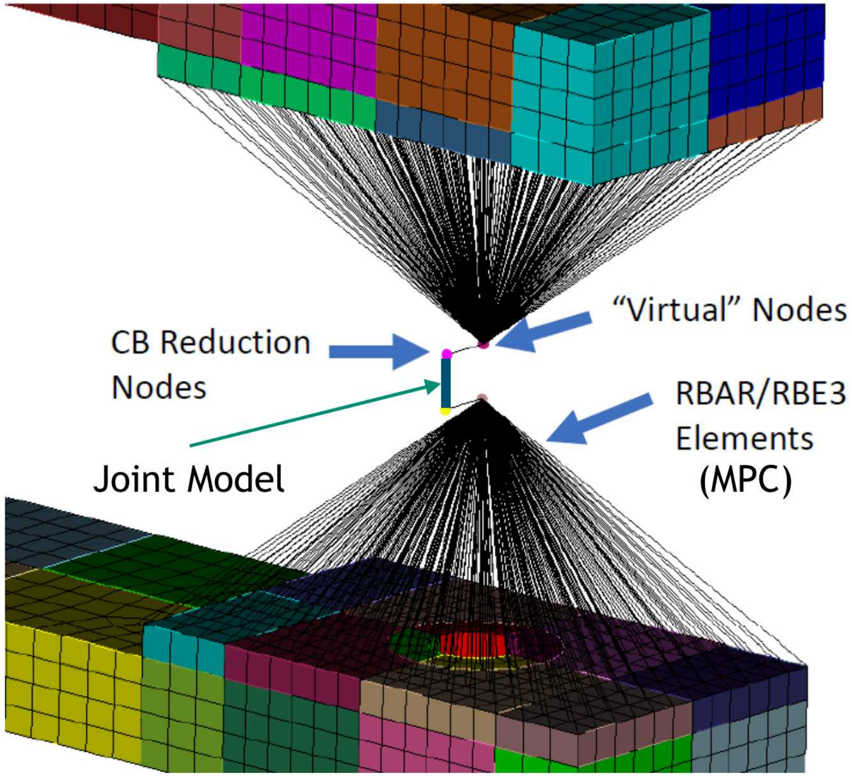

Morphing Wing – Contact Interfaces

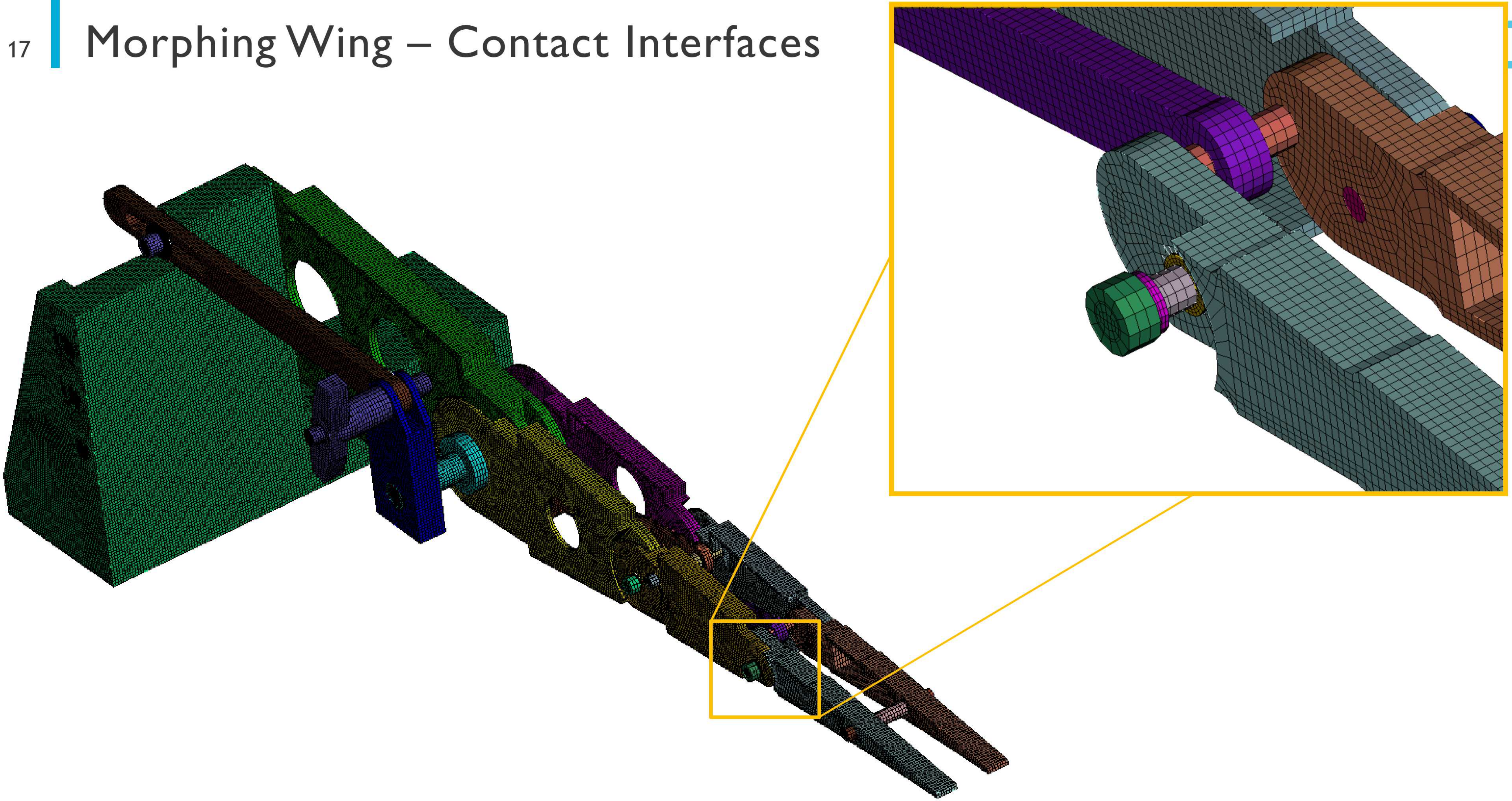

Morphing Wing – Spidering Process

Original surface assigned for contact

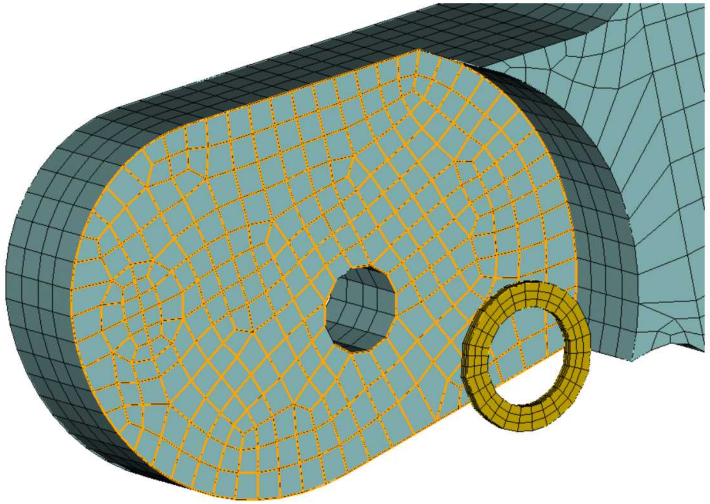

Contact surface output from preload analysis

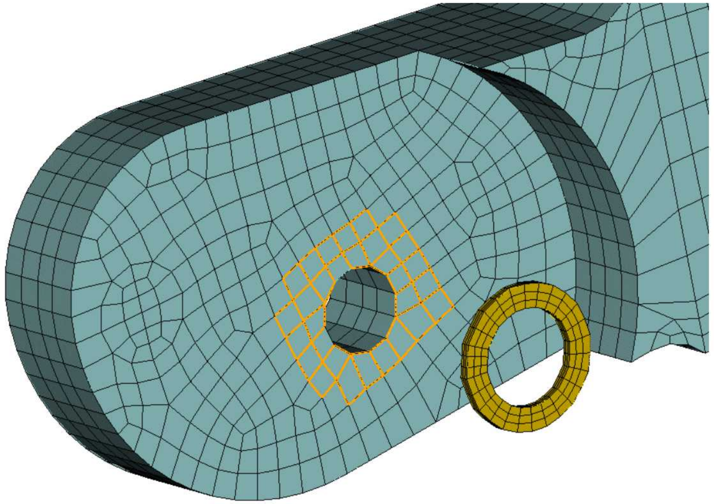

Spider created using nodes from preload contact surface

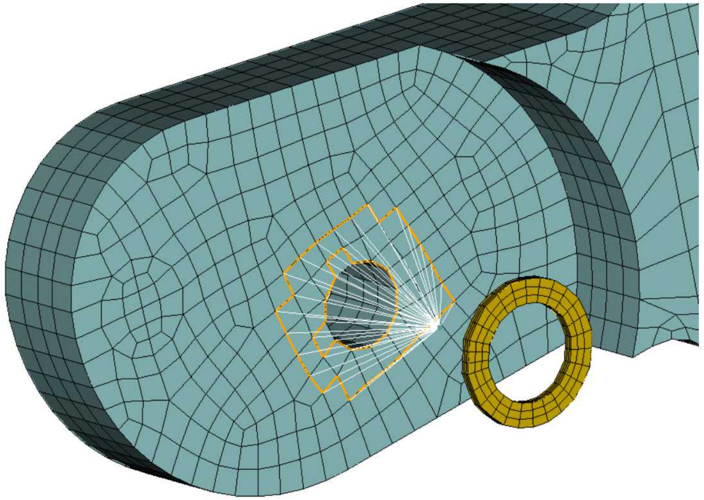

Morphing Wing – Spidering Process

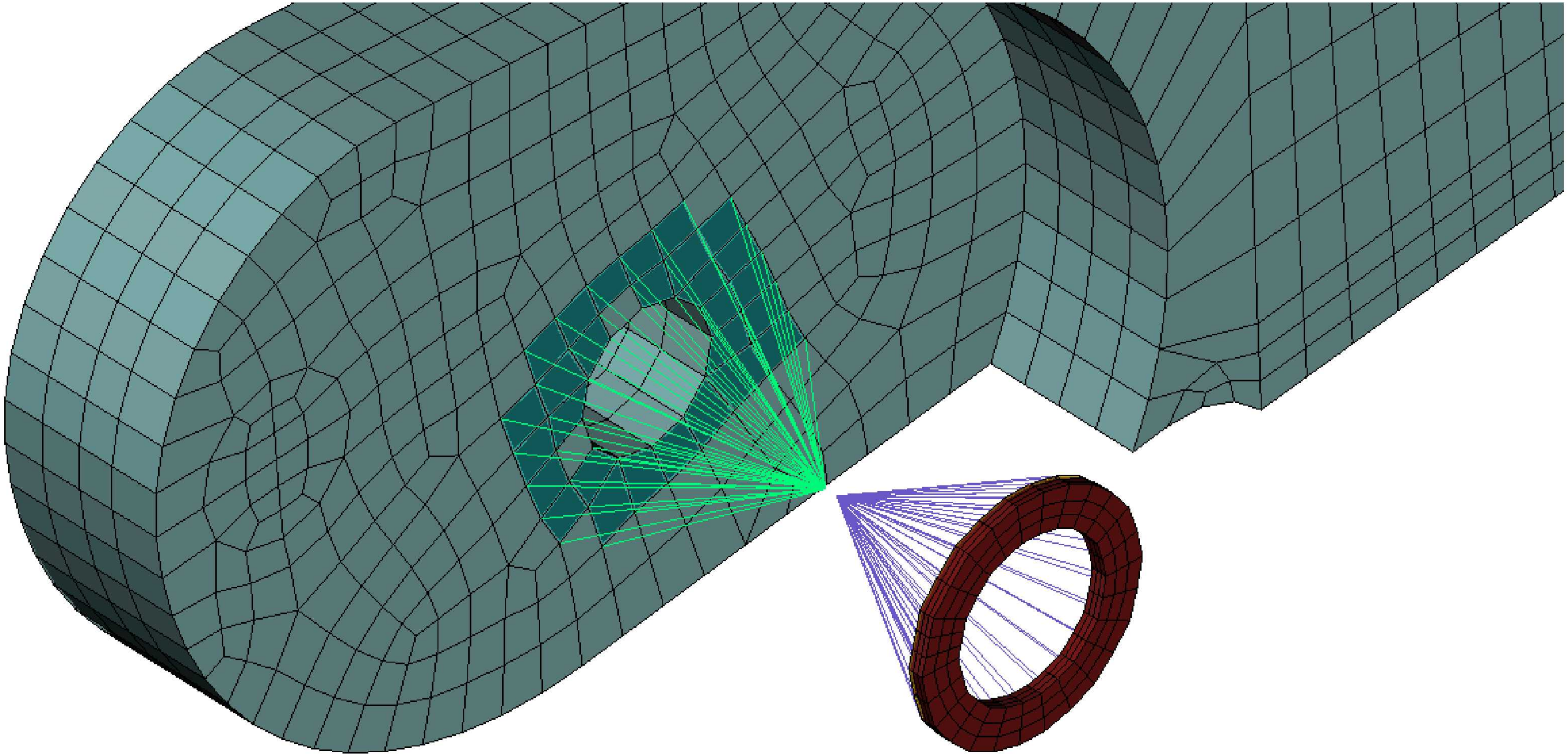

Morphing Wing – Full Model With Multi-Point Constraints Assigned

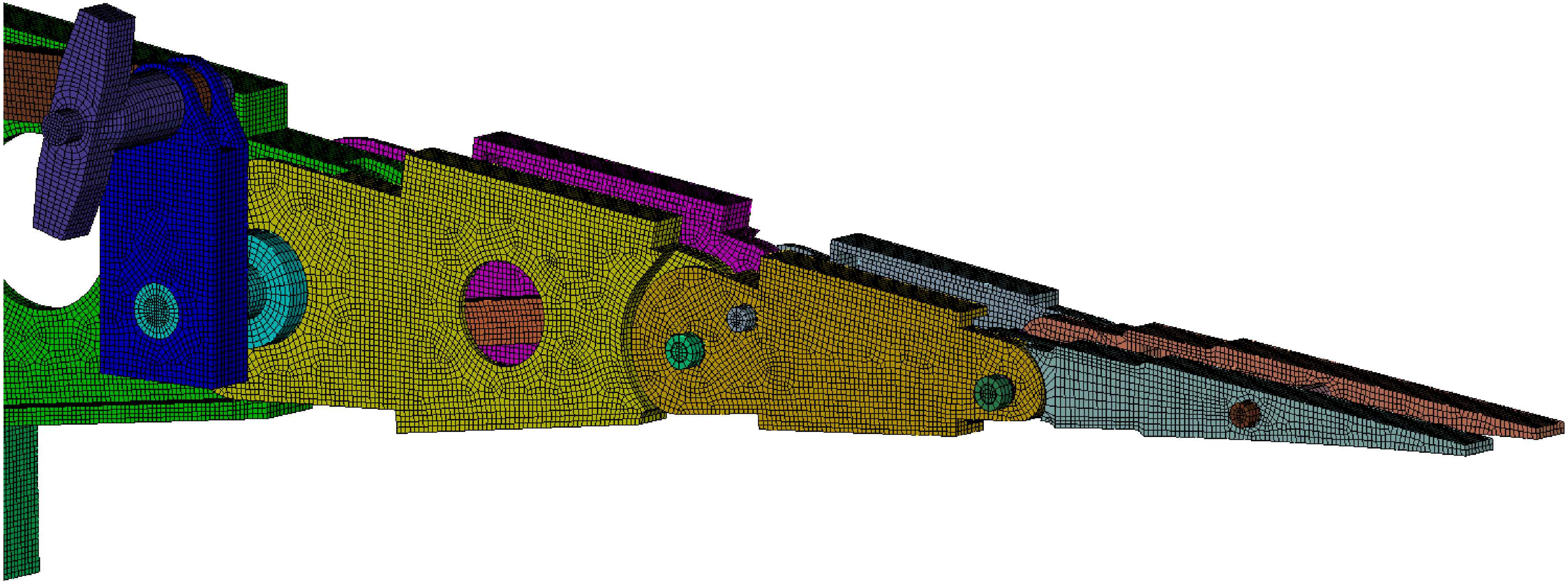

Rotational Stiffness Sensitivity Study

- Adjust rotational stiffness of the structure to see effect on the natural frequency of the 2nd Mode

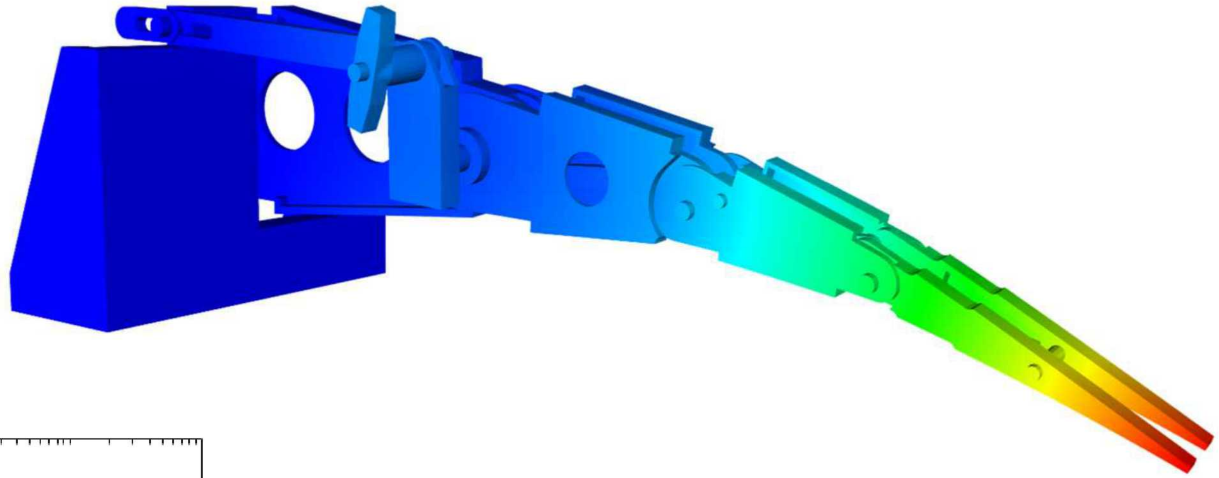

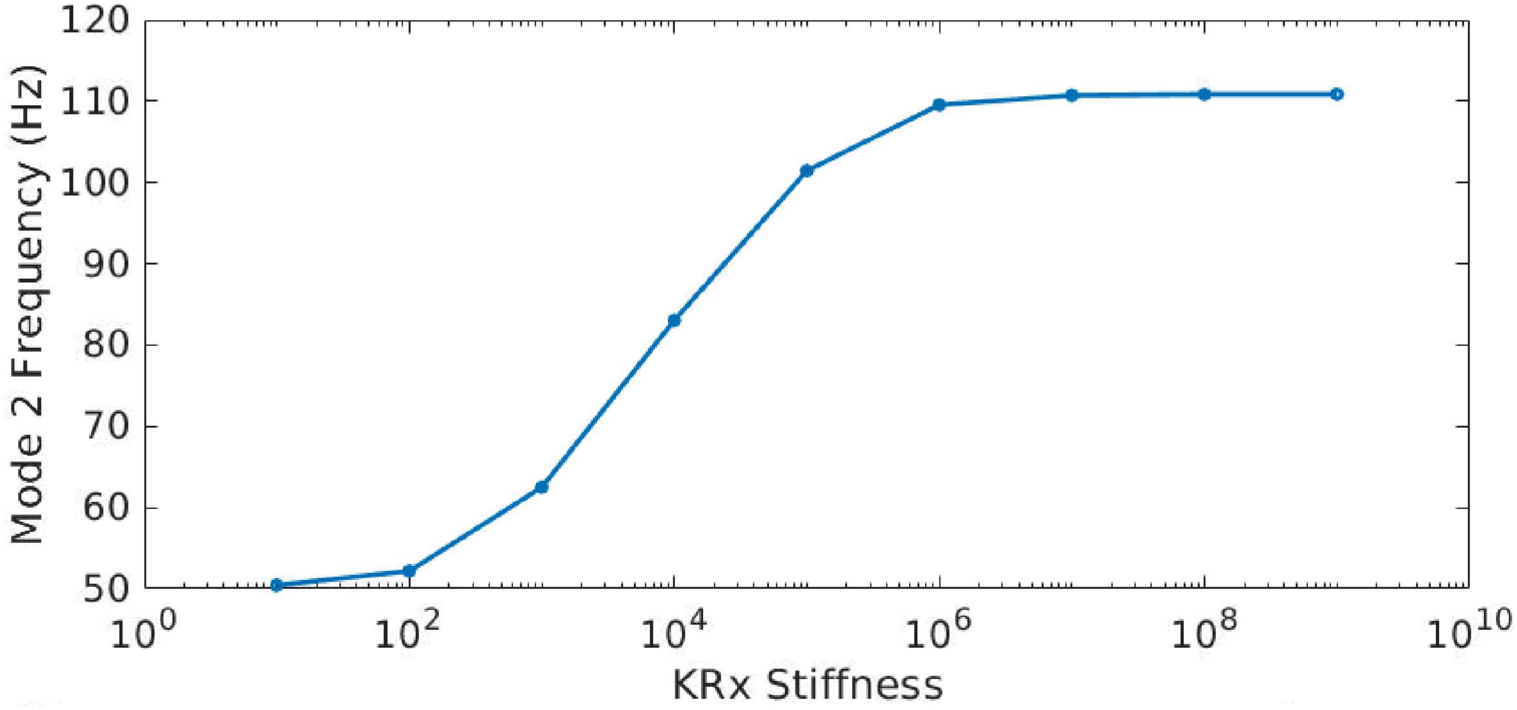

Future Work

- Calibrate Reduced Order Model to match the linear natural frequencies about the preloaded state
- Apply nonlinear hysteretic elements and update to match the full order quasi-static frequency and damping curves
- Add hyper elastic compliant skin around the rib for a more realistic model
- Gauge additional reduction techniques on this industrial model

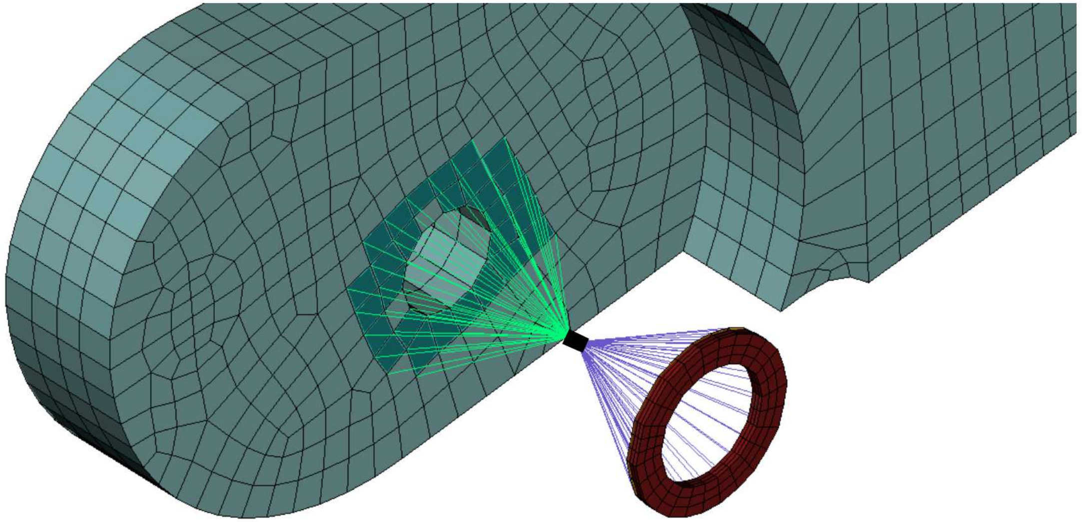

Joint model

Concluding Remarks

- Applied the QSMA framework on an industrial scale structure
  - Utilized two methods for preload (test vs. representative operative condition)
  - Both methods were able to generate quasi-static frequency and damping curves
- Developed a spidered reduced order model that can be updated to match the full order model
- These methods have been typically done on bolted connections vs. the pin/hole frictional connections for this model
- High fidelity nonlinear finite element models are key for future successful virtual testing demonstrations. They present several challenges to make advanced response predictions with confidence.

Acknowledgements

This research was conducted at the 2020 Nonlinear Mechanics and Dynamics Research Institute hosted by Sandia National Laboratories and the University of New Mexico.

Sandia National Laboratories is a multimission laboratory managed and operated by National Technology and Engineering Solutions of Sandia, LLC., a wholly owned subsidiary of Honeywell International, Inc., for the U.S. Department of Energy's National Nuclear Security Administration under contract DE-NA-0003525.

Additional Slides

Tools to Capture Joint Nonlinearity – Iwan Element

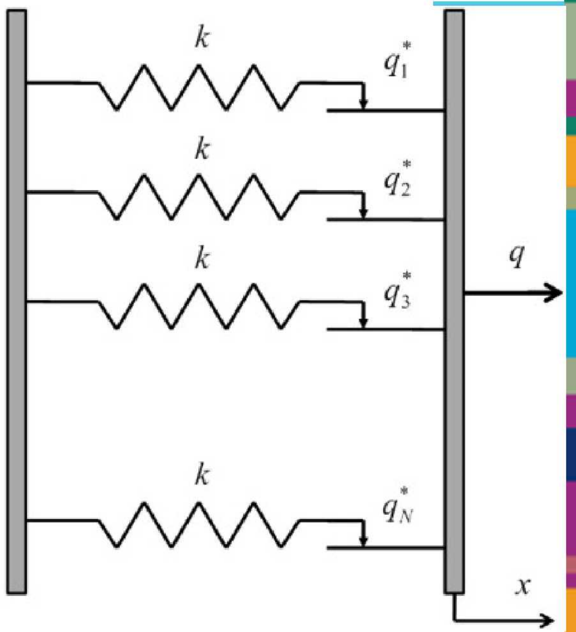

A whole joint model that uses **four parameters** to characterize the amplitude dependent behavior

Multiple Jenkin's slider elements in parallel

F_S	The force necessary to cause macroslip
K_T	The tangential stiffness of the Jenkins elements (i.e. the joint stiffness when no slip occurs)
χ	The exponent that describes the slope of the energy dissipation curve
β	The ratio of the number of Jenkins elements that slip before micro-slip and then at macroslip

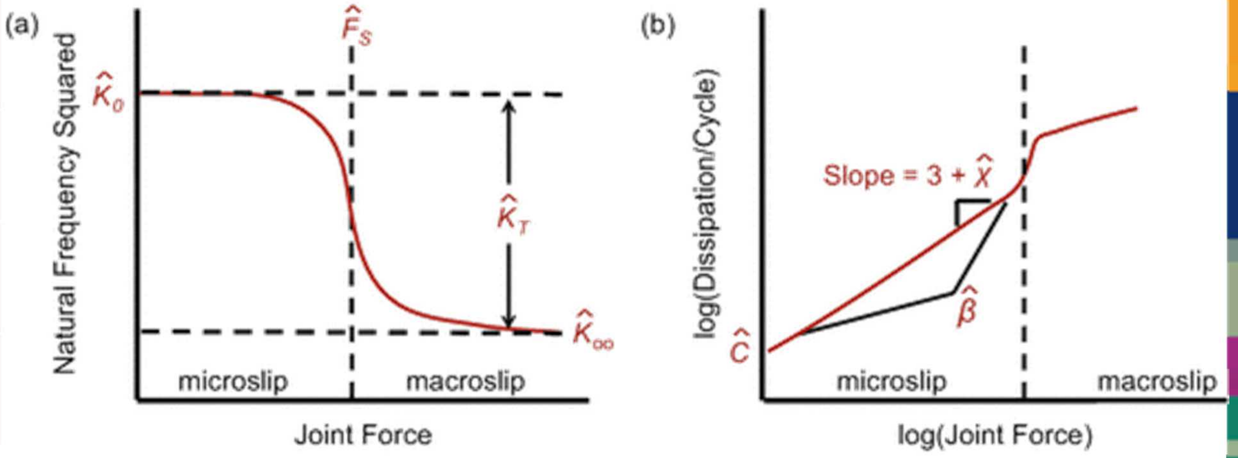

D. J. Segalman, "A Four-Parameter Iwan Model for Lap-Type Joints," *Journal of Applied Mechanics*, vol. 72, no. 5, pp. 752–760, Sep. 2005.

Mode 2 Mode Shape GIF

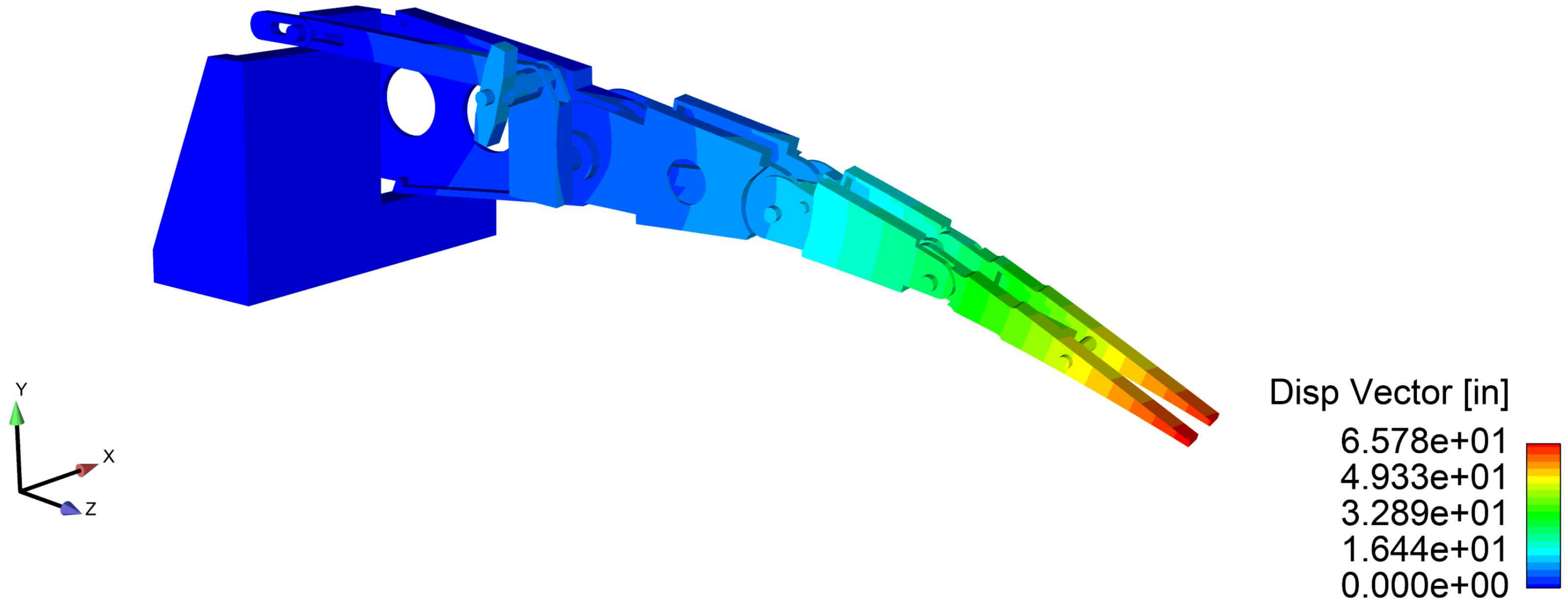

Correlation of ROMs of a Threaded Fastener

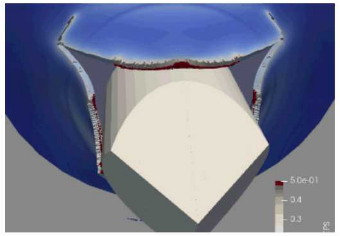

Students:

Avaneesh Murugesan, Michael Sheng, and Kevin Moreno

Mentors:

Neal Hubbard, John Mersch, Jonel Ortiz, Emily Miller, Jeff Smith, and Tariq Kharishi

Sandia National Laboratories is a multimission laboratory managed and operated by National Technology & Engineering Solutions of Sandia, LLC, a wholly owned subsidiary of Honeywell International Inc., for the U.S. Department of Energy's National Nuclear Security Administration under contract DE-NA0003525.

Presentation Contents

- Introduction
- Model Set-up
- Initial Predictions
- Calibrated Models
- Intermediate Angles Results
- Conclusion

Introduction

Motivation: How many fasteners?

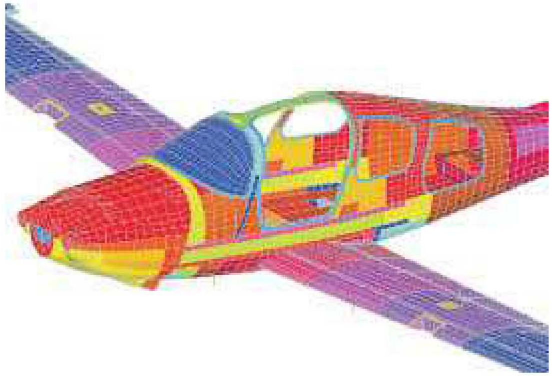

HURLEY, T. AND VANDEMBURG, J., "SMALL AIRPLANE CRASHWORTHINESS DESIGN GUIDE" 2002.

- Fasteners are everywhere: from phones to cars to planes
- Failure can lead to minor inconveniences to major catastrophes
- High-fidelity models of threaded fasteners computationally expensive
- Reduced-order models (ROMs) can be an effective method to replicate the response

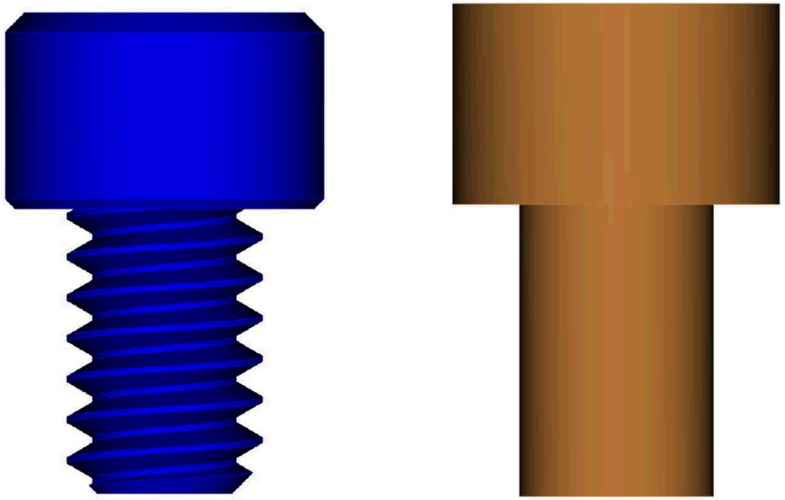

ORTIZ, J., "COMMONLY USED PRELOADING METHODS," 2019.

Project Goals

- Generate **blind predictions** for ROMs based on **nominal parameters**
- Calibrate **plastic response** of the ROMs to **experimental data** from collaboration with UNM
- Evaluate the **plastic response** of **intermediate angles** using calibrated model

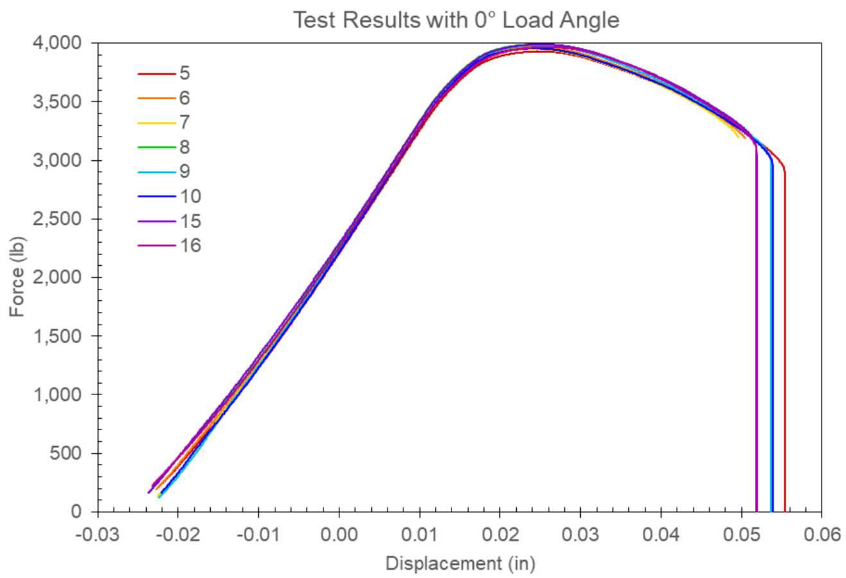

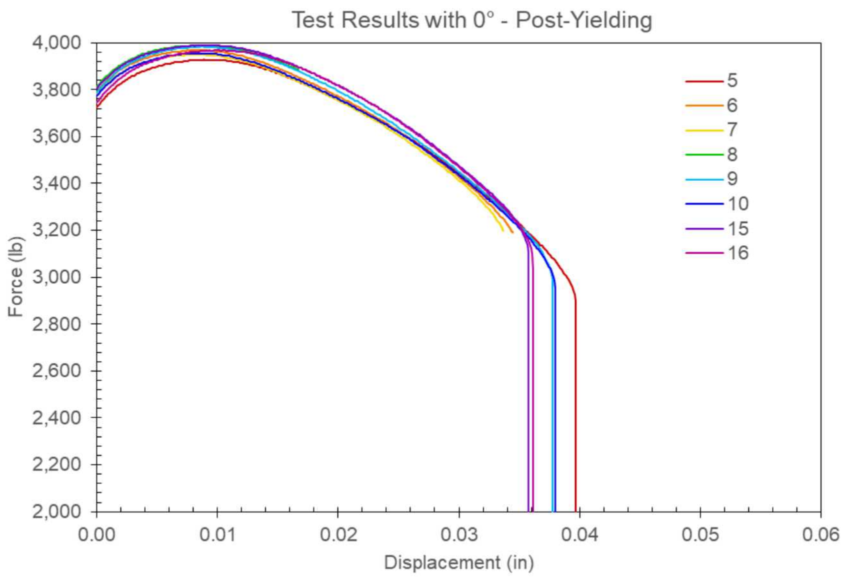

Model Set-up

Fixture Model

- D-rings with holes from 0° – 90° spaced 15° apart
- Fastener held in by bushings
- Model must be defeatured for meshing
  - Removed clevis assembly and detailed features
  - Webcut half of the fixture geometry on the symmetric plane
  - Placed clevis rods at each load angle
  - Used a fine mesh for the bushings and fastener if one was included

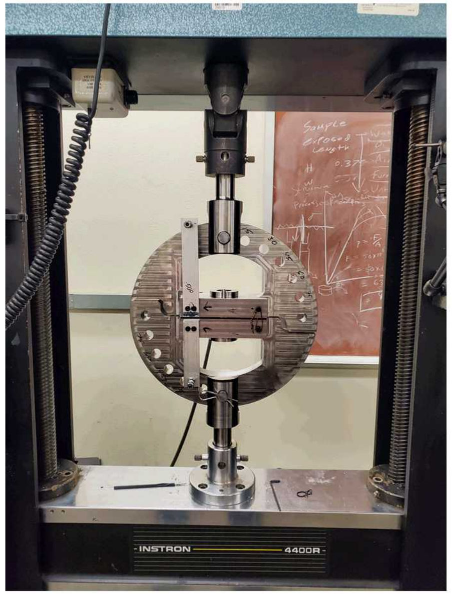

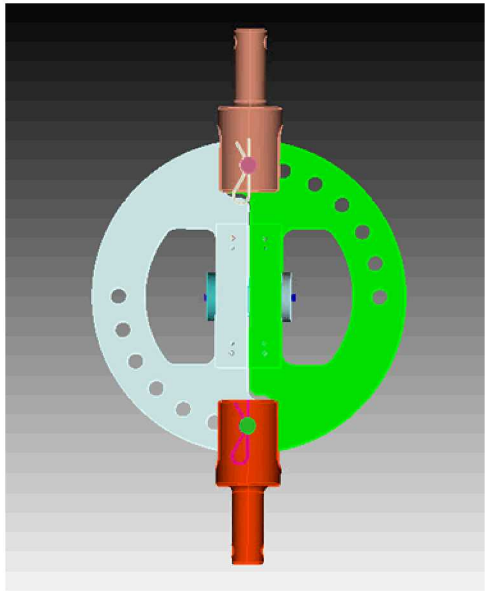

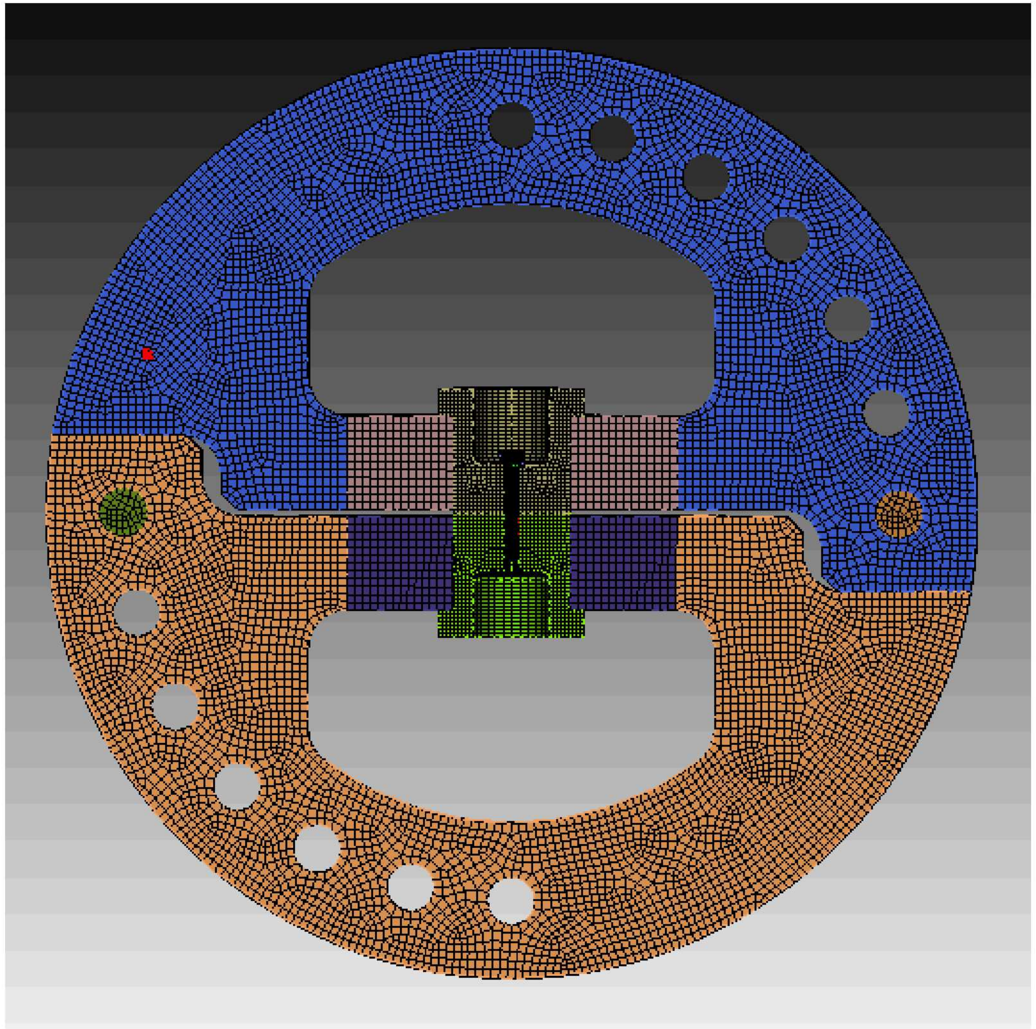

Reduced Ordered Models

- Spot Weld
  - Applies a force-displacement relationship in tension and shear to a node-side set pair
- One-Block Plug
  - Single set of material properties
  - Calibrated to tensile data
- Two-Block Plug
  - Two sets of material properties
  - Tensile region calibrated to tensile data
  - Shear region calibrated to shear data

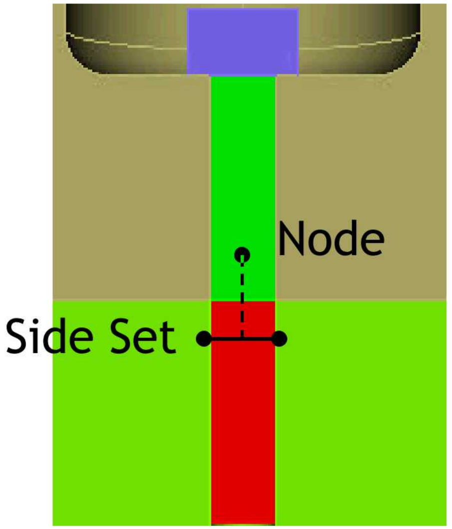

Spot Weld

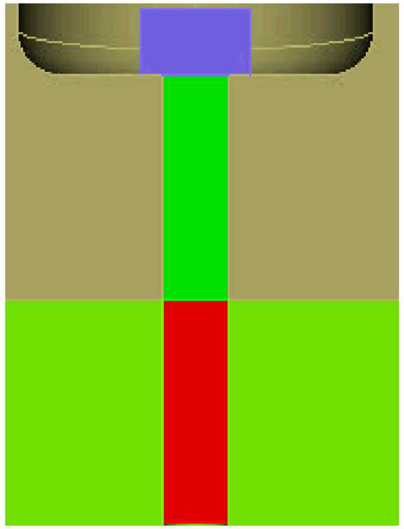

One Block Plug

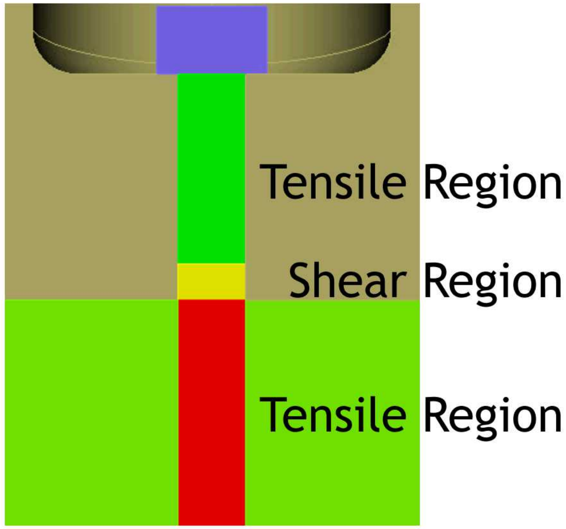

Two Block Plug

Material

- **Fixture 4340 Steel**
  - Young's Modulus: 30.4e6 psi
  - Density: 7.33 g/cc
  - Poisson's Ratio: 0.32
  - Yield Stress: 142.7 ksi
- **Fastener (A574) Tensile Region**
  - Effective Young's Modulus*: 21.1e6 psi
  - Yield Stress: 155 ksi
  - Poisson's Ratio: 0.3
- **Fastener (A574) Shear Region**
  - Effective Yield Stress: 90 ksi (~60% of tensile region)
  - Rest as Tensile Region

*Effective Young's Modulus

$$\frac{F}{A} = E\frac{\Delta x}{L} \longrightarrow E_2 = \frac{A_1}{A_2}E_1$$

- **Spot Weld Tension and Shear Functions**

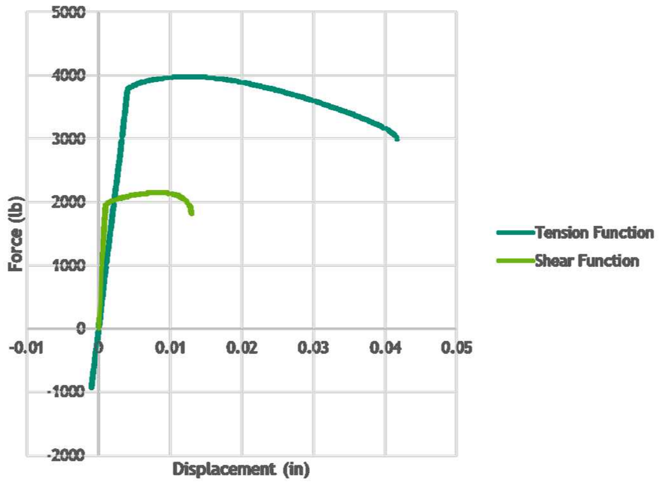

- **Spot Weld Failure Envelope**

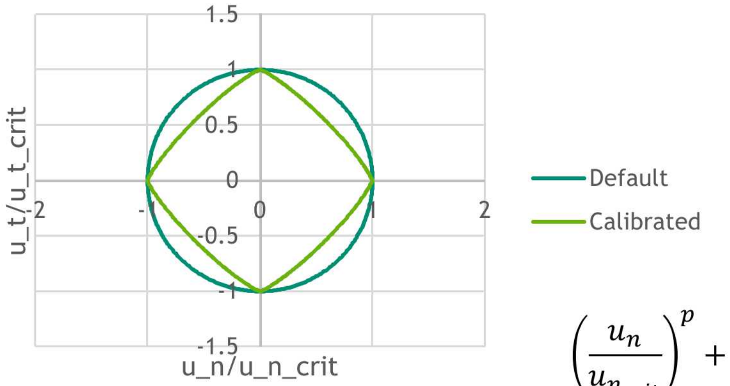

$$\left(\frac{u_n}{u_{n_{crit}}}\right)^p + \left(\frac{u_t}{u_{t_{crit}}}\right)^p \geq 1.0$$

Loading and BC

General

- Experimental loading condition
  - Fixed Constraint
  - Prescribed Displacement in x
- Symmetry in Y to account for half model
- Surface contacts

Spot Weld

- Rigid surfaces for spot weld

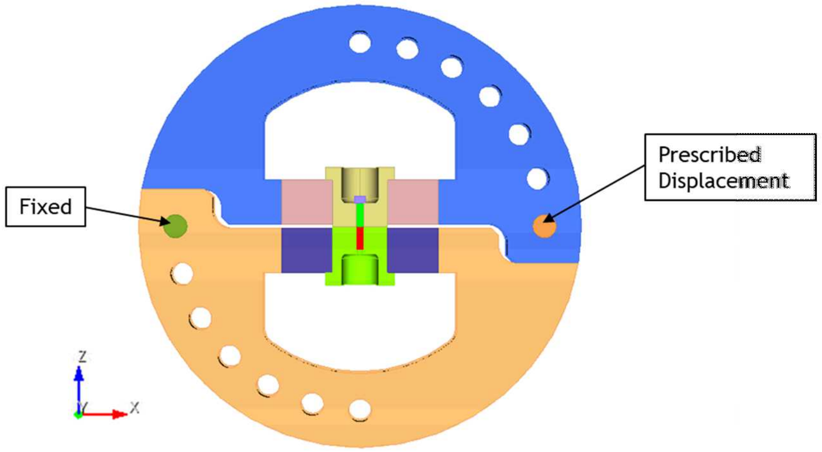

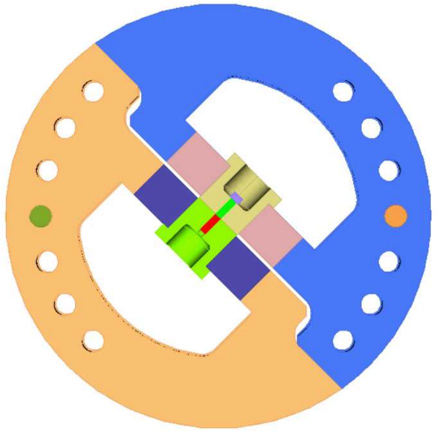

Initial Results

Initial Prediction - Tension

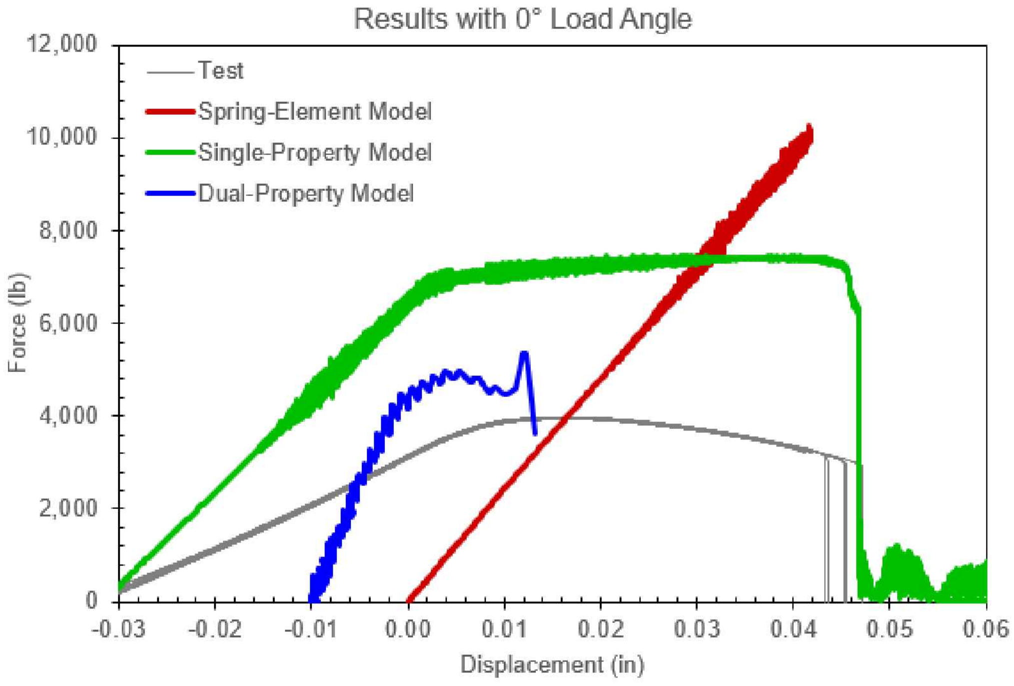

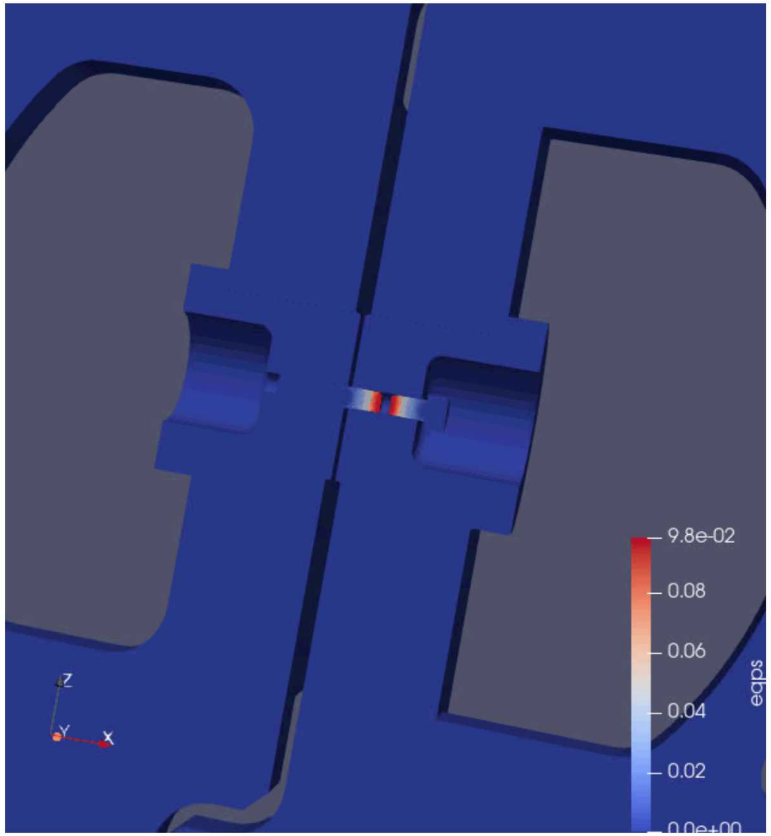

Initial Prediction - Shear

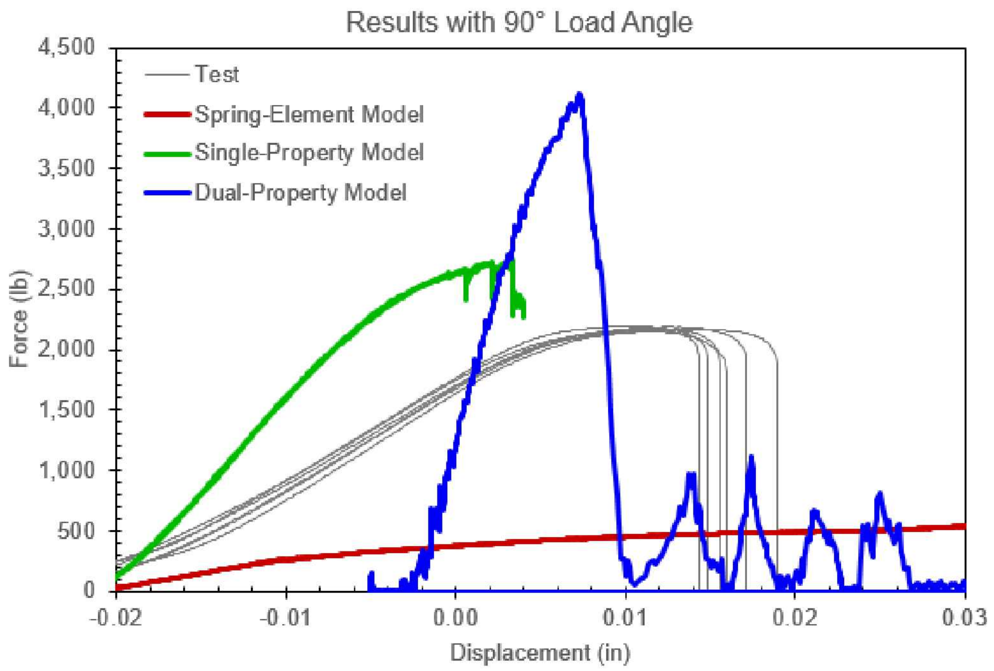

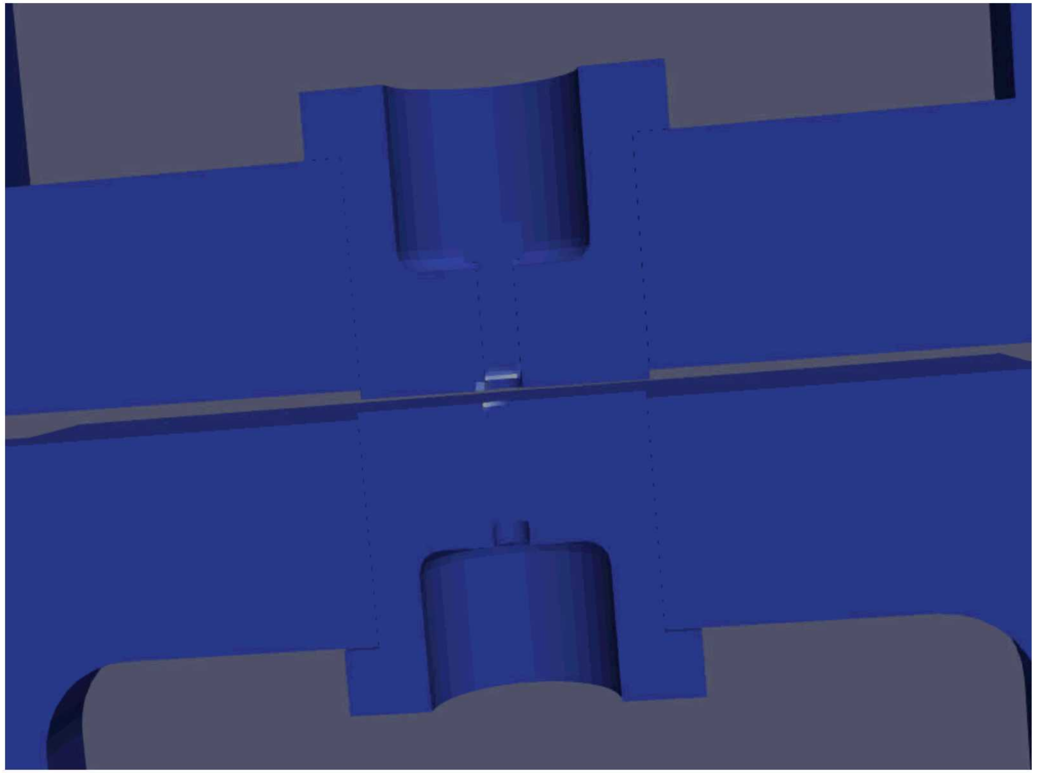

Calibrated Models: Results

Calibrated Results: Tensile and Shear

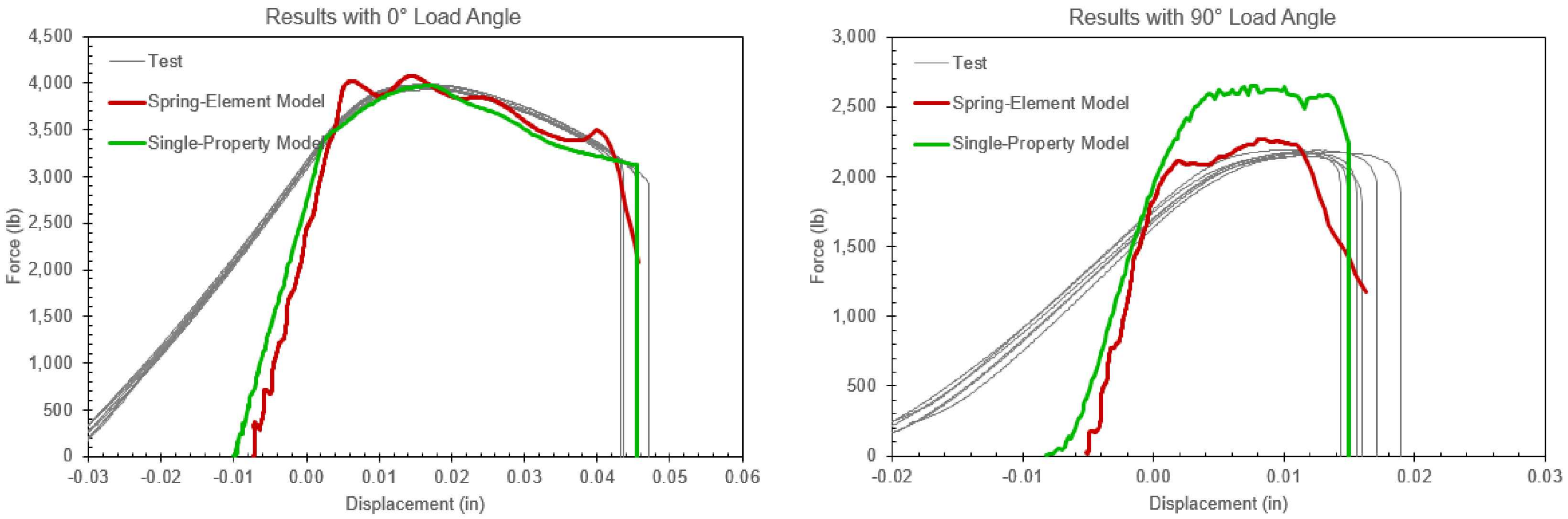

Intermediate Angles: Results

Intermediate Angles after Calibration

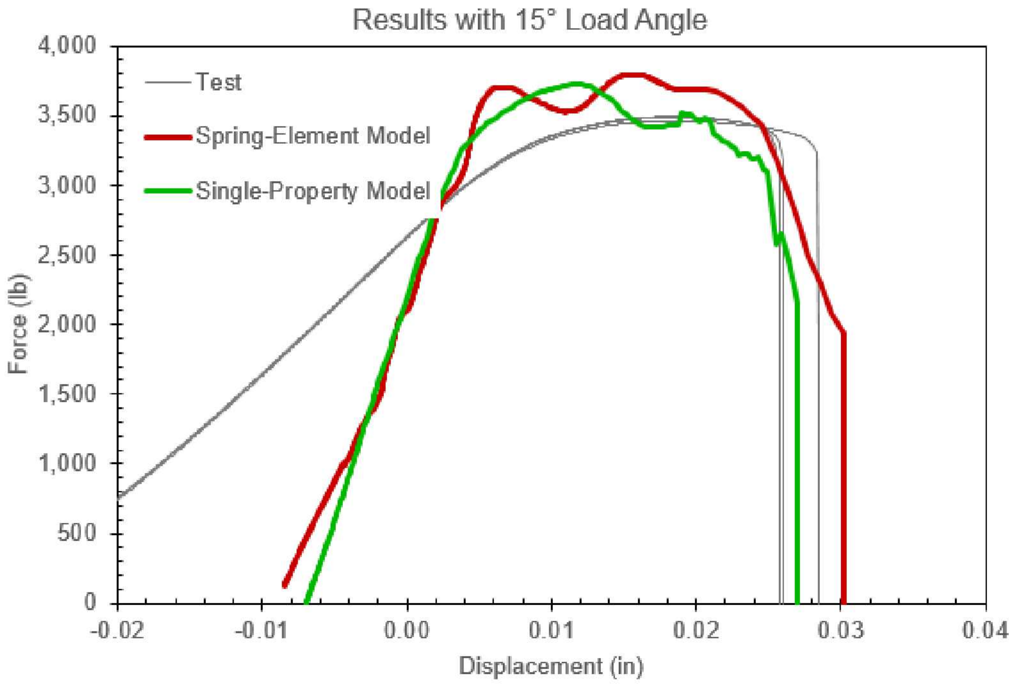

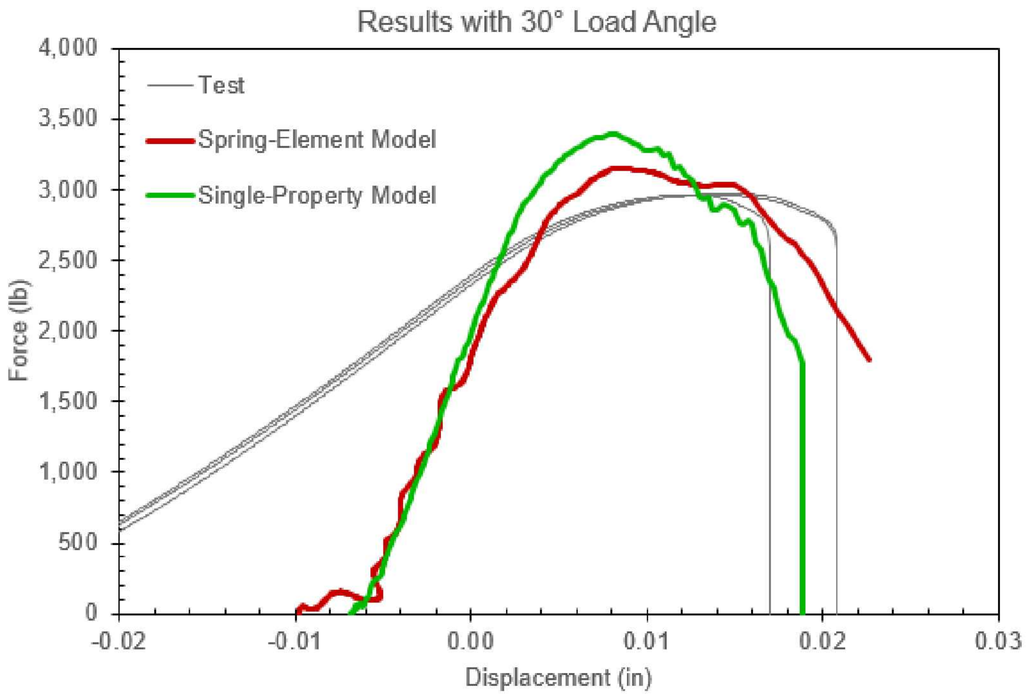

Intermediate Angles after Calibration

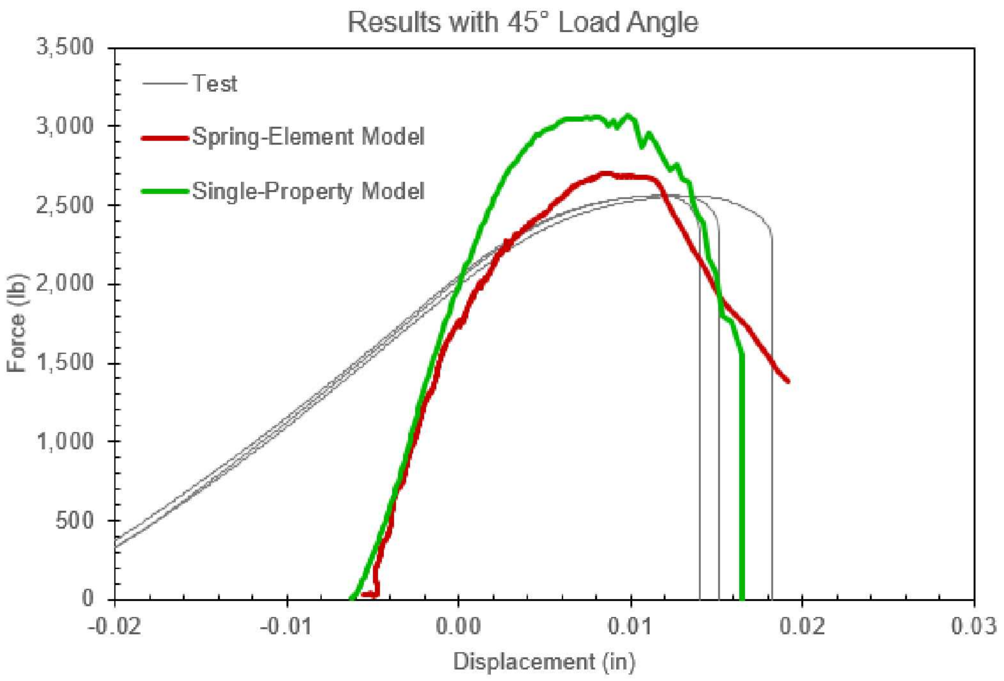

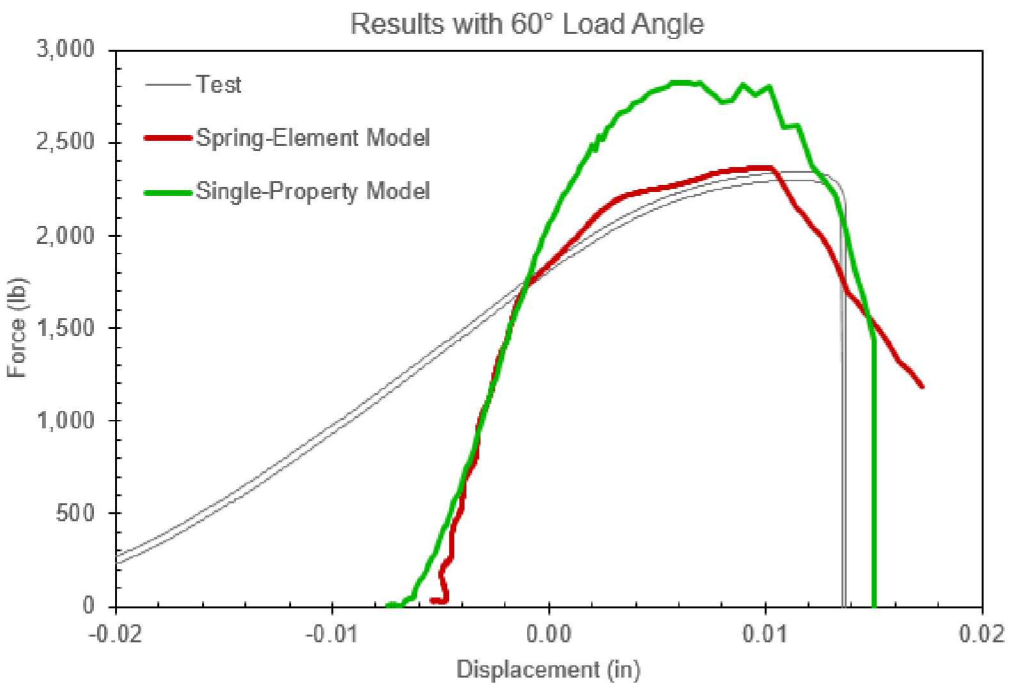

Intermediate Angles after Calibration

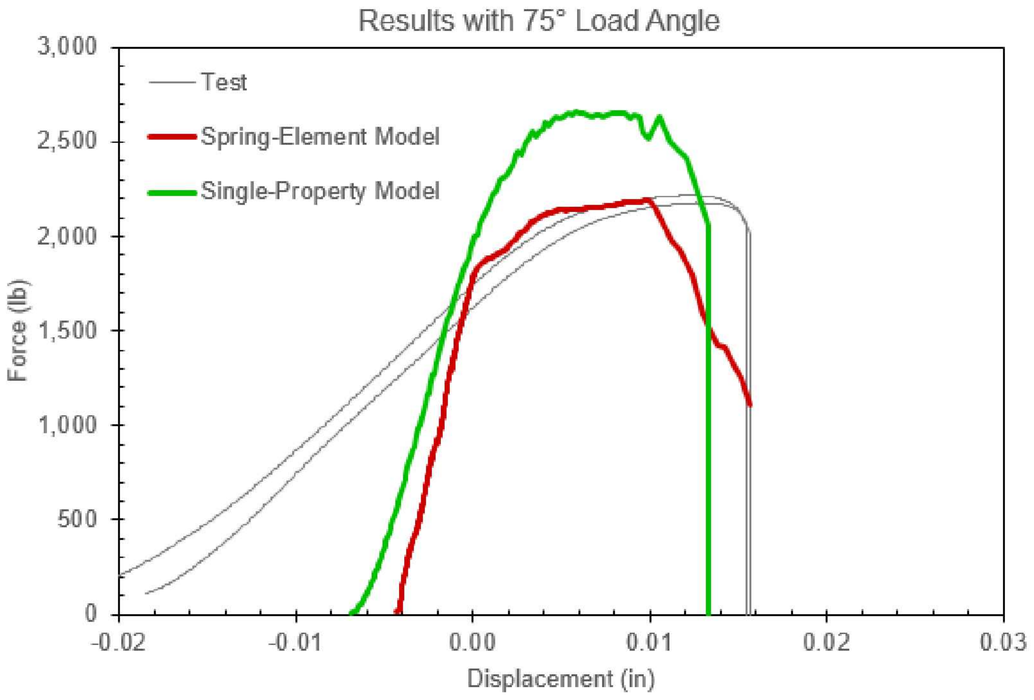

Conclusion

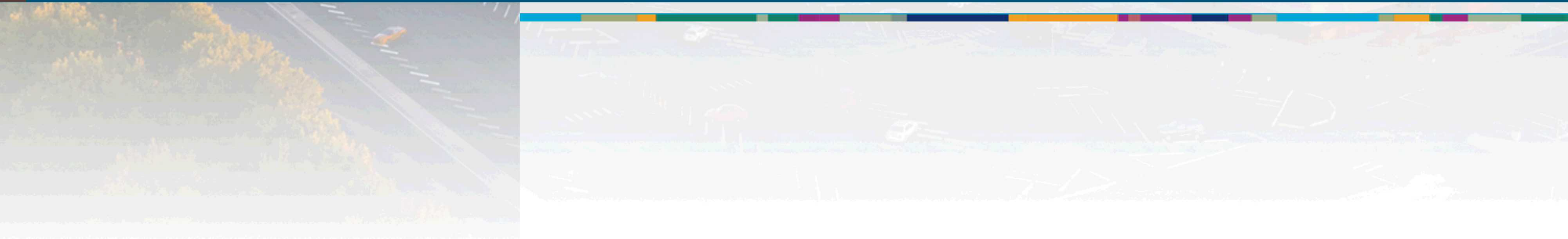

Concluding Remarks

Spring Model Hardening follows the magnitude of the curve and failure point quite effectively

One Block Plug takes longer to tune but can follow the Load/Displacement of a particular angle

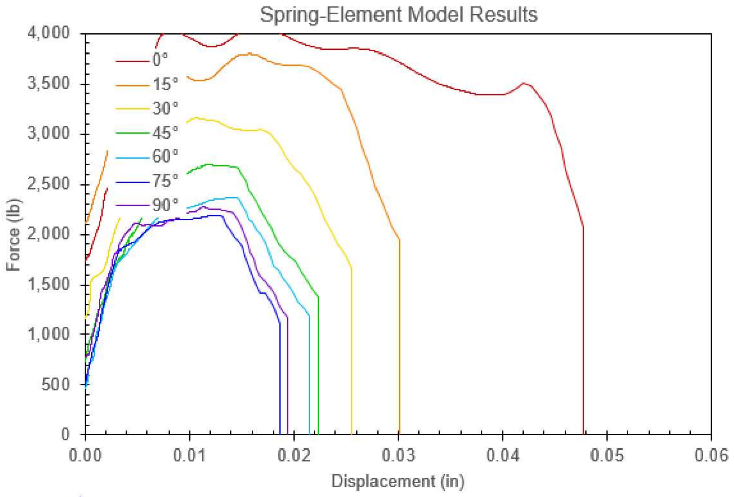

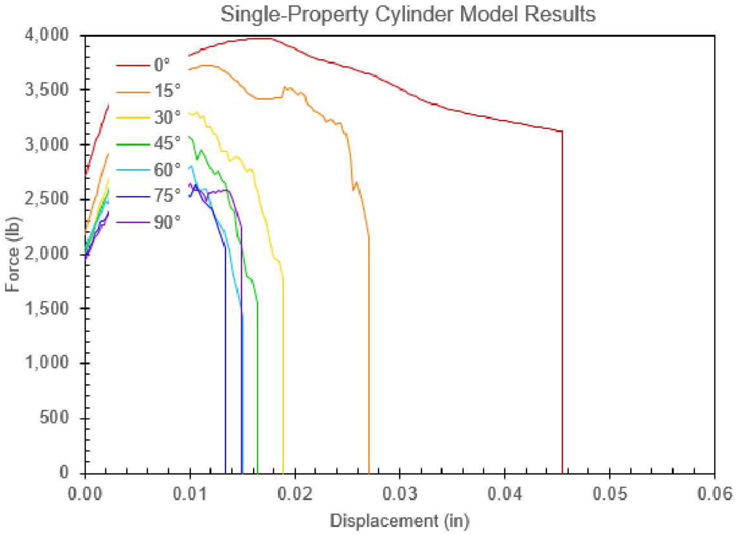

Acknowledgements

This research was conducted at the 2020 Nonlinear Mechanics and Dynamics Research Institute hosted by Sandia National Laboratories and the University of New Mexico.

Sandia National Laboratories is a multimission laboratory managed and operated by National Technology and Engineering Solutions of Sandia, LLC., a wholly owned subsidiary of Honeywell International, Inc., for the U.S. Department of Energy's National Nuclear Security Administration under contract DE-NA-0003525.

Thank you!

Questions?

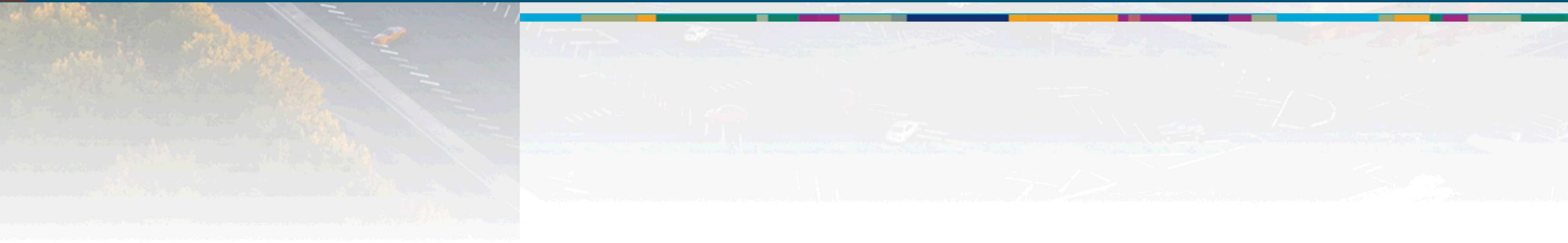

NNM Force Appropriation Pre-test Prediction of Assembly using Calibrated Component and Modal Shaker Models

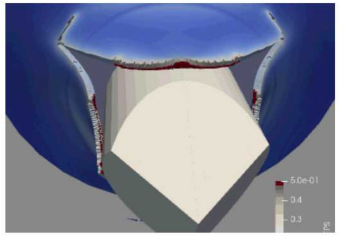

Students:

Arun Malla, Eric Robbins, and Trent Schreiber

Mentors:

Benjamin Pacini, Robert Kuether, Daniel Roettgen, Simone Manzato, and Fernando Moreu

Content slide

I. Introduction

Background and Motivation

- Despite its effect on multiple aspects of structural dynamics, nonlinearity is under-considered and often neglected in industrial design and qualification
- To develop understanding of nonlinear structural dynamics, Seimens Industry Software attempted system identification on a demo aluminum aircraft (Fig. 1) [1]
- But, dynamics of the full system (wing+pylon+fixture) were too complex

Solution: Begin with isolated fixture-pylon structure

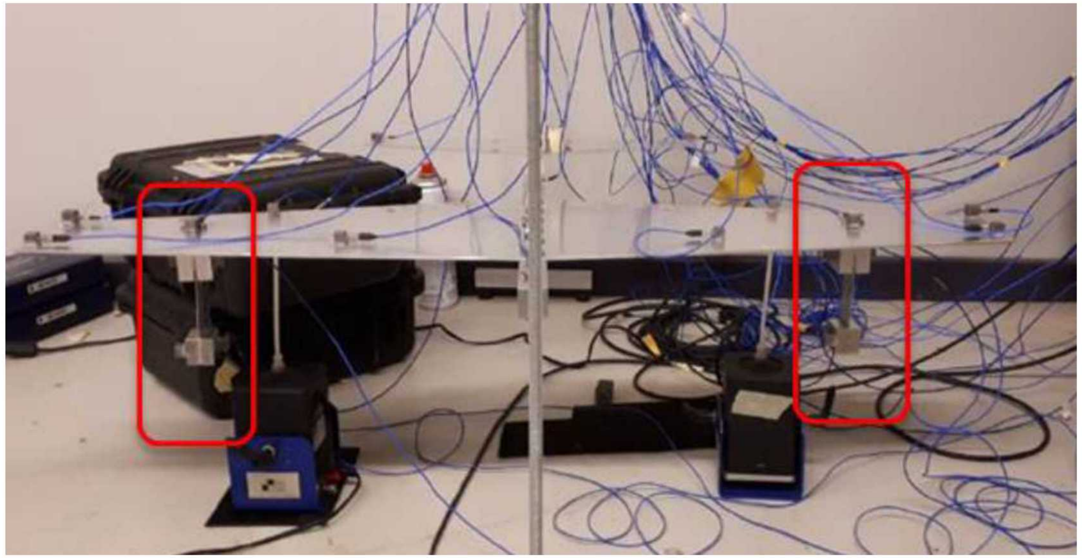

Fig. 1: Siemens demo aluminum aircraft [1]

Previous NOMAD Work

- A NOMAD 2019 research group studied the isolated fixture-pylon structure [2]
- Experiments were conducted on the setup shown in Fig. 2
  - Shaker was used to excite fixture-pylon structure
  - Data collected through accelerometers

Results:

Experimental data

Basic nonlinear model

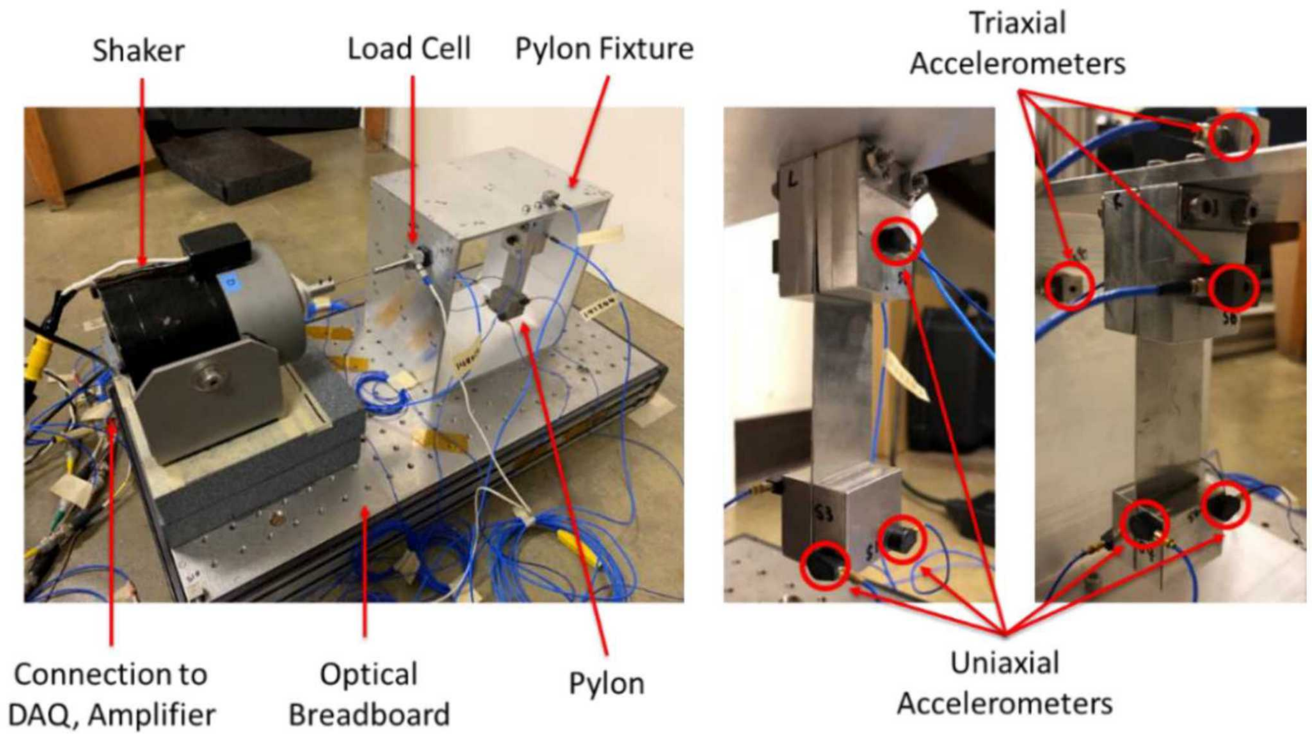

Fig. 2: Sandia isolated fixture-pylon test setup

Current Work

The NOMAD 2020 project builds upon the previous results by:

- Analyzing experimental data
- Further developing the nonlinear model of the fixture-pylon assembly
- Calibrating fixture-pylon model against experimental data
- Combining fixture-pylon model with linear model of the wing structure
- Analyzing the fixture-pylon and wing-pylon-fixture models
- Simulating experiments by coupling wing-pylon model to a shaker model

First step: Analyzing fixture-pylon experimental data

Experimental Data Analysis

Previous experiments resulted in sine spectra data from accelerometers

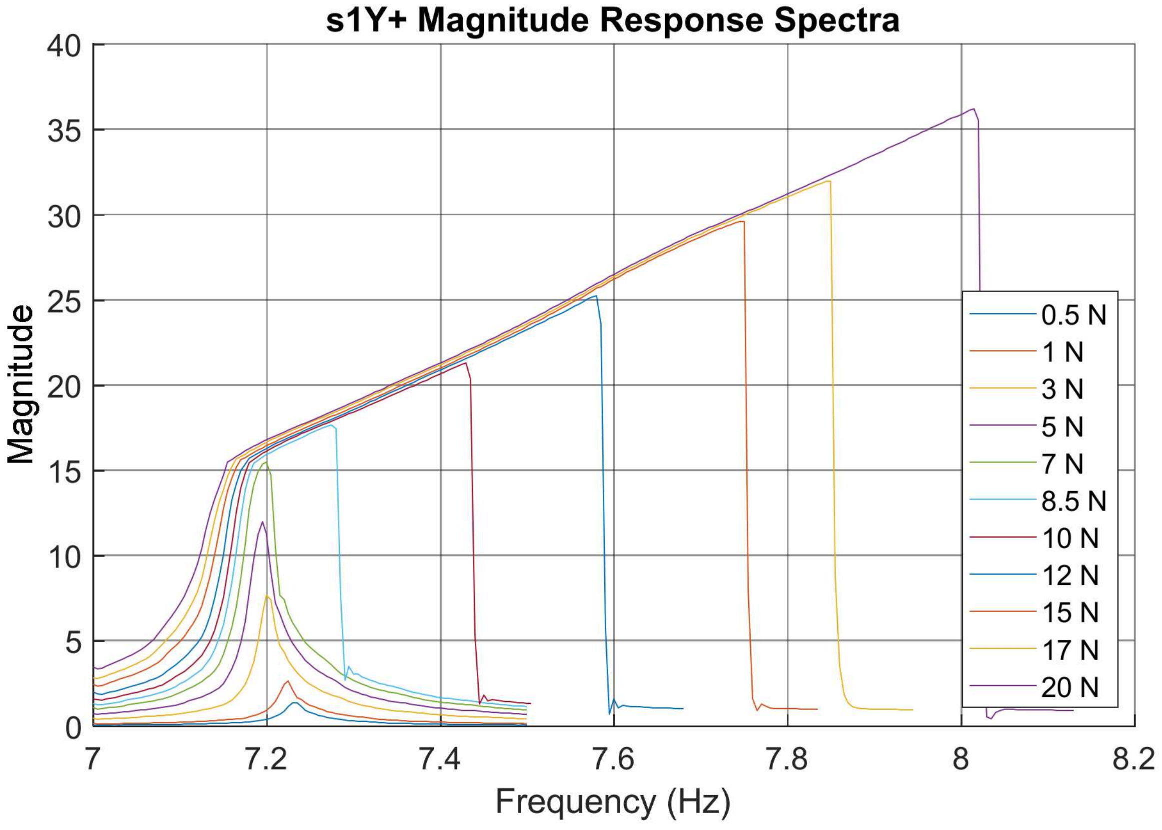

Fig. 3: Sine spectra magnitude response

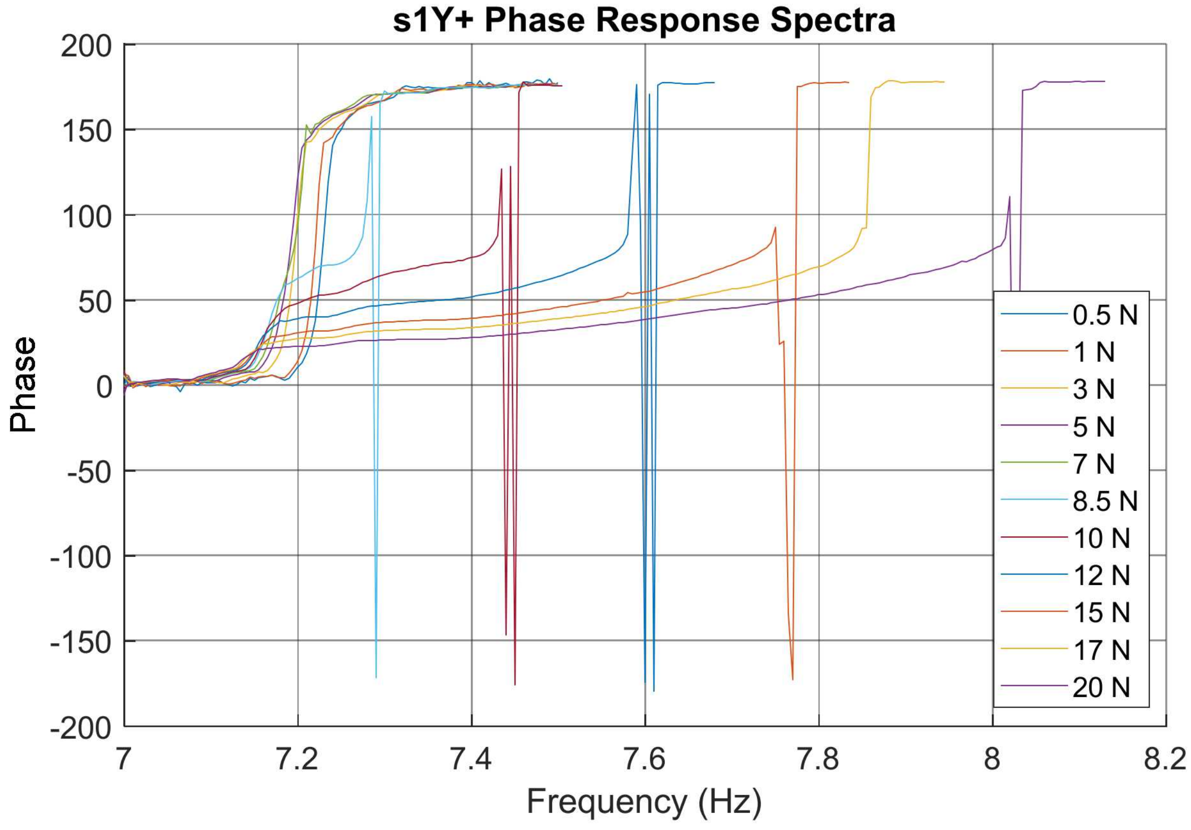

Fig. 4: Sine spectra phase response

Experimental Data Analysis (cont.)

From test data, we extracted backbone curves

- Backbone curves are a useful tool for understanding nonlinear behavior
- Backbone aligned with peaks of magnitude response

Backbone curves

=

Starting point

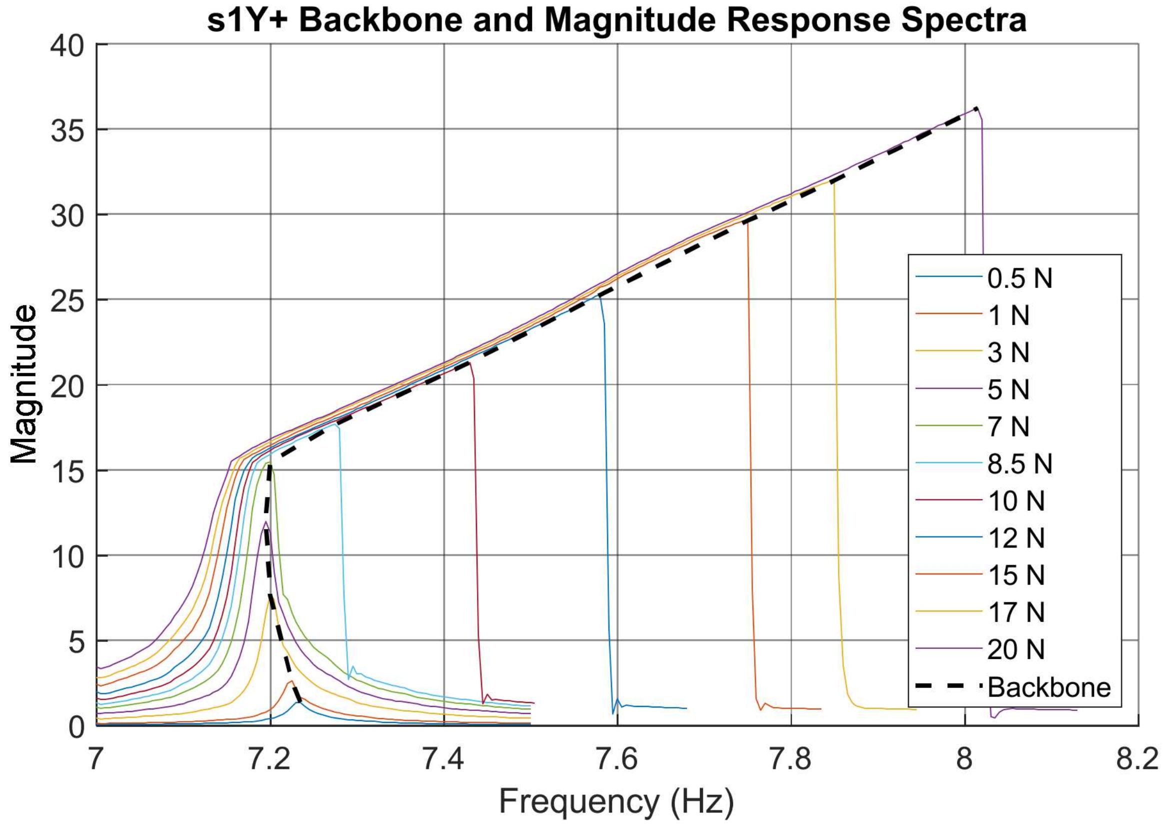

Fig. 5: s1Y+ backbone curve and magnitude response from sine spectra experimental data

II. Fixture-Pylon Assembly

Fixture-Pylon ROM

- To compare the experimental data to a numerical model, a linear finite element model was created for the fixture-pylon assembly using CUBIT
- To reduce the degrees of freedom (DOFs) in the model, a Craig-Bampton (CB) reduction was run in Sierra SD to obtain a reduced order model (ROM) [3-4]
  - This takes the full model with thousands of DOFs and reduces it to a more manageable model with only 7 retained DOFs (virtual nodes, accelerometers, and drive point)

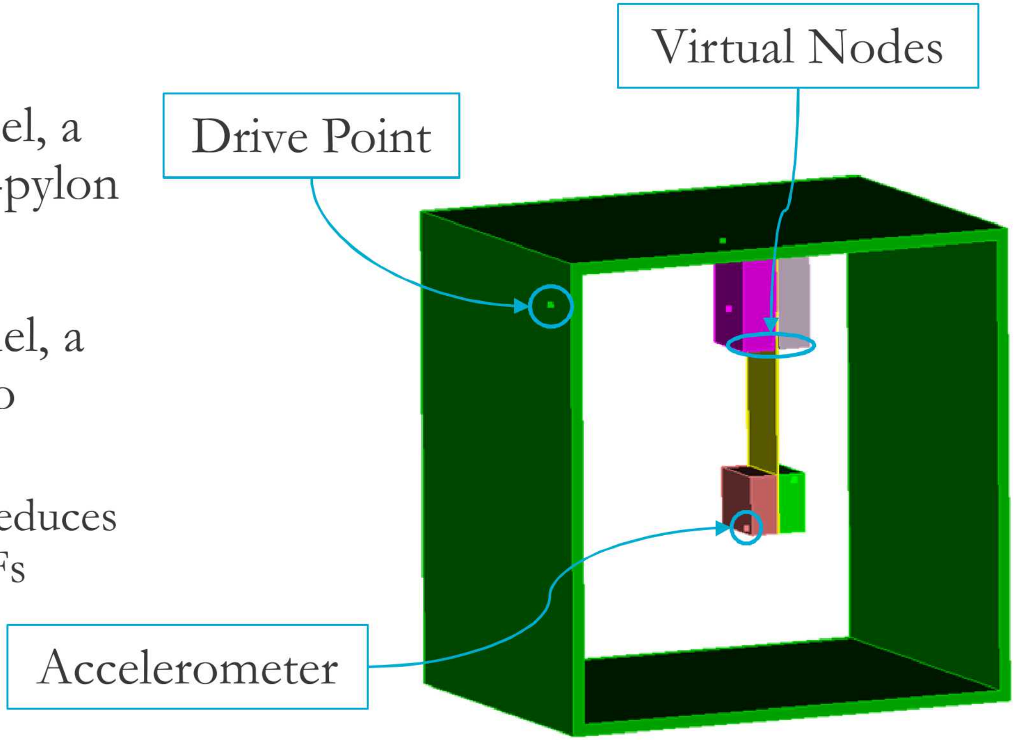

Fig. 6: Fixture-pylon CAD assembly

Reduce the full model to something more manageable:

Full model → CB reduction → Linear ROM

Fixture-Pylon ROM (cont.)

- The linear ROM from Sierra provides the mass and stiffness matrices for the fixture-pylon
  - Damping matrix is computed using proportional damping
- To convert the linear ROM to a nonlinear model, virtual nodes were tied to the pylon block so that a nonlinear restoring force could be added to the equations of motion (EOMs)
- EOMs of nonlinear dynamic system:

$$\underbrace{M\ddot{x}(t) + C\dot{x}(t) + Kx(t)}_{\text{Linear ROM (Sierra Output)}} + f_{nl}\{x(t)\} = u$$

Linear ROM
(Sierra Output)

Nonlinear restoring force between virtual nodes (MATLAB)

Add nonlinear element

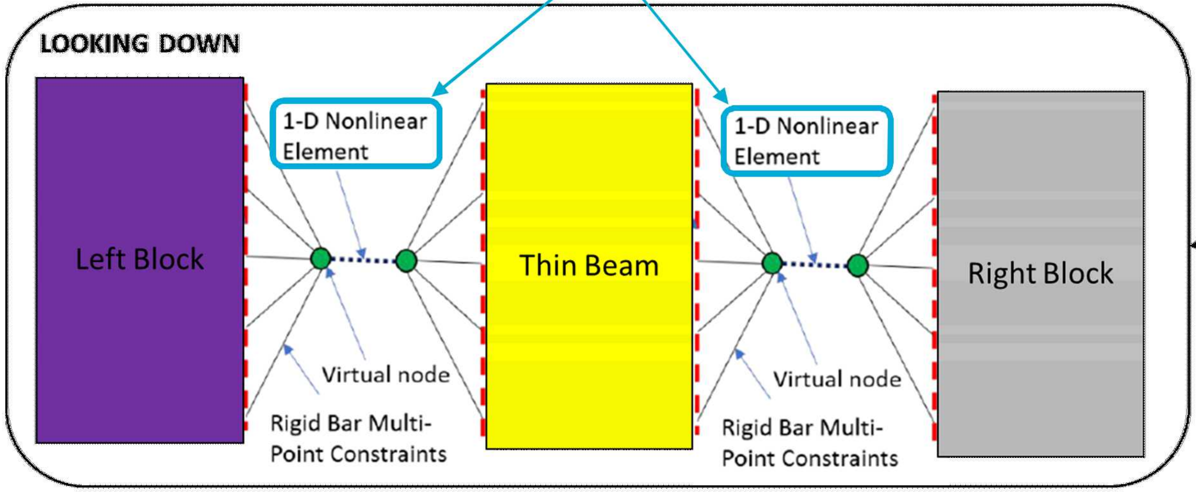

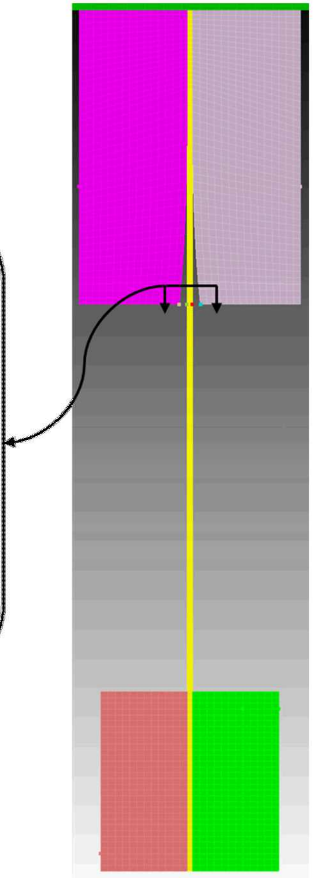

Fig. 7: Virtual nodes in pylon block

Nonlinear Normal Mode (NNM) Theory

- For an unforced, undamped system, an NNM is defined as a **response that is periodic but not necessarily synchronous** [5-6]
- A multi-degree of freedom system will have multiple NNMs
- NNMs are often illustrated in a frequency - energy plot (FEP) (Fig. 8), which shows how a system's natural frequency changes with energy input into the system
- Each point along the NNM in the FEP corresponds to a different time-history response
- Multi-harmonic balance (MHB) is one of several numerical methods used to compute NNMs

NNMs are computed using MHB and illustrated in frequency - energy plots

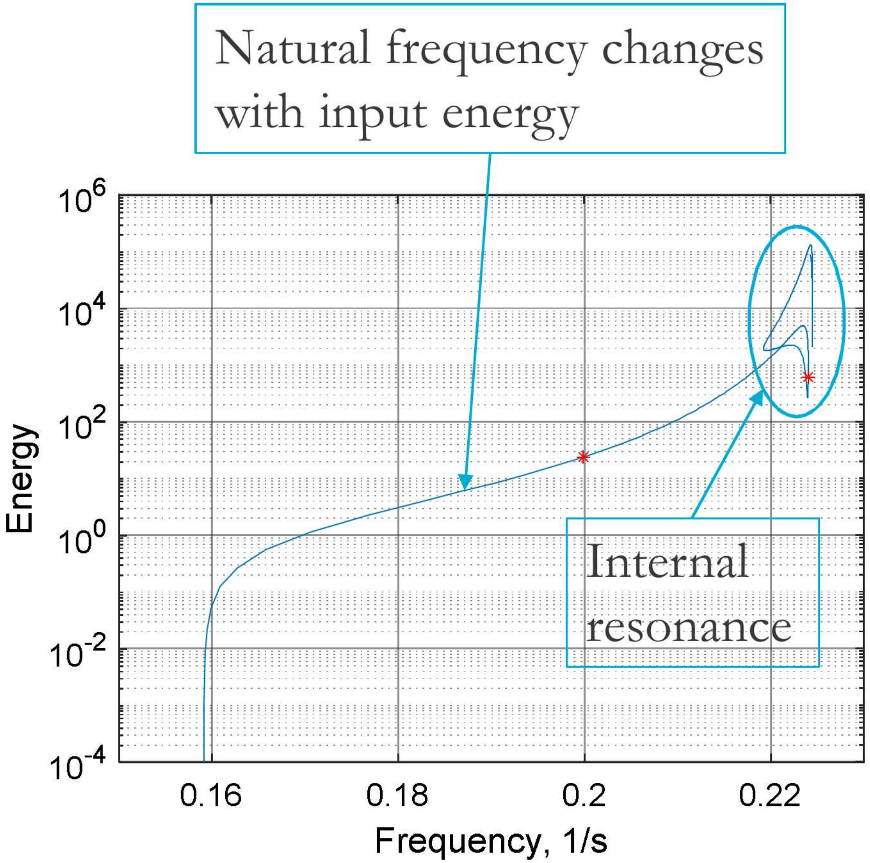

Fig. 8: Frequency - energy curve for 1st NNM of sample system

Calibrating ROM Nonlinearity

Two options were considered for nonlinear elements:

- Cubic spring element (Fig. 9)
  - $f_{\mathrm{nl}}(\Delta x) = k_{NL}(\Delta x)^3$
  - Parameters:
    - k_{NL} - nonlinear spring constant

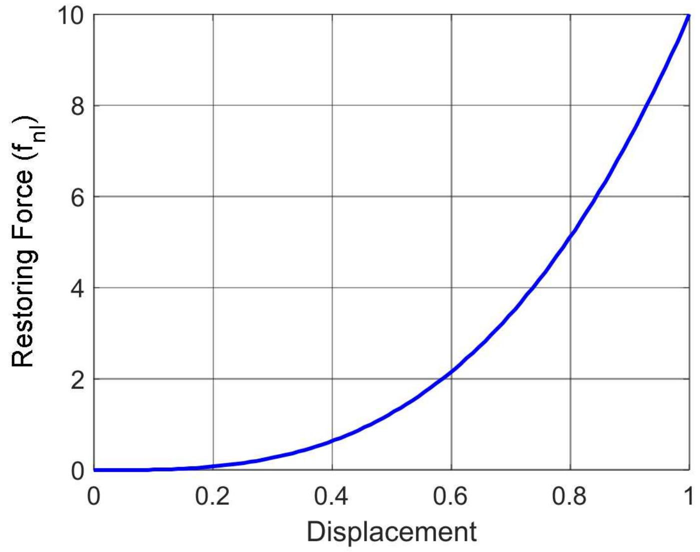

Fig. 9: f_{nl} for cubic spring element

- Gap-spring element (Fig. 10)
  - $f_{nl}(\Delta x) = \begin{cases} 0 \; for \; \Delta x \leq x_{gap} \\ k_{pen}(\Delta x - x_{gap}) \; for \; \Delta x > x_{gap} \end{cases}$
  - Parameters:
    - k_{pen} - linear penalty spring constant
    - x_{gap} - gap width

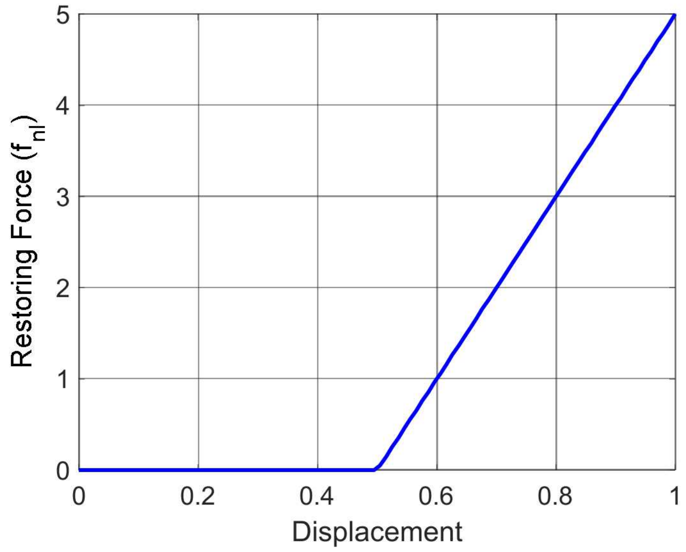

Fig. 10: f_{nl} for gap-spring element

Calibrating ROM Nonlinearity (cont.)

With cubic spring (Fig. 11) and gap-spring (Fig. 12) elements, NNM backbone curves were determined and compared to experimental data

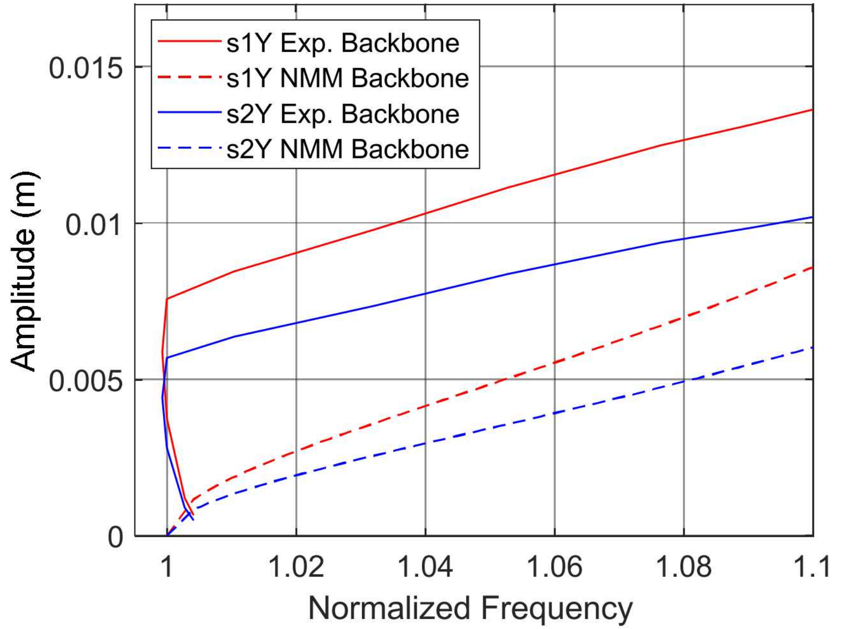

Fig. 11: Cubic spring element backbone comparison

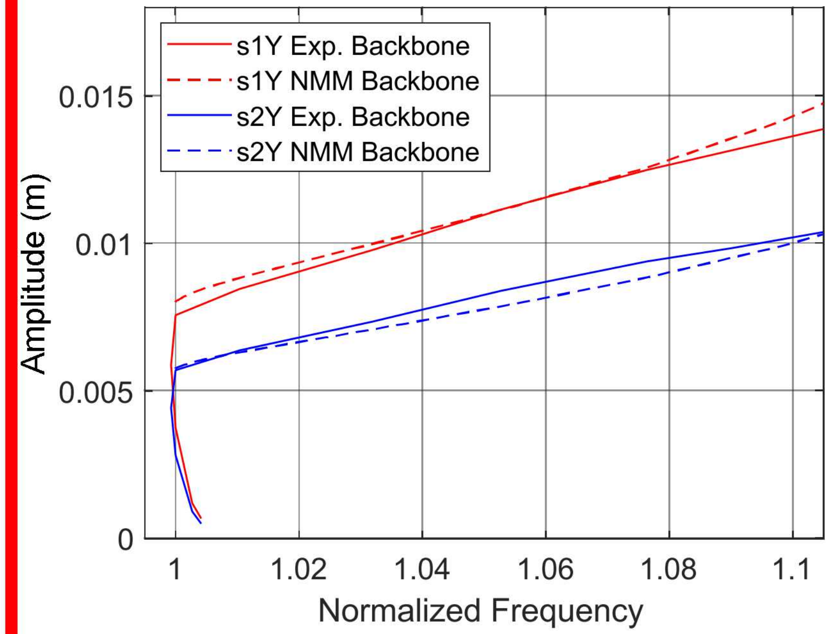

Fig. 12: Gap-spring element backbone comparison

Selected:

<u>**Gap-spring element**</u>

$$k_{pen} = \mathbf{7 * 10\hat{}4}\ N/m$$
$$x_{gap} = \mathbf{0.68}\ mm$$

Stepped Sine Validation

A stepped sine test simulation was performed to verify that the gap-spring nonlinearity accurately captures the nonlinear dynamics in the pylon-fixture ROM in comparison to the NOMAD 2019 experimental results

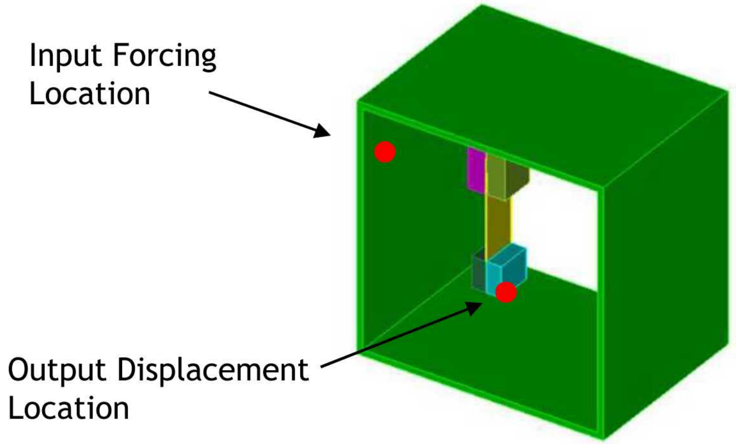

Fig. 13: Fixture-pylon system with marked input and output nodes

A stepped sine test simulation will verify if the calibrated ROM is in agreement with the experimental data

Stepped Sine Validation (cont.)

- Despite some variation in stiffness effects, the simulation results compared relatively well with the experimental results
- Nearly all linear-peak regions occurred at a slightly higher frequency and most nonlinear-peaks were slightly smaller in magnitude, compared to the experimental results

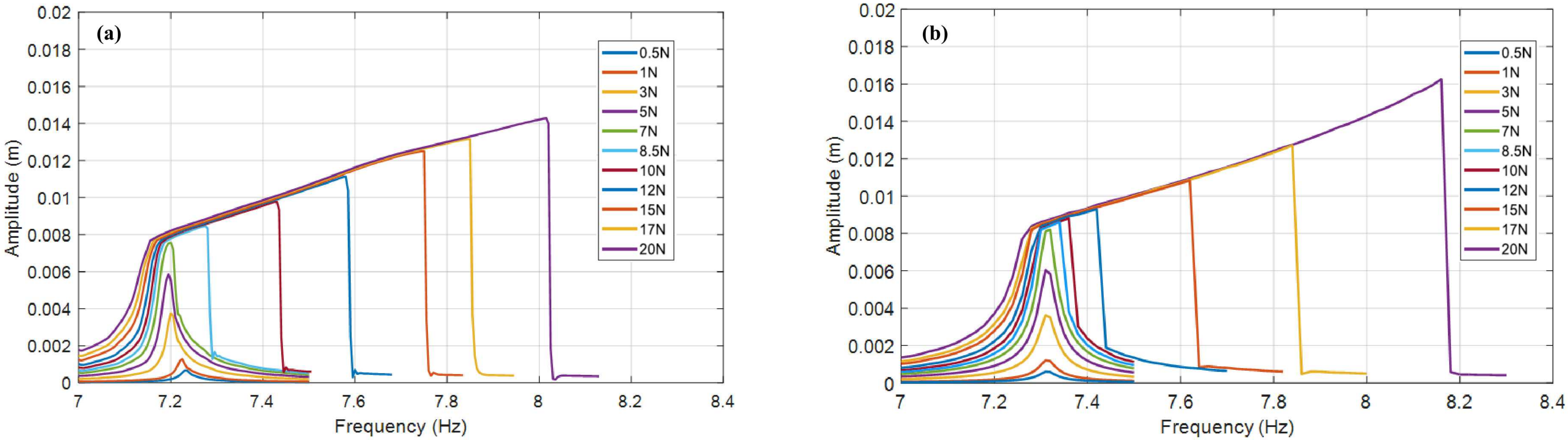

Fig. 14: Comparison of results from NOMAD 2019 experiment (a) and stepped sine simulation (b)

Stepped Sine Validation (cont.)

- Despite some variation in stiffness effects, the simulation results compared relatively well with the experimental results
- Nearly all linear-peak regions occurred at a slightly higher frequency and most nonlinear-peaks were slightly smaller in magnitude, compared to the experimental results

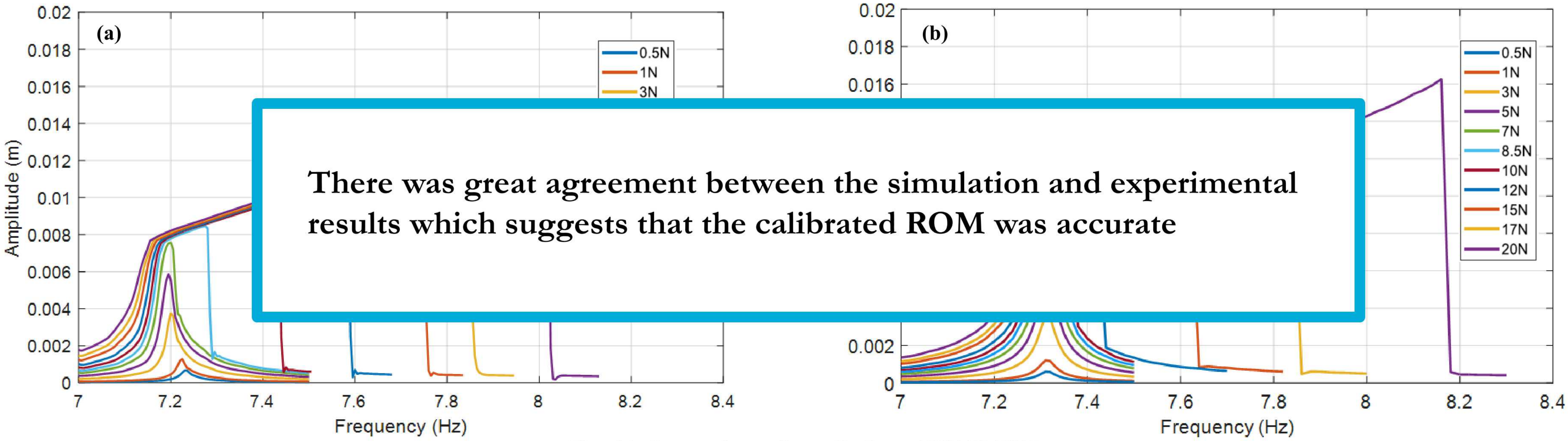

There was great agreement between the simulation and experimental results which suggests that the calibrated ROM was accurate

Fig. 14: Comparison of results from NOMAD 2019 experiment (a) and stepped sine simulation (b)

III. Full Assembly

Wing-Pylon ROM

- Next step: Attach the calibrated pylon to the wing
- Following similar methods as the fixture-pylon model, a linear finite element model of the next-level wing-pylon assembly was created
- Craig-Bampton reduction was applied using Sierra SD to obtain the linear ROM
  - DOFs for the accelerometers, virtual nodes, and drive points were retained
- The calibrated gap-spring element in the pylon block was added to the linear ROM to describe the nonlinear EOMs

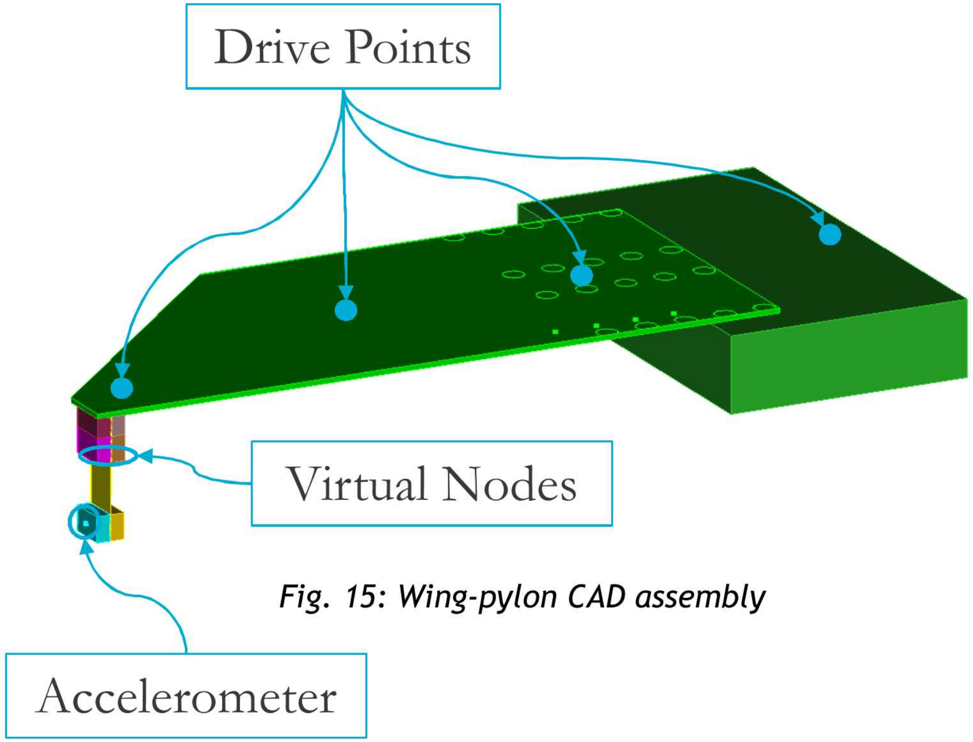

Fig. 15: Wing-pylon CAD assembly

Linear wing-pylon ROM from Sierra + **Calibrated gap-spring element in pylon** = **Nonlinear EOMs**

$$\boldsymbol{M}\ddot{\boldsymbol{x}}(\boldsymbol{t}) + \boldsymbol{C}\dot{\boldsymbol{x}}(\boldsymbol{t}) + \boldsymbol{K}\boldsymbol{x}(\boldsymbol{t})$$

$$\boldsymbol{f}_{\boldsymbol{nl}}\{\boldsymbol{x}(\boldsymbol{t})\}$$

$$\boldsymbol{M}\ddot{\boldsymbol{x}}(\boldsymbol{t}) + \boldsymbol{C}\dot{\boldsymbol{x}}(\boldsymbol{t}) + \boldsymbol{K}\boldsymbol{x}(\boldsymbol{t}) + \boldsymbol{f}_{\boldsymbol{nl}}\{\boldsymbol{x}(\boldsymbol{t})\} = \boldsymbol{u}$$

Wing-Pylon ROM (cont.)

Mode shapes for linear wing-pylon model:

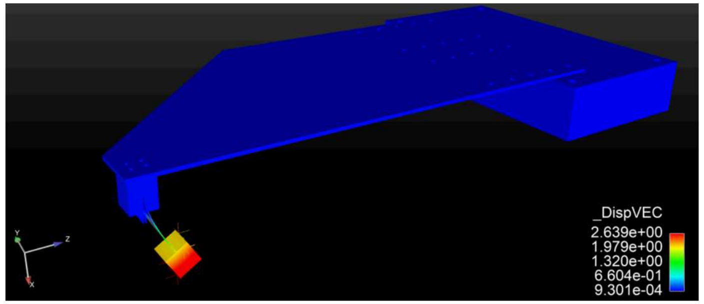

Fig. 16: Mode 1 (7.30 Hz)

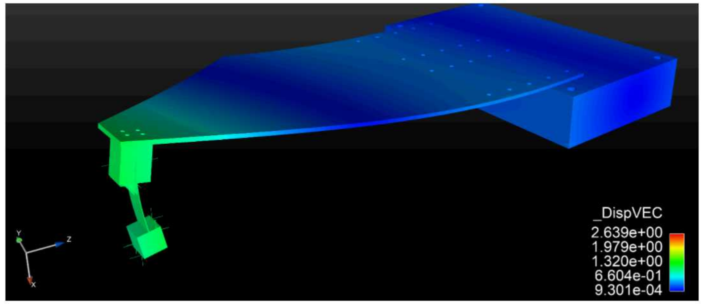

Fig. 17: Mode 2 (22.20 Hz)

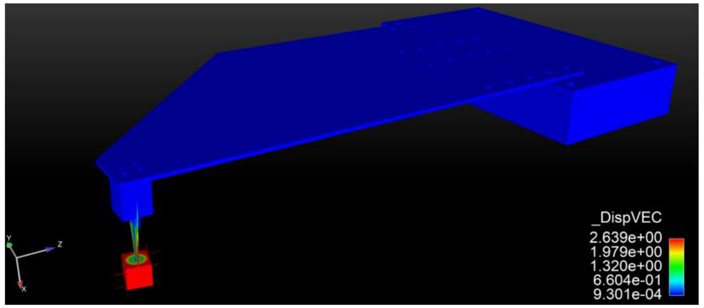

Fig. 18: Mode 3 (47.28 Hz)

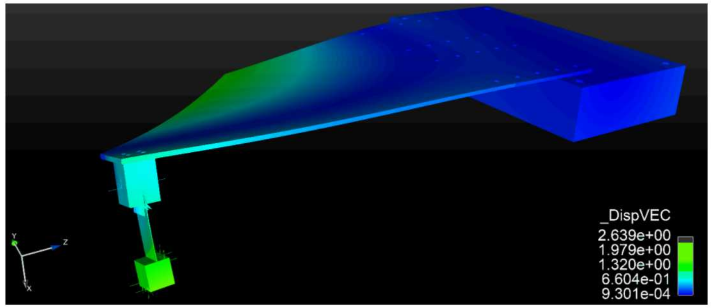

Fig. 19: Mode 4 (49.22 Hz)

Note: mode numbers refer to elastic modes

Multi-Harmonic Balance Method

- The MHB method was utilized to identify NNMs and any possible internal resonances for the calibrated wing-pylon ROM
- Mode 2 was of interest because the bending of the wing resulted in bending of the pylon beam which produced large displacements in the lower pylon block
- Large displacements in the pylon initiated the nonlinear behavior in the gap-spring element

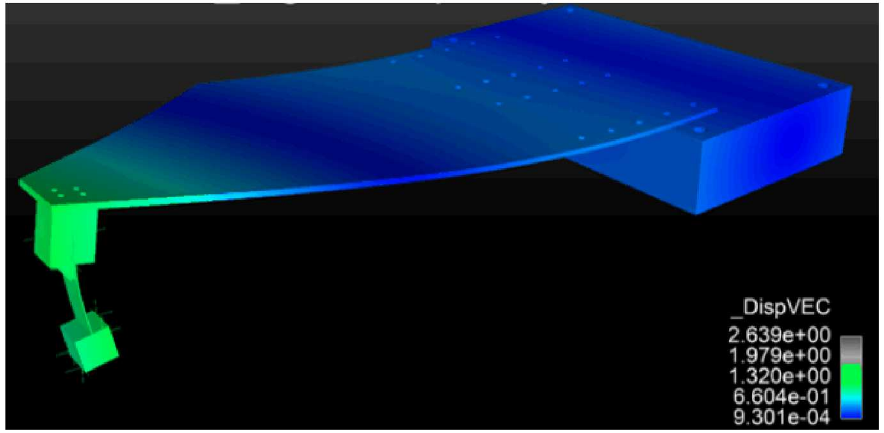

Fig. 20: Mode 2 (22.20 Hz)

Mode 2 was considered for further investigation based on the large wing and pylon bending mode shapes

Multi-Harmonic Balance Method (cont.)

- NNM 2 contained a small frequency shift which remained extremely close to linear mode 2 resonant frequency
- This can easily be overlooked if only a linear analysis is considered thus reinforcing the significance of nonlinear analyses
- An internal resonance was identified on a tongue of NNM 2

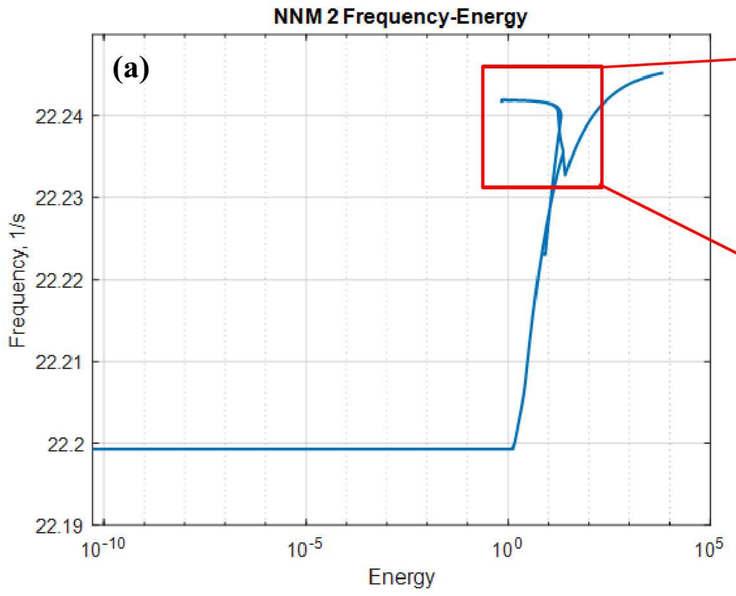

Fig. 21: NNM 2 of the Wing-Pylon Assembly

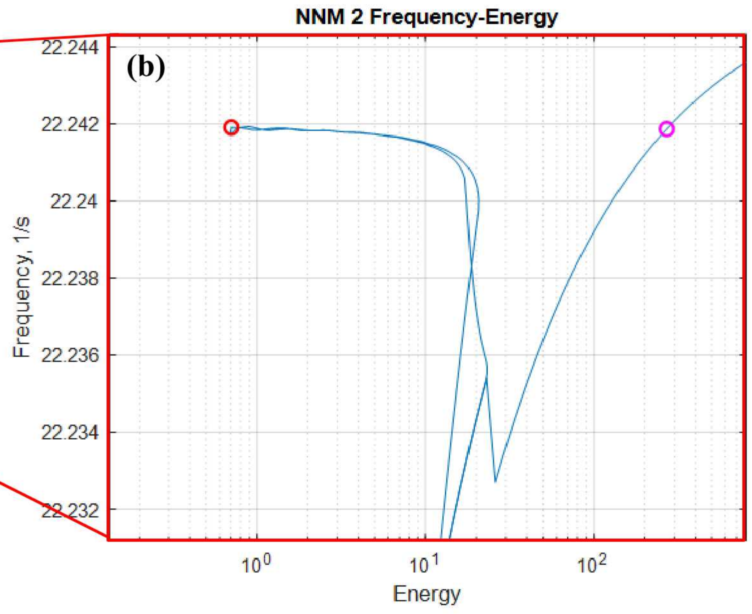

Fig. 22: NNM 2 with Identified Internal Resonance and Single Harmonic Points

Multi-Harmonic Balance Method (cont.)

- A 1:5 internal resonance was identified between NNM 2 and 7 on the wing-pylon ROM; the red point in (a) is the tongue of the internal resonance between the two NNM's
- The internal resonance can easily be seen in the displacement time-history (b) where multiple ratios of 1:5 harmonics exist
- Single harmonic motion exists (c) in NNM 2 as well which is described by the magenta point in (a)

NNM 2 remained very close to its linear mode and additionally contained a 1:5 internal resonance with NNM 7

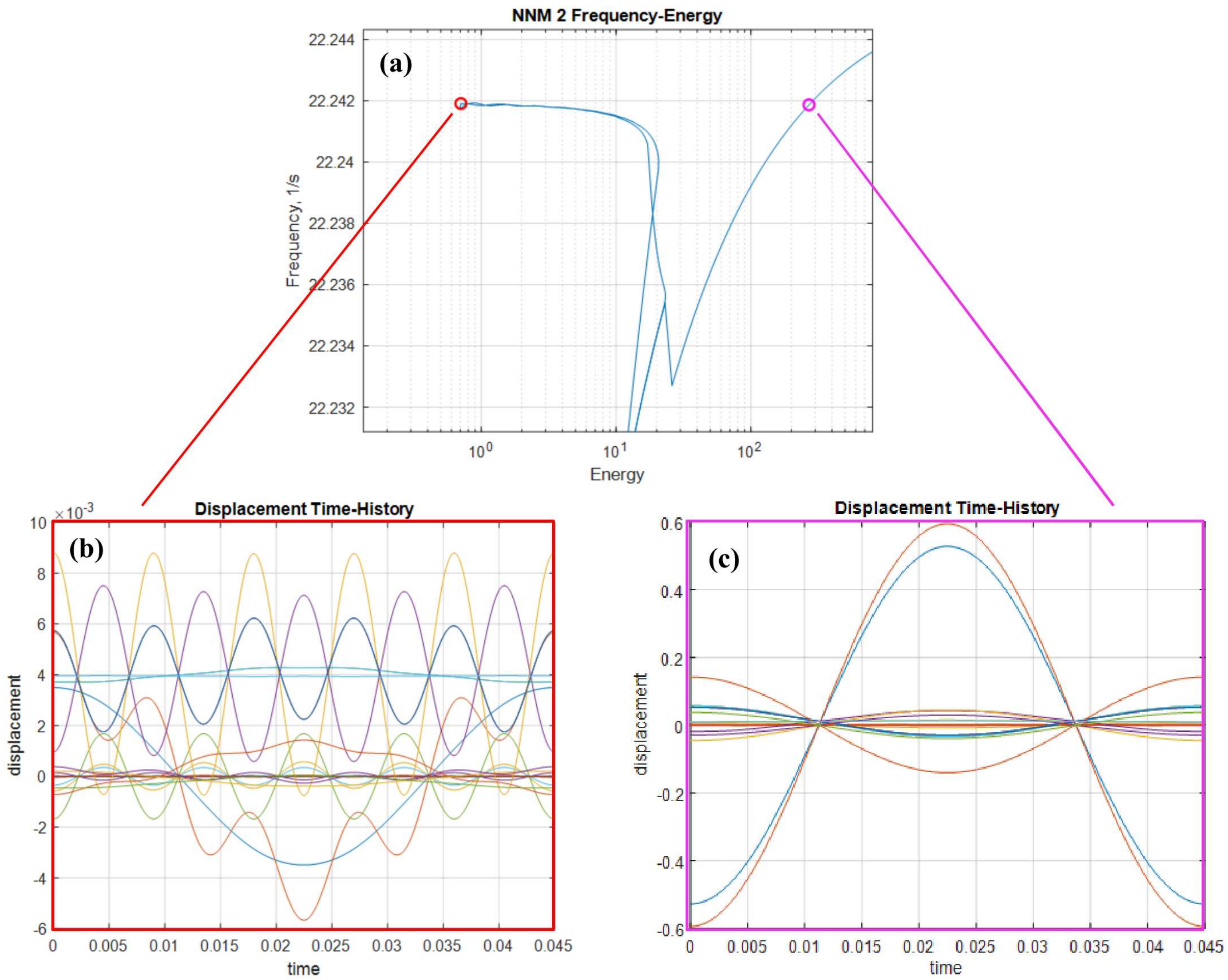

Fig. 23: Displacement Time-Hitories of Identified Internal Resonance and Single Harmonic Motion

Multi-Harmonic Balance Method (cont.)

- The modal interaction between the NNM's 2 and 7 are depicted in plot (b) where NNM 7 was scaled down by an integer of 5 and only computed to the 5th harmonic (there are more harmonics and internal resonances on NNM 7)
- This essentially means when mode 2 is excited mode 7 can experience large displacement amplitude responses

(a)

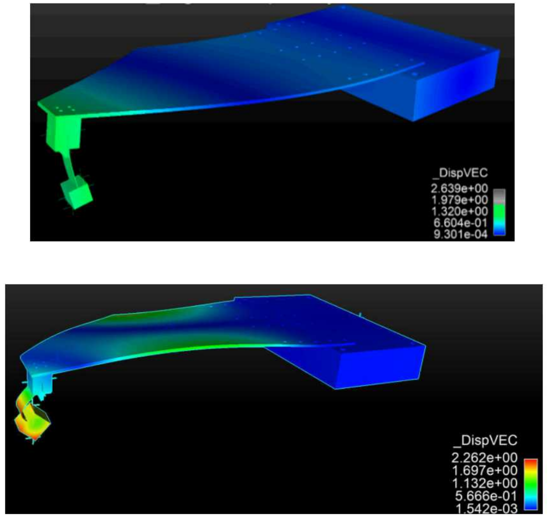

Fig. 24: Linear Modes 2 and 7 Mode Shapes

(b)

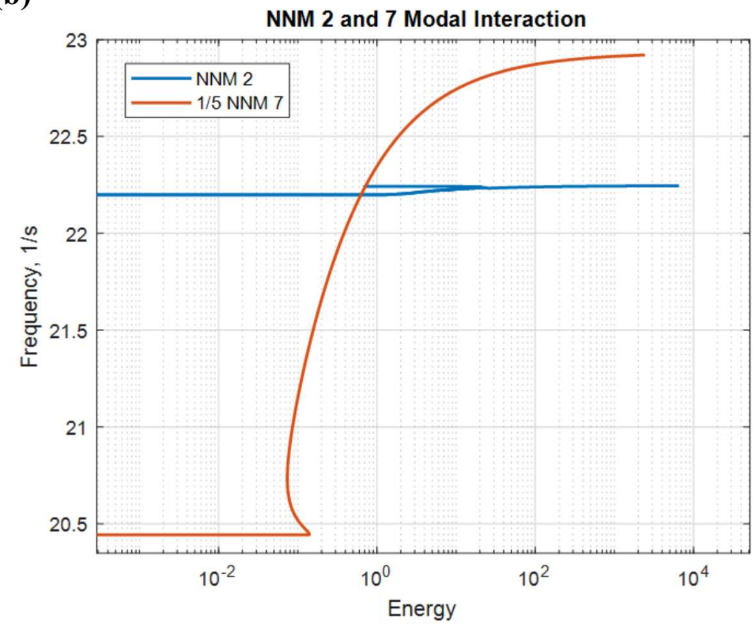

Fig. 25: NNM 2 and 7 Modal Interaction

(c)

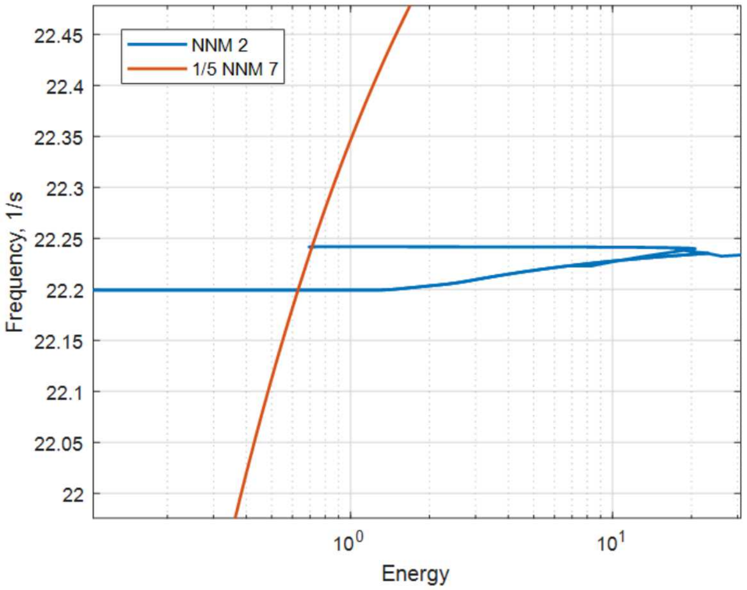

Fig. 26 NNM 2 and 7 Internal Resonance Crossing

Multi-Harmonic Balance Method (cont.)

- The modal interaction between the NNM's 2 and 7 are depicted in plot (b) where NNM 7 was scaled down by an integer of 5 and only computed to the 5th harmonic (there are more harmonics and internal resonances on NNM 7)
- This essentially means when mode 2 is excited mode 7 can experience large displacement amplitude responses

(a)

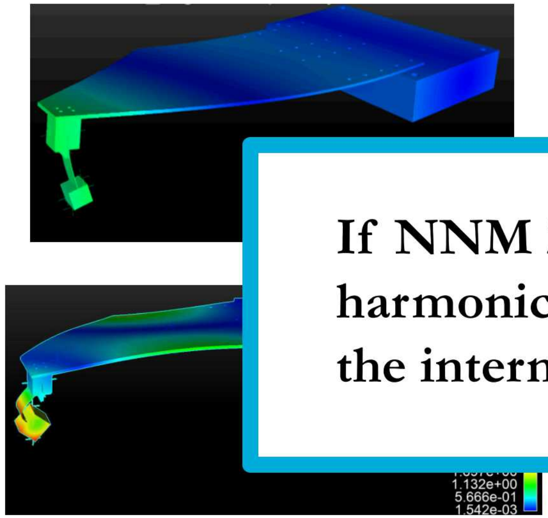

(b)

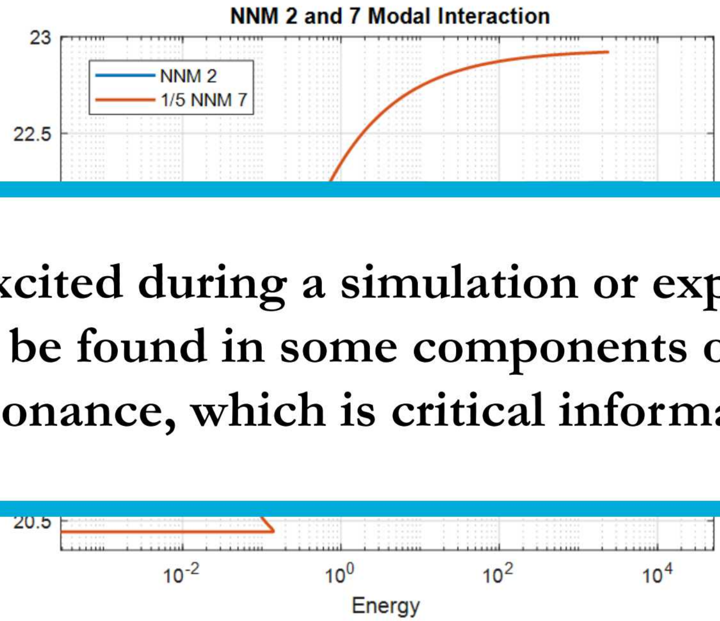

(c)

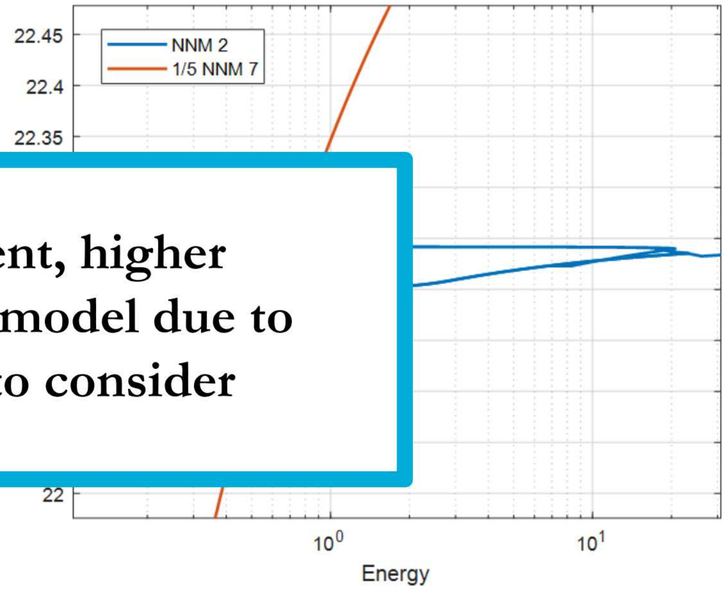

If NNM 2 is excited during a simulation or experiment, higher harmonics can be found in some components of the model due to the internal resonance, which is critical information to consider

Fig. 24: Linear Modes 2 and 7 Mode Shapes

Fig. 25: NNM 2 and 7 Modal Interaction

Fig. 26 NNM 2 and 7 Internal Resonance Crossing

IV. Virtual Experiments

Shaker Model

To account for physical limitations of the shaker, a previously calibrated electro-mechanical shaker model was substructured to the wing-pylon ROM for simulated experiments using the force appropriation method

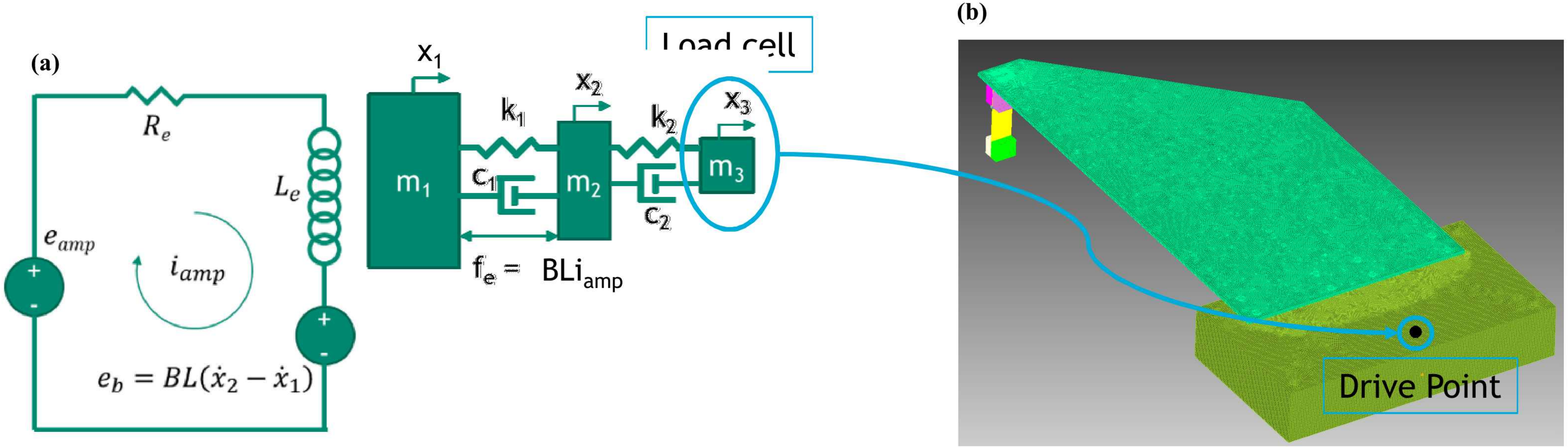

Fig. 27: Virtual shaker model (a) and wing-pylon finite element model (b)

Note: Shaker input voltage is the <u>only</u> input to the substructured shaker, wing, pylon system

Force Appropriation Method

- Phase lag quadrature criterion: A single NNM is isolated if the structure vibrates with a phase lag of 90° with respect to the input signal
- Force appropriation testing relies on the phase lag quadrature criterion
  - The structure is excited at different forcing frequencies until a 90° phase difference is achieved
  - NNMs can be identified one at a time using this method
- Simulated force appropriation experiments were performed for the wing-pylon assembly
  - A controller varied the frequency of the shaker input voltage until quadrature was achieved
  - The amplitude of the input voltage was then increased and the process repeated; thus constructing the frequency-energy plot (FEP) for NNMs of interest

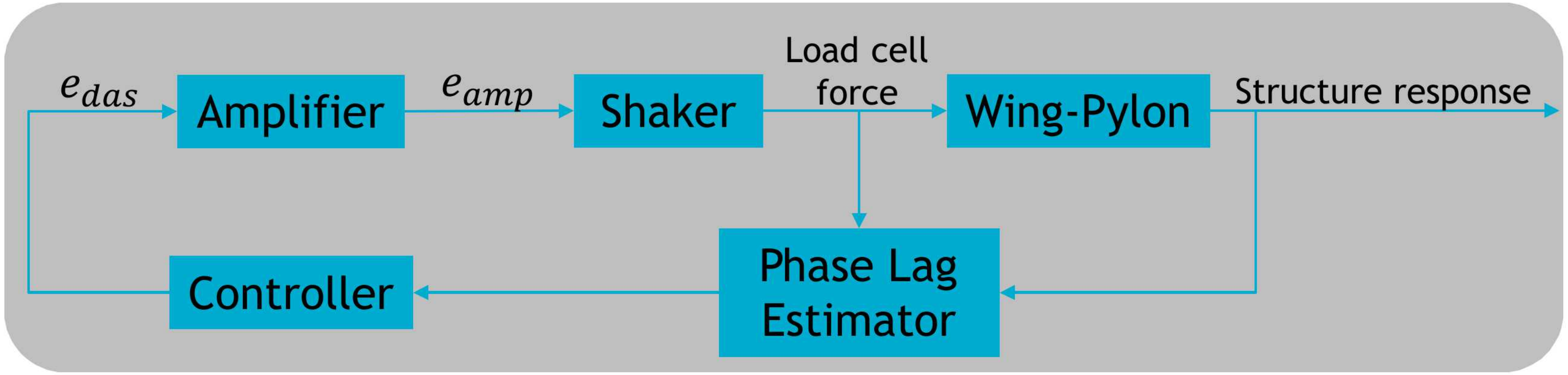

Fig. 28: Block diagram of force appropriation testing

Force Appropriation Method (cont.)

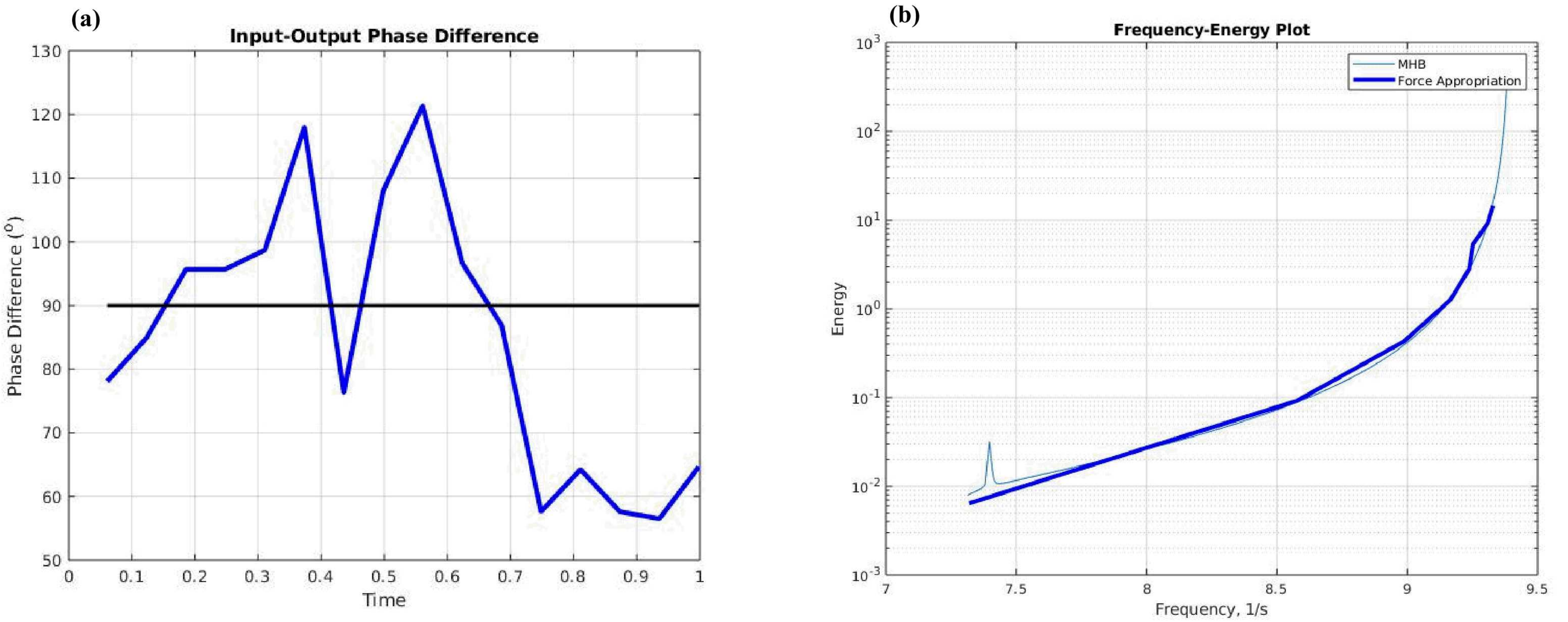

Fig. 29: NNM 1 phase lag quadrature quality (a) and FEP (b)

Further work needs to be conducted to achieve better quadrature

V. Conclusions

Results, Conclusions and Future Work

Results

- NNMs were successfully characterized using computational methods such as force appropriation and multi-harmonic balance
- Models were accurately validated against experimental data and finite element software
- It was shown that the study of NNMs can yield insights into nonlinear systems, such as the presence and behavior of internal resonances as well as the frequency-energy dependence of nonlinear modes
- To simulate a physical experiment, a calibrated shaker model was substructured to the wing-pylon model

Future Work:

- Fine-tune simulation model to accurately simulate second and higher modes
- Experimental testing of the physical wing-pylon assembly to validate NNMs and internal resonances between different combinations of modes
- Further investigations can be conducted on the effect of other system parameters such as wing length

THANK YOU

References

[1] Cooper, S.B., et al. *Investigating Nonlinearities in a Demo Aircraft Structure Under Sine Excitation*. 2020. Cham: Springer International Publishing.

[2] Ligeikis, C., et al., Modeling and Experimental Validation of a Pylon Subassembly Mockup with Multiple Nonlinearities, in 38th International Modal Analysis Conference (IMAC XXXVIII), 2020, Houston, TX.

[3] Craig, R.R.J. and M.C.C. Bampton, Coupling of Substructures for Dynamic Analysis. AIAA Journal, 1968. 6(7): p. 1313-1319.

[4] Craig, R.R.J. and A.J. Kurdila, Fundamentals of Structural Dynamics. 2nd ed. 2006, New York: John Wiley and Sons.

[5] Kerschen, G., et al., Nonlinear normal modes. Part I. A useful framework for the structural dynamicist. Mechanical Systems and Signal Processing, 2009.

[6] Haller, G., Ponsioen, S., Nonlinear normal modes and spectral submanifolds: Existence, uniqueness, and use in model reduction. Nonlinear Dynamics, 2016.

[7] T. Detroux, L. Renson, L. Masset, and G. Kerschen, "The harmonic balance method for bifurcation analysis of large-scale nonlinear mechanical systems," *Computer Methods in Applied Mechanics and Engineering*, vol. 296, pp. 18-38, 2015/11/01/ 2015, doi: https://doi.org/10.1016/j.cma.2015.07.017

Acknowledgements

This research was conducted at the 2020 Nonlinear Mechanics and Dynamics Research Institute hosted by Sandia National Laboratories and the University of New Mexico.

Sandia National Laboratories is a multimission laboratory managed and operated by National Technology and Engineering Solutions of Sandia, LLC., a wholly owned subsidiary of Honeywell International, Inc., for the U.S. Department of Energy's National Nuclear Security Administration under contract DE-NA-0003525.

X. graveyard of rejected slides

Background and Motivation

- Despite its effect on multiple aspects of structural dynamics, nonlinearity is under-considered and often neglected in industrial design and qualification
- Further development of experimental and computational identification techniques is essential to understanding nonlinear structural dynamics
- To this end, a previous Sandia research group studied an isolated pylon structure and developed a nonlinear model to replicate the experimental response [1]
  - Pylon design originated from a demo aluminum aircraft (Fig. 1) created by Seimens Industry Software [2]
- Goals included:
  - To understand how localized nonlinearities can influence the global modes of a system
  - To investigate how nonlinearity in engine pylon subassemblies could be positively exploited

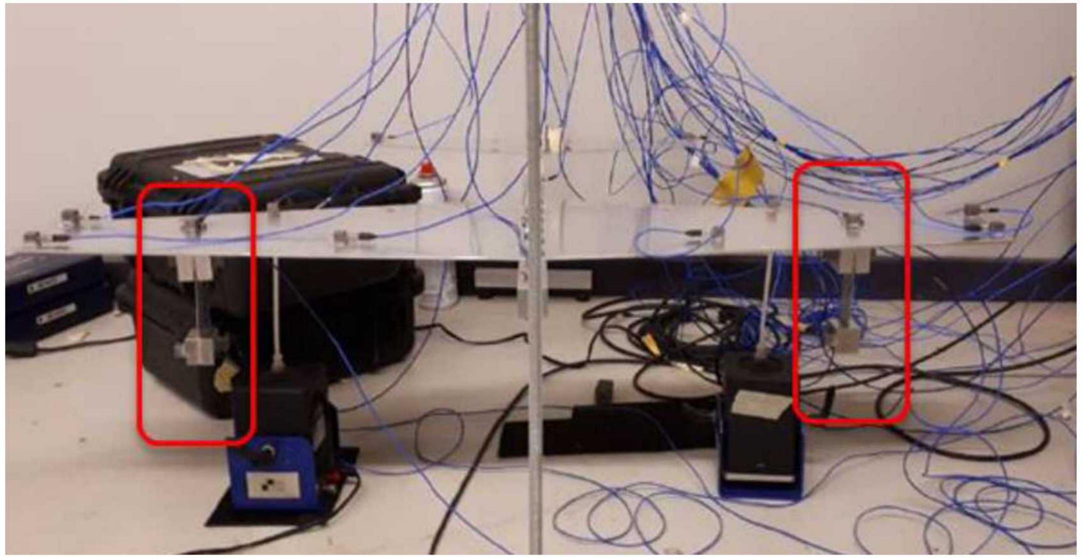

Fig. 1: Siemens demo aluminum aircraft [2]

Overview of Current Work

- NOMAD 2019 experiments were conducted on an isolated pylon mounted to a rigid fixture (Fig. 2)
- This study builds upon the previous results by:
  - Developing a nonlinear Craig-Bampton (CB) reduced order model (ROM) for the pylon-fixture assembly
  - Applying nonlinear normal mode (NNM) theory to the pylon-fixture ROM
  - Identifying pylon-fixture nonlinearity by comparison with experimental data
  - Combining pylon-fixture ROM with a linear CB ROM of the wing structure
  - Simulating nonlinear force appropriation experiments by coupling wing-pylon ROM to a calibrated electromechanical model of a shaker

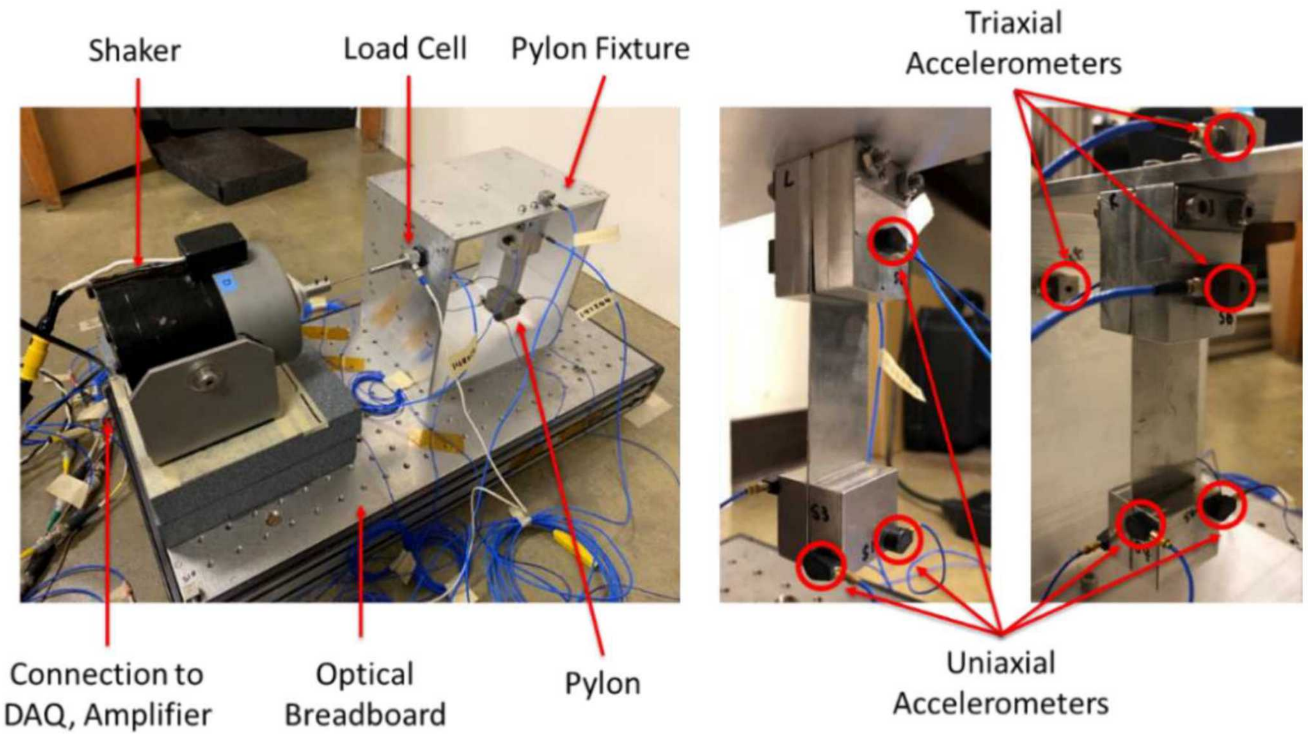

Fig. 2: Sandia isolated fixture-pylon test setup

Preliminary Data Analysis

- Previous experiments on the fixture-pylon system yielded complex sine spectra data at accelerometer locations $s1Y+$ and $s2Y$- for a series of forcing amplitudes
- To determine frequency backbones, data was separated into phase and magnitude components to locate quadrature points for each amplitude (Fig. 3)
  - Quadrature: The point where input-output phase difference = 90°. Here, damping and input forces are balanced

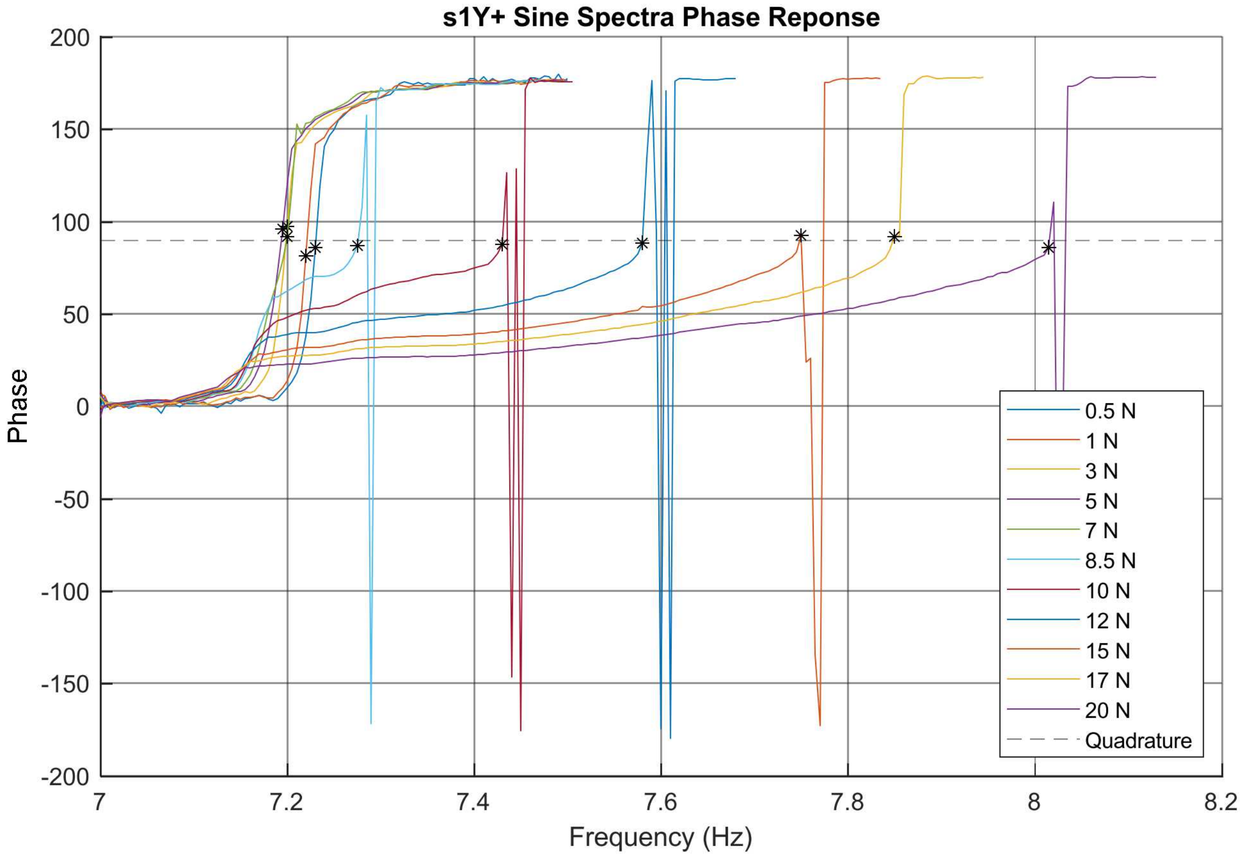

Fig. 3: Sine spectra phase response, values closest to quadrature marked

Fixture-Pylon ROM (cont.)

- Using the mass and stiffness matrices from the CB ROM, the nonlinear, undamped equations of motion with no external force were written as:

$$\boldsymbol{M}_{\boldsymbol{ROM}}\ddot{\boldsymbol{x}}_{\boldsymbol{ROM}} + \boldsymbol{K}_{\boldsymbol{ROM}}\boldsymbol{x}_{\boldsymbol{ROM}} + \boldsymbol{f}_{\boldsymbol{nl}} = \{\boldsymbol{0}\}$$

  - Where $\boldsymbol{f}_{\boldsymbol{nl}}$ is the conservative nonlinear restoring force (0 at all DOFs except virtual nodes)

- The NNMs of this model were calculated using the multi-harmonic balance (MHB) method, which represents the approximate NNM solution as a Fourier series [5]:

$$\mathbf{x}_{\boldsymbol{ROM}}(t) = \frac{\mathbf{c}_0^x}{\sqrt{2}} + \sum_{k=1}^{N_h}[\mathbf{s}_k^x \sin(k\omega t) + \mathbf{c}_k^x \cos(k\omega t)]$$

  - Where $\boldsymbol{c}_0^x, \boldsymbol{s}_k^x$, and $\boldsymbol{c}_k^x$ are Fourier coefficients

- These Fourier series were converted to a set of nonlinear algebraic equations and solved numerically to obtain a branch of predicted NNM solutions [6-7]

Calibrating ROM Nonlinearity

Two options were considered for the nonlinear elements between the pylon and pylon blocks

- Cubic spring element, dependent on interface points x_1 (pylon) and x_2 (block)
  - Force: $f_{NL}(x_1, x_2) = k_{NL}(x_2 - x_1)^3$
  - Potential energy: $PE_{NL}(x_1, x_2) = \frac{1}{4} k_{NL}(x_2 - x_1)^4$
  - Where k_{NL} was the nonlinear spring constant of the cubic spring

- Gap-spring element, dependent on interface points x_1, x_3 (pylon) and x_2, x_4 (blocks)
  - Force: $f_{gap}(x_1, x_2, x_3, x_4) = \begin{cases} k_{pen}(\delta_{12} - x_{gap})\ for\ \delta_{12} > x_{gap} \\ k_{pen}(\delta_{34} - x_{gap})\ for\ \delta_{34} > x_{gap} \\ 0\ otherwise \end{cases}$
  - Potential energy: $PE_{gap}(x_1, x_2, x_3, x_4) = \begin{cases} \frac{1}{2} k_{pen}(\delta_{12} - x_{gap})^2\ for\ \delta_{12} > x_{gap} \\ \frac{1}{2} k_{pen}(\delta_{34} - x_{gap})^2\ for\ \delta_{34} > x_{gap} \\ 0\ otherwise \end{cases}$
  - Where:
    - k_{pen} was the linear spring constant of the penalty spring
    - x_{gap} was the gap width on either side of the pylon
    - $\delta_{12} = x_1 - x_2$
    - $\delta_{34} = x_3 - x_4$.

Calibrating ROM Nonlinearity (cont.)

NNM displacement backbones at points $s1Y$ and $s2Y$ were compared to experimental data

- Gap-spring element was selected

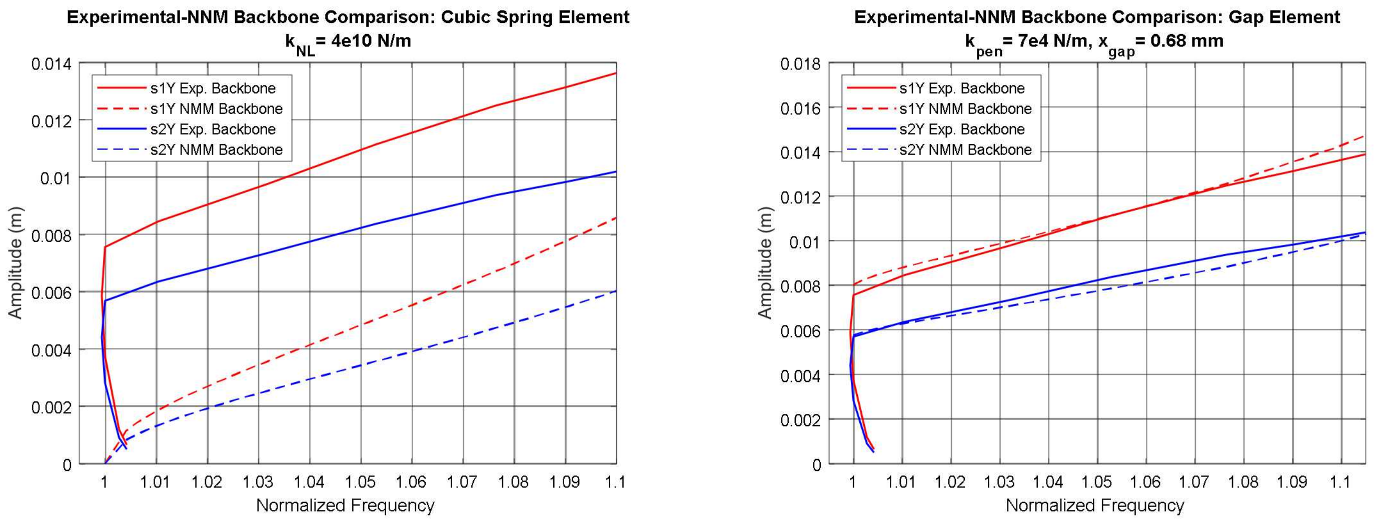

Fig. 8: Cubic/gap-spring element backbone comparison

Gap-spring element parameters k_{pen} and x_{gap} were varied to determine effects and calibrate model to experimental data

Final parameter values:

- $k_{pen} = 7 * 10^4\ N/m$
- $x_{gap} = 0.68\ mm$

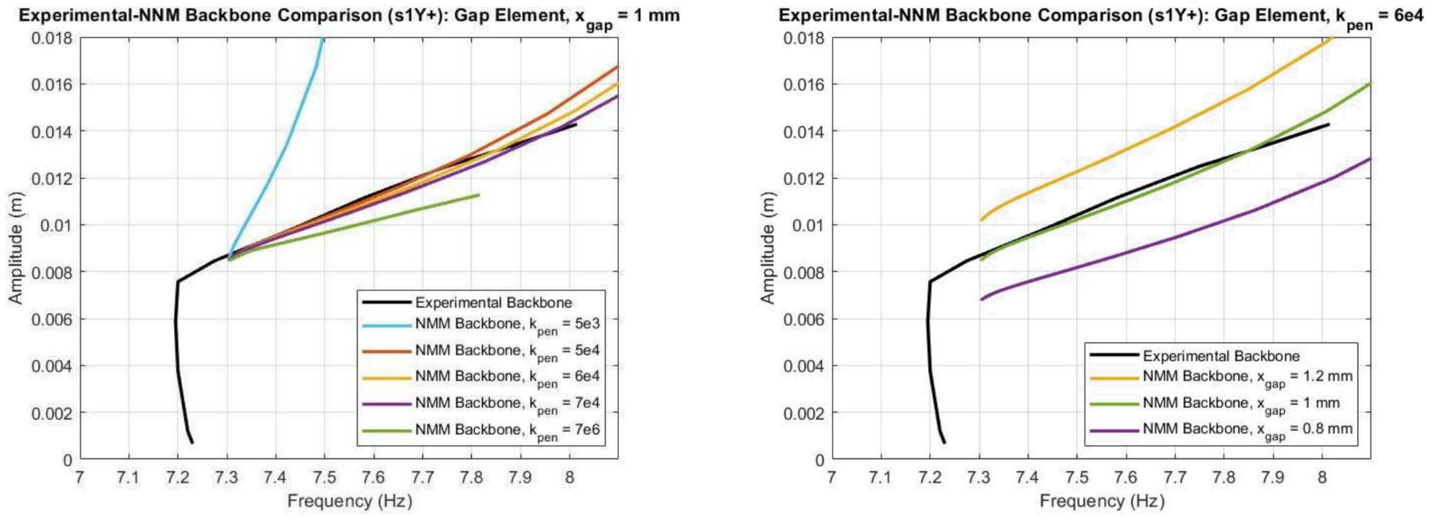

Fig. 9: Effect of gap element parameters

Adding Damping to ROM

- Rayleigh mass and stiffness proportional damping was used to obtain the damping matrix
- Different combinations of natural frequencies and damping ratios were tested in order to identify the combination that produced results closest to the experimental response
- Based on the results from preliminary stepped sine test simulations, it was determined that the properties from the combination of mode 1 and mode 3 produced the most accurate damping coefficients

Table 1: Modal Properties of Pylon-Fixture NOMAD 2019

Mode	*1*	*2*	*3*	*4*	*5*
f_{exp} (Hz)	7.25	45.79	78.07	96.30	134.75
f_{FEA} (Hz)	7.23	47.28	80.48	99.89	134.73
% difference	0.41	3.20	3.04	3.66	0.015
ζ_{exp} (%)	0.12	1.76	0.39	0.95	0.35

(a)

$$\begin{bmatrix} \xi_i \\ \xi_j \end{bmatrix} = \frac{1}{2} \begin{bmatrix} \frac{1}{\omega_i} & \omega_i \\ \frac{1}{\omega_j} & \omega_j \end{bmatrix} \begin{bmatrix} \eta \\ \delta \end{bmatrix}$$

(b)

$$C = \eta\, M + \delta\, K$$

Shaker Model

To account for the dynamics of a shaker in virtual experiments, a previously calibrated electro-mechanical model was utilized

Shaker system equations of motion:

$$BL(\dot{x}_2 - \dot{x}_1) + L_e \dot{i}_{amp} - e_{amp} + R_e i_{amp} = 0$$

$$\frac{1}{k_a}\dot{e}_{amp} + \frac{\omega_b}{k_a} e_{amp} = e_{das}$$

$$m_1\ddot{x}_1 + c_1(\dot{x}_1 - \dot{x}_2) + k_1(x_1 - x_2) + BL \cdot i_{amp} = 0$$

$$m_2\ddot{x}_2 + c_1(\dot{x}_2 - \dot{x}_1) + c_2(\dot{x}_2 - \dot{x}_3) + k_1(x_2 - x_1) + k_2(x_2 - x_3) - BL \cdot i_{amp} = 0$$

$$m_3\ddot{x}_3 + c_2(\dot{x}_3 - \dot{x}_2) + k_2(x_3 - x_2) = 0$$

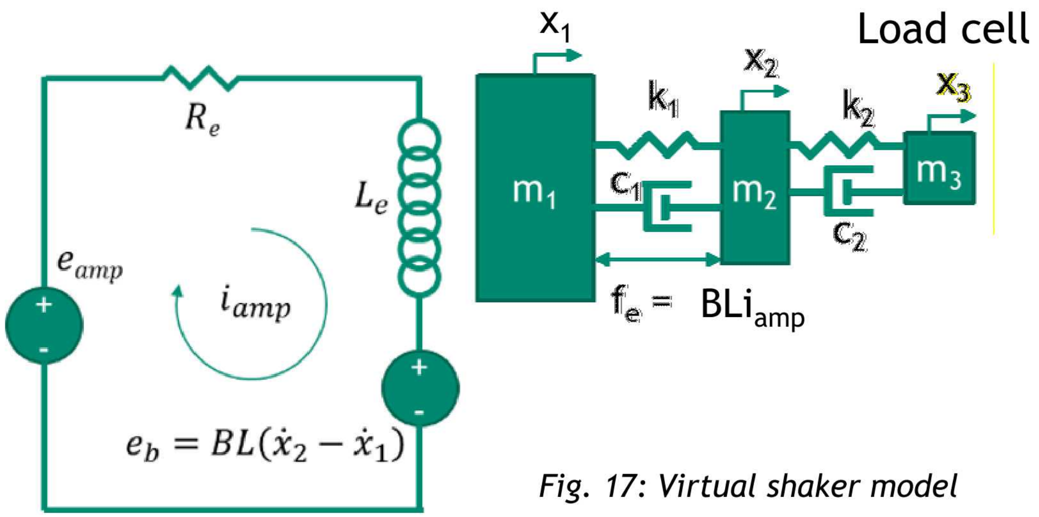

Fig. 17: Virtual shaker model

Note: e_{das} = voltage output from data acquisition system (used as the <u>only</u> input to the shaker, wing, pylon model)
e_{amp} = voltage output from amplifier

State-Space Formulation & Substructuring

Wing-pylon equations of motion:

$$\boldsymbol{M_{ROM}\ddot{x}_{ROM} + C_{ROM}\dot{x}_{ROM} + K_{ROM}x_{ROM} + f_{nl,ROM} = \{0\}}$$

State-space representation for shaker, wing, pylon model (unconstrained):

$$\mathbf{A} \cdot \dot{\boldsymbol{\gamma}} = \mathbf{B} \cdot \boldsymbol{\gamma} + \boldsymbol{f_{nl}} + \boldsymbol{C} \cdot \boldsymbol{e_{das}}$$

$$\underbrace{\begin{bmatrix} 1 & 0 & 0 & 0 & 0 & 0 & 0 & 0 & 0 & 0 \\ 0 & 1 & 0 & 0 & 0 & 0 & 0 & 0 & 0 & 0 \\ 0 & 0 & 1 & 0 & 0 & 0 & 0 & 0 & 0 & 0 \\ 0 & 0 & 0 & L_e & 0 & 0 & 0 & 0 & 0 & 0 \\ 0 & 0 & 0 & 0 & 1 & 0 & 0 & 0 & 0 & 0 \\ 0 & 0 & 0 & 0 & 0 & I_{41\times41} & 0 & 0 & 0 & 0 \\ 0 & 0 & 0 & 0 & 0 & 0 & m_1 & 0 & 0 & 0 \\ 0 & 0 & 0 & 0 & 0 & 0 & 0 & m_2 & 0 & 0 \\ 0 & 0 & 0 & 0 & 0 & 0 & 0 & 0 & m_3 & 0 \\ 0 & 0 & 0 & 0 & 0 & 0 & 0 & 0 & 0 & M_{ROM} \end{bmatrix}_{90\times90}}_{A} \cdot \underbrace{\begin{Bmatrix} \dot{x}_1 \\ \dot{x}_2 \\ \dot{x}_3 \\ \dot{i}_{amp} \\ \dot{e}_{amp} \\ \dot{x}_{ROM} \\ \ddot{x}_1 \\ \ddot{x}_2 \\ \ddot{x}_3 \\ \ddot{x}_{ROM} \end{Bmatrix}_{90\times1}}_{\dot{\gamma}} =$$

Continued on next slide

State-Space Formulation & Substructuring (cont.)

$$
= \underbrace{\begin{bmatrix}
0 & 0 & 0 & 0 & 0 & 0 & 1 & 0 & 0 & 0 \\
0 & 0 & 0 & 0 & 0 & 0 & 0 & 1 & 0 & 0 \\
0 & 0 & 0 & 0 & 0 & 0 & 0 & 0 & 1 & 0 \\
0 & 0 & 0 & -R_e & 1 & 0 & BL & -BL & 0 & 0 \\
0 & 0 & 0 & 0 & -\omega_b & 0 & 0 & 0 & 0 & 0 \\
0 & 0 & 0 & 0 & 0 & 0 & 0 & 0 & 0 & I_{41\times41} \\
-k_1 & k_1 & 0 & -BL & 0 & 0 & -c_1 & c_1 & 0 & 0 \\
k_1 & -(k_1+k_2) & k_2 & BL & 0 & 0 & c_1 & -(c_1+c_2) & c_2 & 0 \\
0 & k_2 & -k_2 & 0 & 0 & 0 & 0 & c_2 & -c_2 & 0 \\
0 & 0 & 0 & 0 & 0 & -K_{ROM} & 0 & 0 & 0 & -C_{ROM}
\end{bmatrix}_{90\times90}}_{B} \cdot \underbrace{\begin{Bmatrix} x_1 \\ x_2 \\ x_3 \\ i_{amp} \\ e_{amp} \\ x_{ROM} \\ \dot{x}_1 \\ \dot{x}_2 \\ \dot{x}_3 \\ \dot{x}_{ROM} \end{Bmatrix}_{90\times1}}_{\gamma}
$$

$$
+ \underbrace{\begin{Bmatrix} 0_{49\times1} \\ -f_{nl,ROM} \end{Bmatrix}_{90\times1}}_{f_{nl}} + \underbrace{\begin{Bmatrix} 0_{4\times1} \\ k_a \\ 0_{85\times1} \end{Bmatrix}_{90\times1}}_{C} \cdot e_{das}
$$

State-Space Formulation & Substructuring (cont.)

Now we need to substructure the shaker to the wing-pylon. To attach the load cell (x_3) to drive point 5 (d5):

$$\gamma = \begin{Bmatrix} x_1 \\ x_2 \\ x_3 \\ i_{amp} \\ e_{amp} \\ q1_{fi} \\ \vdots \\ d1 \\ d3 \\ d2 \\ d4 \\ d5 \\ \dot{x}_1 \\ \dot{x}_2 \\ \dot{x}_3 \\ \dot{q}1_{fi} \\ \vdots \\ \dot{d}1 \\ \dot{d}3 \\ \dot{d}2 \\ \dot{d}4 \\ \dot{d}5 \end{Bmatrix}_{90\times 1} = \underbrace{\begin{bmatrix} 1 & 0 & 0 & 0 & \cdots & 0 & 0 & 0 & 0 & 0 & \cdots & 0 & 0 \\ 0 & 1 & 0 & 0 & \cdots & 0 & 0 & 0 & 0 & 0 & \cdots & 0 & 0 \\ 0 & 0 & 0 & 0 & \cdots & 1 & 0 & 0 & 0 & 0 & \cdots & 0 & 0 \\ 0 & 0 & 1 & 0 & \cdots & 0 & 0 & 0 & 0 & 0 & \cdots & 0 & 0 \\ 0 & 0 & 0 & 1 & \cdots & 0 & 0 & 0 & 0 & 0 & \cdots & 0 & 0 \\ \vdots & \vdots & \vdots & \vdots & \ddots & \vdots & \vdots & \vdots & \vdots & \vdots & \vdots & \vdots & \vdots \\ 0 & 0 & 0 & 0 & \cdots & 1 & 0 & 0 & 0 & 0 & \cdots & 0 & 0 \\ 0 & 0 & 0 & 0 & \cdots & 0 & 1 & 0 & 0 & 0 & \cdots & 0 & 0 \\ 0 & 0 & 0 & 0 & \cdots & 0 & 0 & 1 & 0 & 0 & \cdots & 0 & 0 \\ 0 & 0 & 0 & 0 & \cdots & 0 & 0 & 0 & 0 & 0 & \cdots & 0 & 1 \\ 0 & 0 & 0 & 0 & \cdots & 0 & 0 & 0 & 1 & 0 & \cdots & 0 & 0 \\ 0 & 0 & 0 & 0 & \cdots & 0 & 0 & 0 & 0 & 1 & \cdots & 0 & 0 \\ \vdots & \vdots & \vdots & \vdots & \vdots & \vdots & \vdots & \vdots & \vdots & \vdots & \ddots & \vdots & \vdots \\ 0 & 0 & 0 & 0 & \cdots & 0 & 0 & 0 & 0 & 0 & \cdots & 1 & 0 \\ 0 & 0 & 0 & 0 & \cdots & 0 & 0 & 0 & 0 & 0 & \cdots & 0 & 1 \end{bmatrix}_{90\times 88}}_{T} \cdot \underbrace{\begin{Bmatrix} x_1 \\ x_2 \\ i_{amp} \\ e_{amp} \\ q1_{fi} \\ \vdots \\ d1 \\ d3 \\ d2 \\ d4 \\ d5 \\ \dot{x}_1 \\ \dot{x}_2 \\ \dot{q}1_{fi} \\ \vdots \\ \dot{d}1 \\ \dot{d}3 \\ \dot{d}2 \\ \dot{d}4 \\ \dot{d}5 \end{Bmatrix}_{88\times 1}}_{z} = [T]\cdot\{z\}$$

Load cell (x_3, $\dot{x}_3$)

Drive point ($d5$, $\dot{d}5$)

State-Space Formulation & Substructuring (cont.)

Using the substructuring transformation matrix, T, constrain the EOMs in state-space:

Substitute $\gamma = T \cdot z$ and pre-multiply both sides by T^T

$$\mathrm{A} \cdot \dot{\gamma} = \mathrm{B} \cdot \gamma + f_{nl} + C \cdot e_{das}$$

$$T^T \mathrm{A} T \dot{z} = T^T \mathrm{B} T \mathrm{z} + T^T f_{nl} + T^T C e_{das}$$

Isolate $\dot{z}$

$$\dot{z} = \underbrace{(T^T A T)^{-1} T^T B T}_{A_z} z + \underbrace{(T^T A T)^{-1} T^T}_{B_{nl}} f_{nl} + \underbrace{(T^T A T)^{-1} T^T C}_{B_z} e_{das}$$

★ $\dot{\boldsymbol{z}} = \boldsymbol{A_z} z + \boldsymbol{B_{nl}} \boldsymbol{f_{nl}} + \boldsymbol{B_z} \boldsymbol{e_{das}}$ (constrained state-space representation)

State-Space Model Validation

A linear version of the constrained state-space model was verified against the full wing-pylon model in Sierra through comparing their frequency-response functions (FRFs)

In the frequency domain, the vector of transfer functions $\boldsymbol{H_{ez}}$ between input voltage e_{das} and output displacements $\boldsymbol{z}$ was defined as:

- $\boldsymbol{H_{ez}} = (i\omega \boldsymbol{I} - \boldsymbol{A_z})^{-1}\boldsymbol{C}$
- Where $\boldsymbol{C}$ was a column vector with the only non-zero entry corresponding to the input, in this case e_{das}

The transfer function vector H_{ef} between input voltage e_{das} and load cell force f_{lc} was defined as:

- $H_{ef} = k_2\left(H_{ez,x_2} - H_{ez,x_{dp}}\right) + c_2(H_{ez,\dot{x}_2} - H_{ez,\dot{x}_{dp}})$
- Where $H_{ez,i}$ = the element of $\boldsymbol{H_{ez}}$ corresponding to DOF i

Thus, the final transfer function H_{zf} between load cell force f_{lc} and selected output displacement z_s was:

- $H_{zf} = \frac{H_{ez,z_s}}{H_{ef}}$

H_{zf} was computed over a range of frequencies and compared to the Sierra-generated FRF

State-Space Model Validation (cont.)

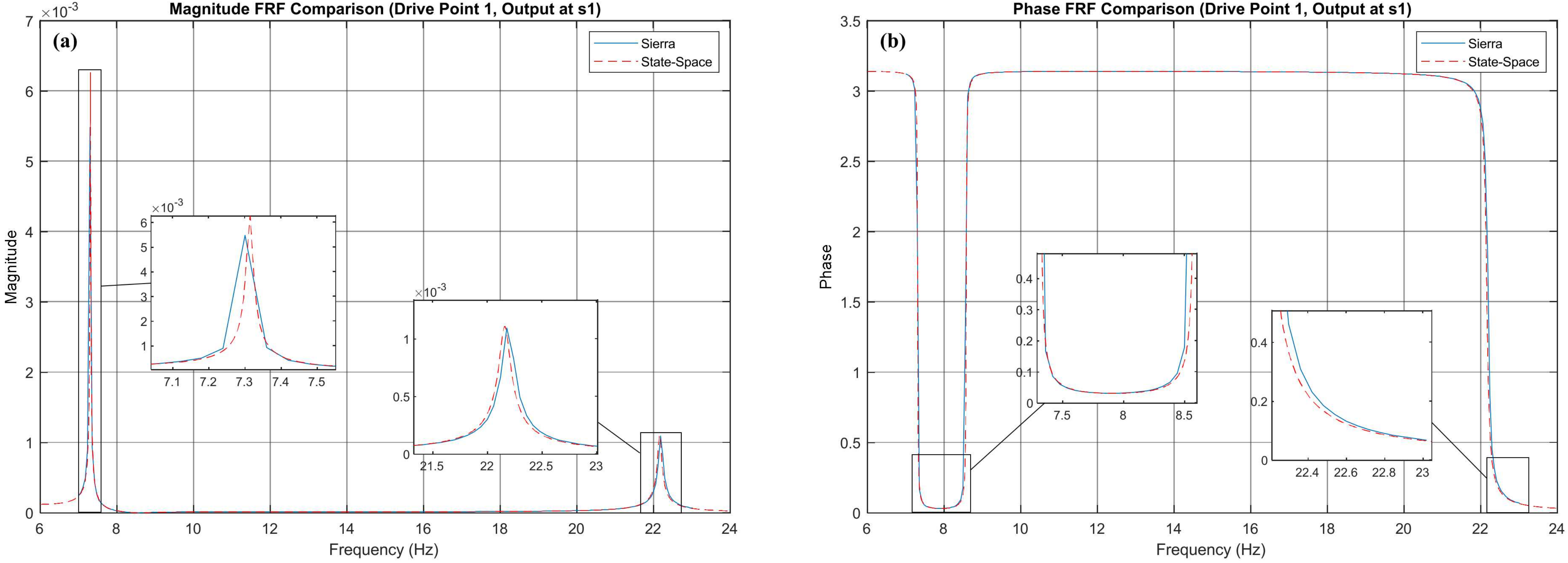

Fig. 18: Magnitude (a) and phase (b) FRF comparison between Sierra and constrained state-space model

Multi-Harmonic Balance Method (cont.)

- NNM 2 spanned through a very low frequency range which resided extremely close to the linear modal frequency
- This can easily be overlooked if only a linear analysis is considered thus reinforcing the significance of nonlinear analyses
- A 1:5 internal resonance was identified between NNM 2 and 7 on the wing-pylon ROM which can easily be seen in the displacement number of harmonics in the plot (c)

NNM 2 remained very close to its linear mode. Additionally, a 1:5 internal resonance was identified

Neural Network Informed Uncertainty Quantification for Structural Dynamics Reduced Order Models

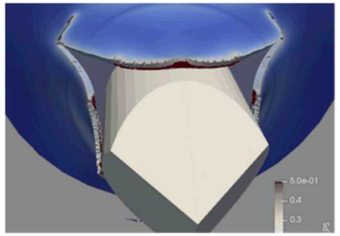

Students:

Ziad Ghanem[1], S. Macrae Montgomery[2], Walker Powell[3]

Mentors:

Adam Brink[4], Eleni Chatzi[5], Carianne Martinez[4], Dane Quinn[6]

[1] University of Texas at Dallas
[2] Woodruff School of Mechanical Engineering, Georgia Institute of Technology
[3] North Carolina State University
[4] Sandia National Laboratories
[5] ETH Zürich
[6] The University of Akron

Outline

- Goals
- Problem Description
  - Physical Problem
  - Reduced-Order Model
- Network Architectures
  - Long-Short Term Memory (LSTM)
  - Deep Koopman Network
- Results
- Conclusions
- Future Work
- References

Goals

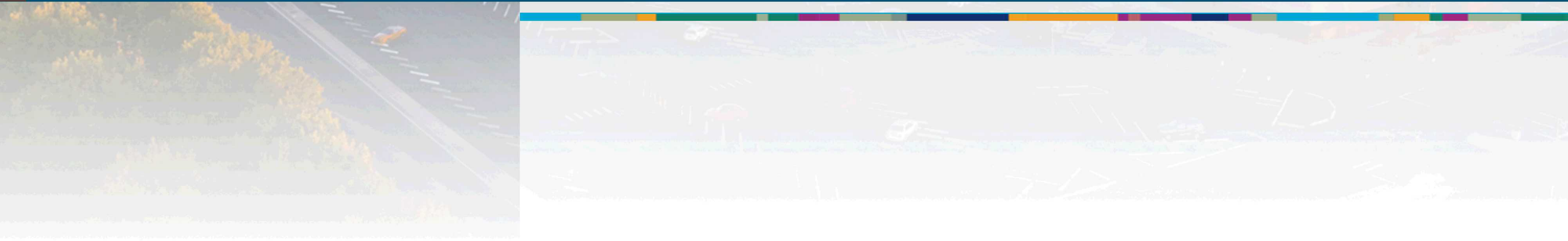

Goals

- Use neural networks to augment reduced-order models (ROMs) for improved prediction
- Learn error behavior to allow for future-time error prediction, either deterministic or statistical
- Use real-time ROM augmentation to more accurately simulate and predict extreme events in physical systems

Problem Description

Physical Problem

- Euler-Bernoulli beam ($L = 1\text{m}$)
- Harmonic forcing at $x = 0.75\text{m}$
- Initial displacement prescribed at $x = 0.5\text{m}$
- 10 equidistant 'sensor' locations
- 4 datasets were generated varying initial conditions and spring constants

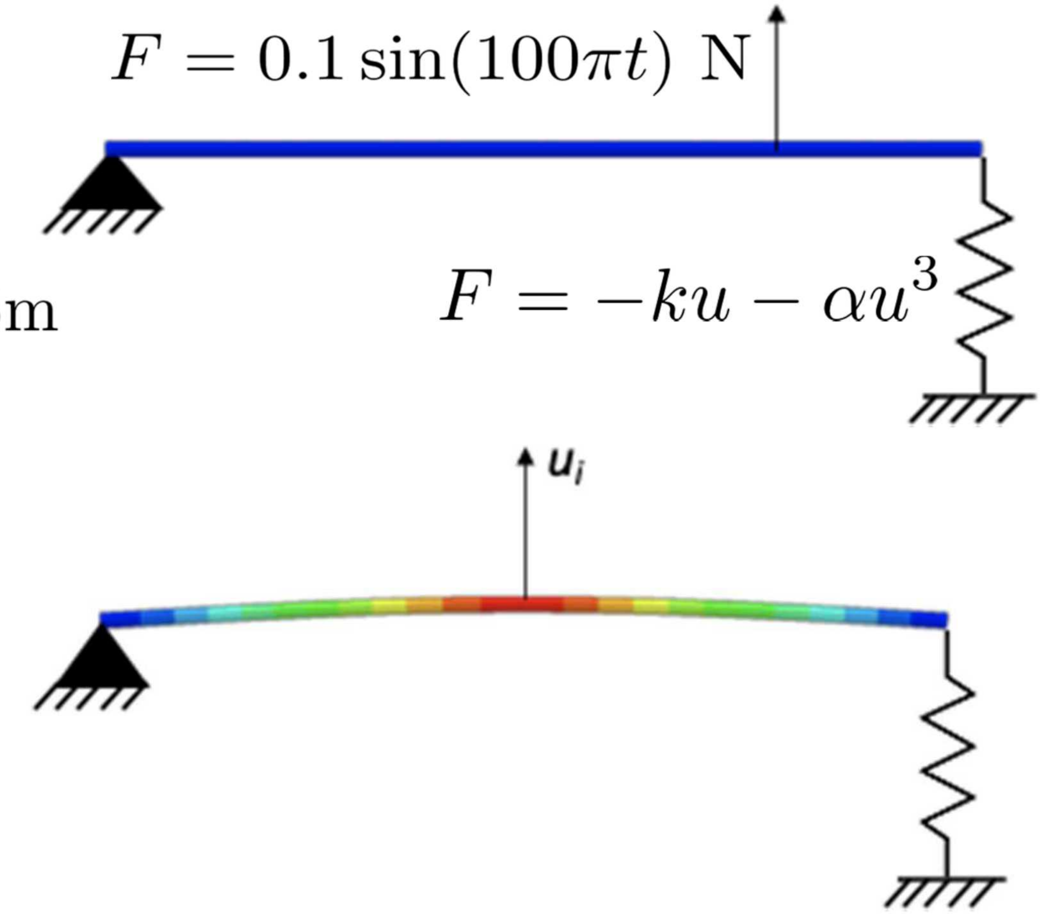

Reduced Order Model

- Galerkin projection onto low-rank basis
- POD basis generated from simulations with varying parameters and initial conditions
- 10 modes retained for each ROM basis
- Fast integration using implicit Runge-Kutta m≈ 0.5ss (each)

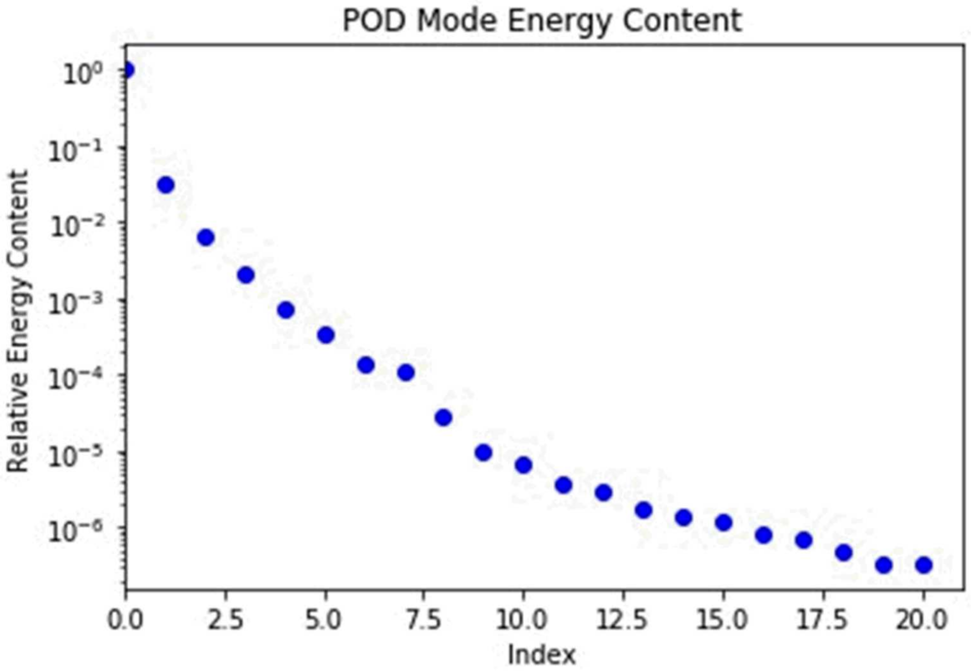

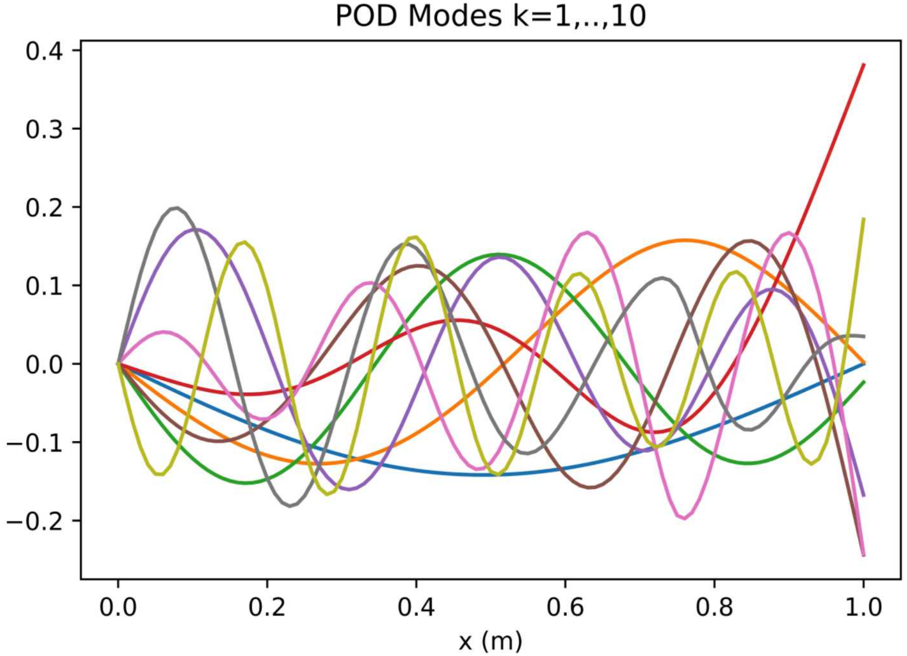

ROM Errors

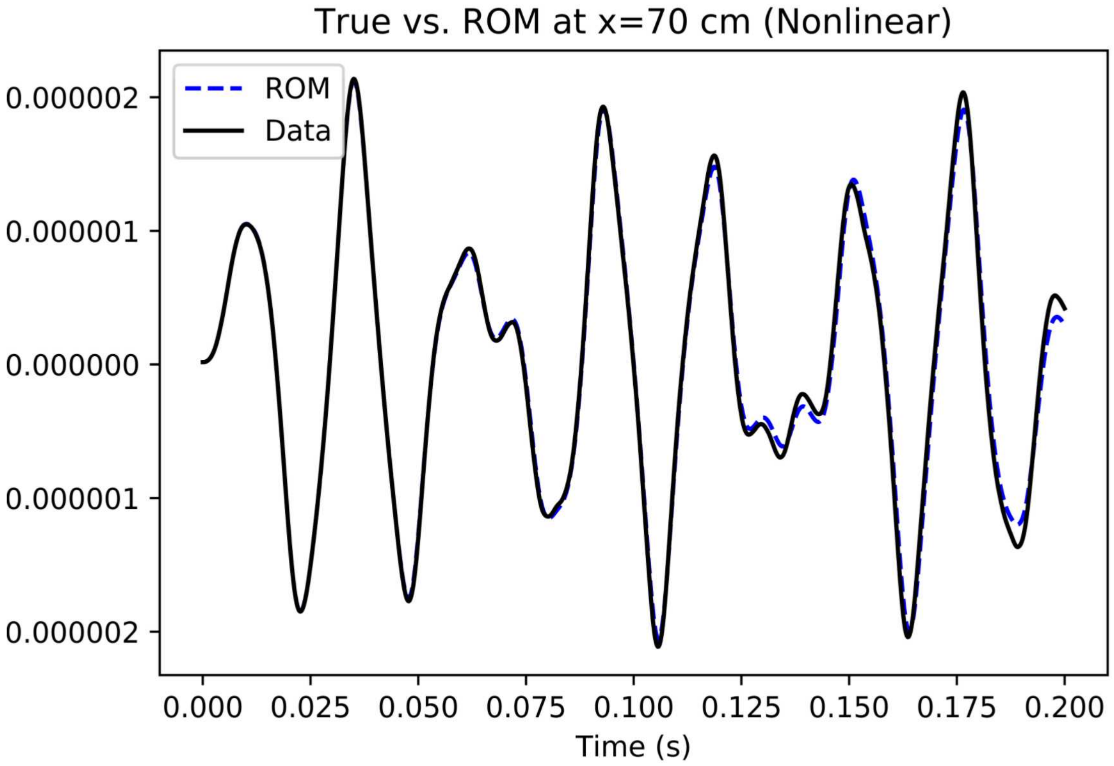

True vs. ROM at x=70 cm (Nonlinear)
ROM
Data
0.000002
0.000001
0.000000
0.000001
0.000002
0.000
0.025
0.050
0.075
0.100
0.125
0.150
0.175
0.200
Time (s)

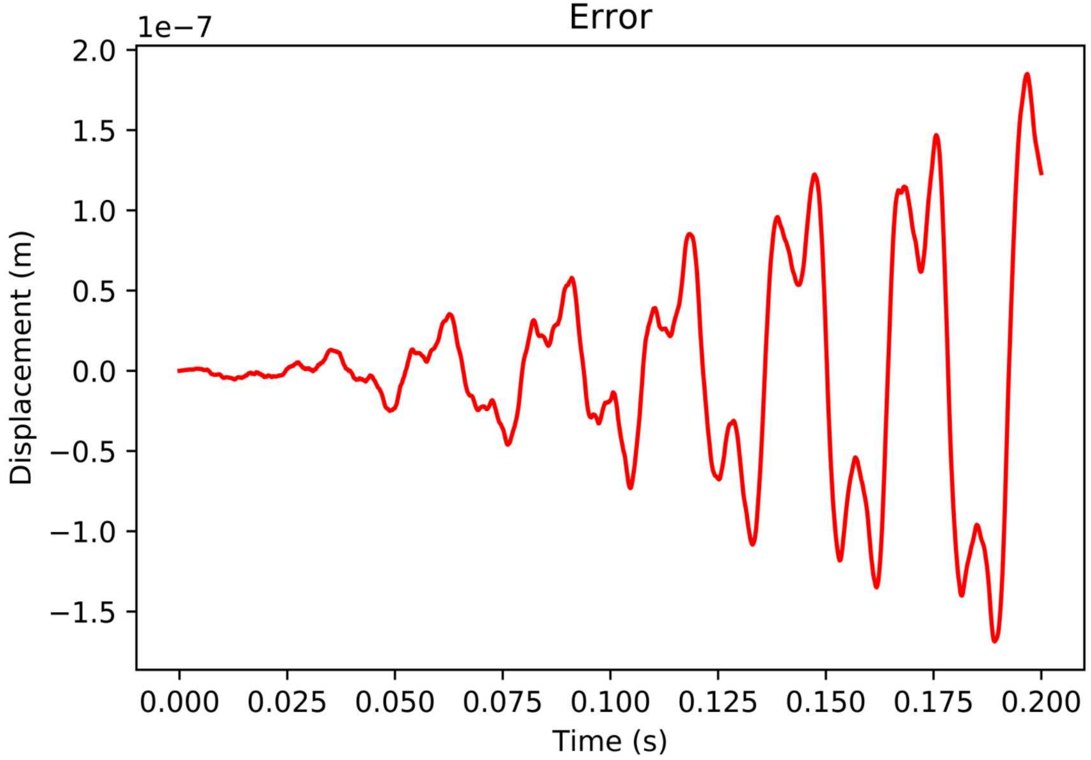

Error
1e−7
2.0
1.5
1.0
0.5
0.0
−0.5
−1.0
−1.5
Displacement (m)
0.000
0.025
0.050
0.075
0.100
0.125
0.150
0.175
0.200
Time (s)

Dynamic Prediction Framework

Instead of learning the map $t \mapsto x(t)$,
learn the map $x(t_n) \to x(t_{n+1})$.

- Often better posed for long time extrapolation
- Easier to characterize growth/decay/oscillations

We use this framework to learn the dynamics of the ROM error

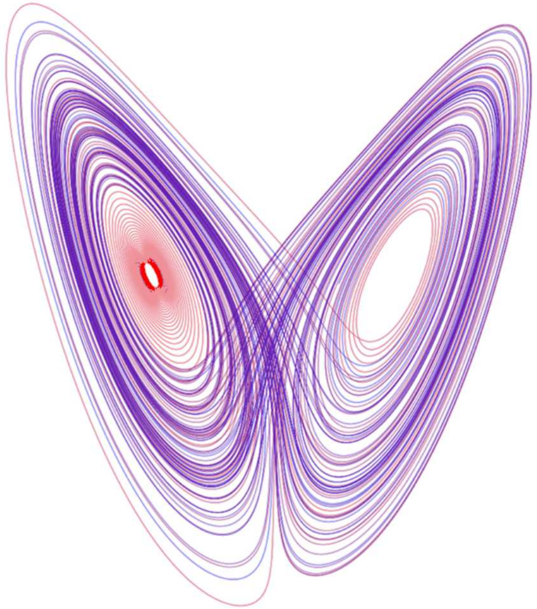

Complex

vs

$$x' = \sigma(y - x)$$
$$y' = x(\rho - z) - y$$
$$z' = xy - \beta z$$

Simple

Network Architectures

Recurrent Neural Nets (RNNs) & Long-Short Term Memory (LSTM)

- RNNs with modified structure which enable them to learn long term dependencies.
- Natural architecture for parsing sequenced inputs or outputs (or both).
- LSTMs exhibit state-dependent context; i.e., they can look back in time a variable number of steps

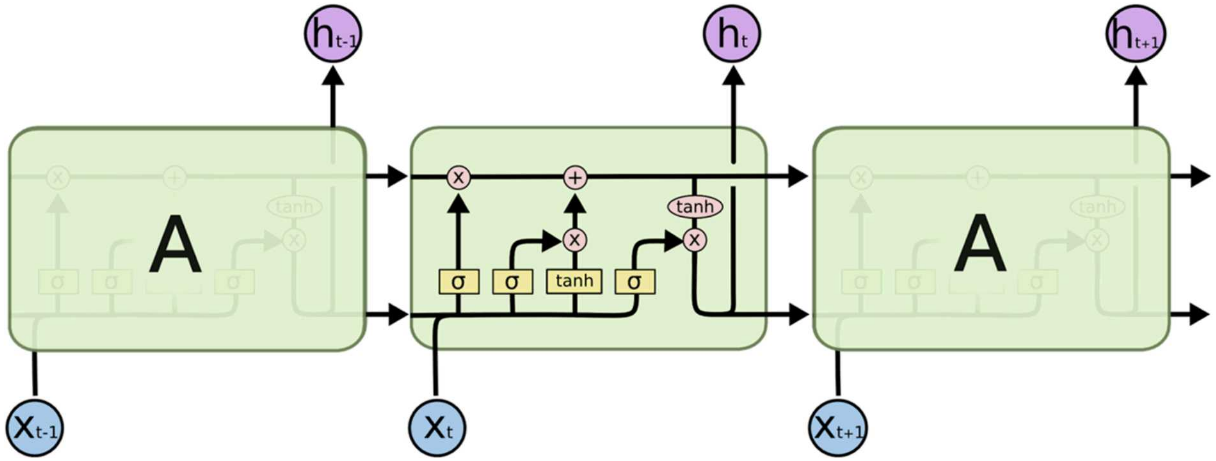

The Koopman Operator

Dynamical system

$$x(t_{n+1}) = f(x(t_n))$$

Koopman Operator

$$K\varphi(x(t_n)) = \varphi(x(t_{n+1}))$$

$$x(t_{n+1}) = \varphi^{-1}(K\varphi(x(t_n)))$$

Koopman Eigenfunctions

$$K\varphi_\lambda(\cdot) = \lambda\varphi_\lambda(\cdot)$$

$$x(t_{n+1}) = \varphi_\lambda^{-1}(\lambda\varphi_\lambda(x(t_n)))$$

Estimating the Koopman operator generates **linear** dynamics in right coordinates, even for nonlinear systems

Koopman eigenfunctions are an efficient choice of embedding, and have physical significance (Mezić 2016)

Deep Koopman Network

- Developed by Lusch et al. to learn Koopman eigenfunctions and use them for predictions
- Full version includes auxiliary network to account for nonlinear adjustments to Koopman eigenvalues corresponding to continuous spectra

Linear Predictive Autoencoder

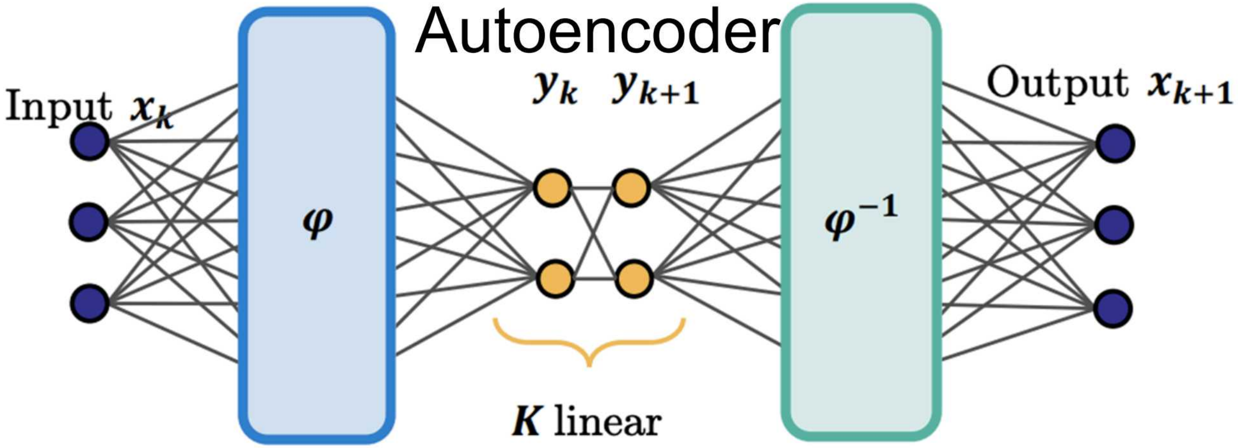

Deep Koopman Network

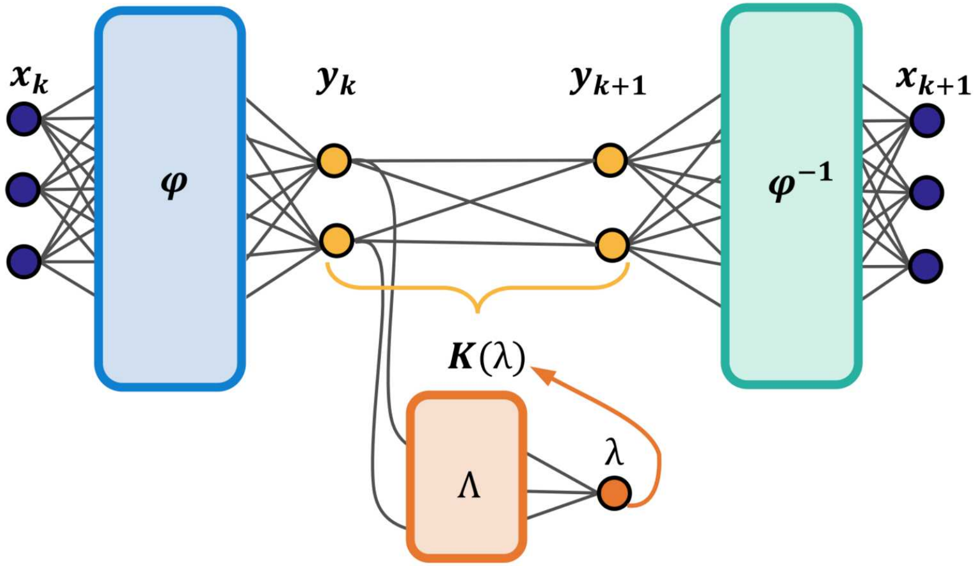

Images from Lusch et

Modified Deep Koopman Network

Our problem is more complex than those considered in Lusch et al.:

- Time dependent forcing (non-autonomous dynamics)
- Varying physical parameters (k, α)
- Unknown dynamics, requiring *a priori* estimation of parts of network architecture

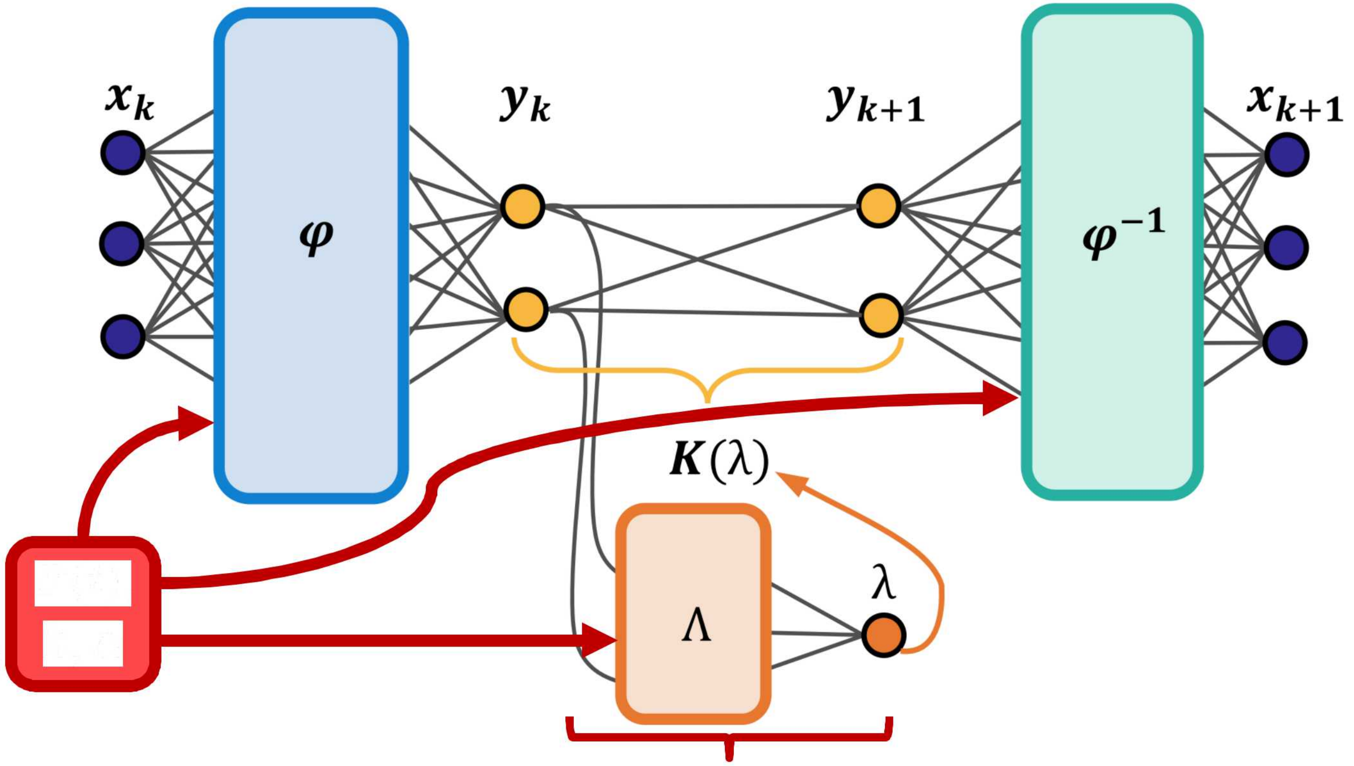

Architecture estimated *a priori*

Results

LSTM Training

- Predicts error time series given ROM displacement time series
- Very fast training (~2s per epoch)
- Completely agnostic to parameter and forcing dependence

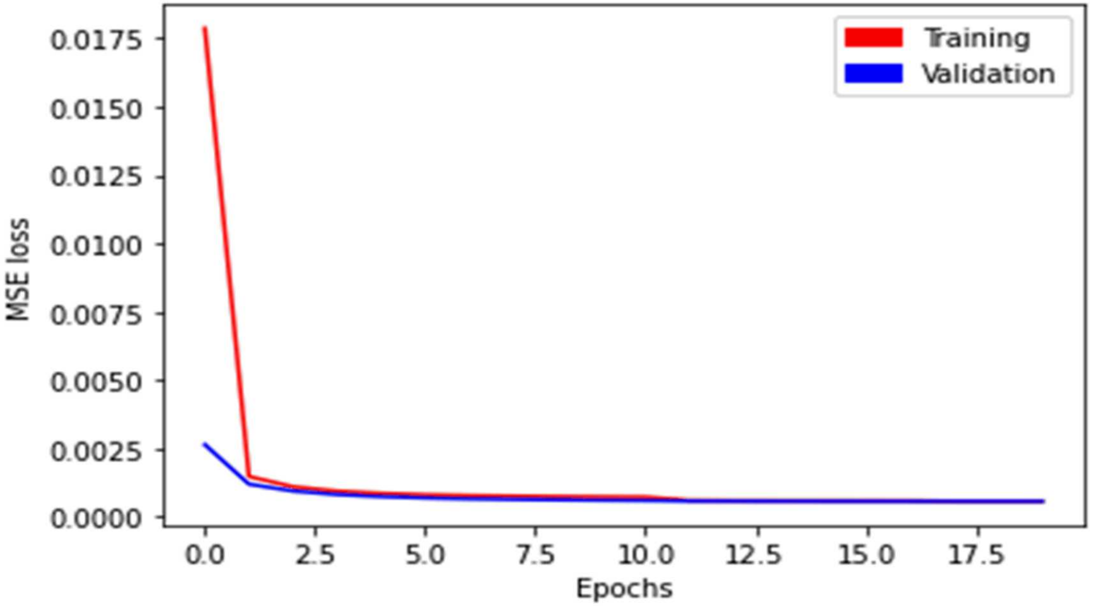

1 Epoch of Training

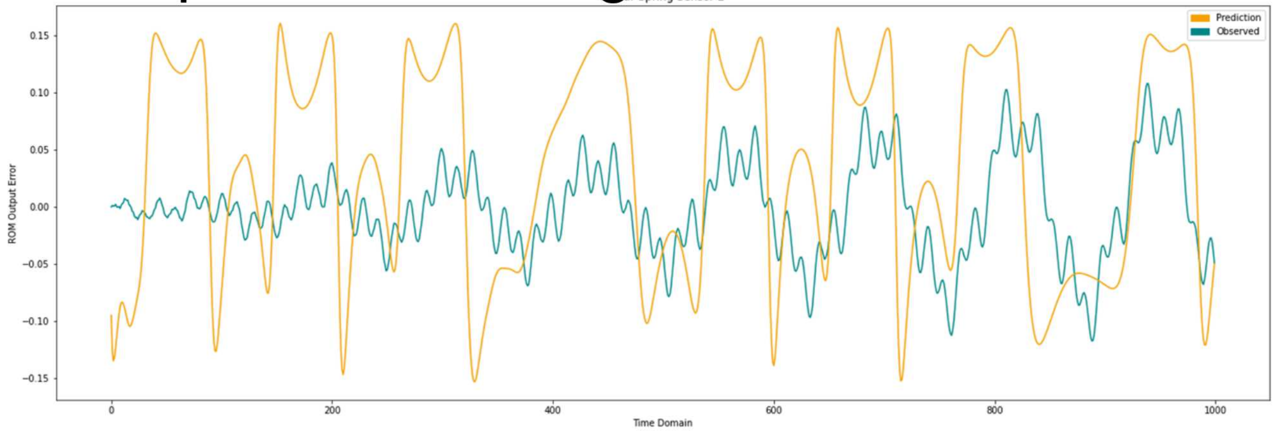

5 Epochs of Training

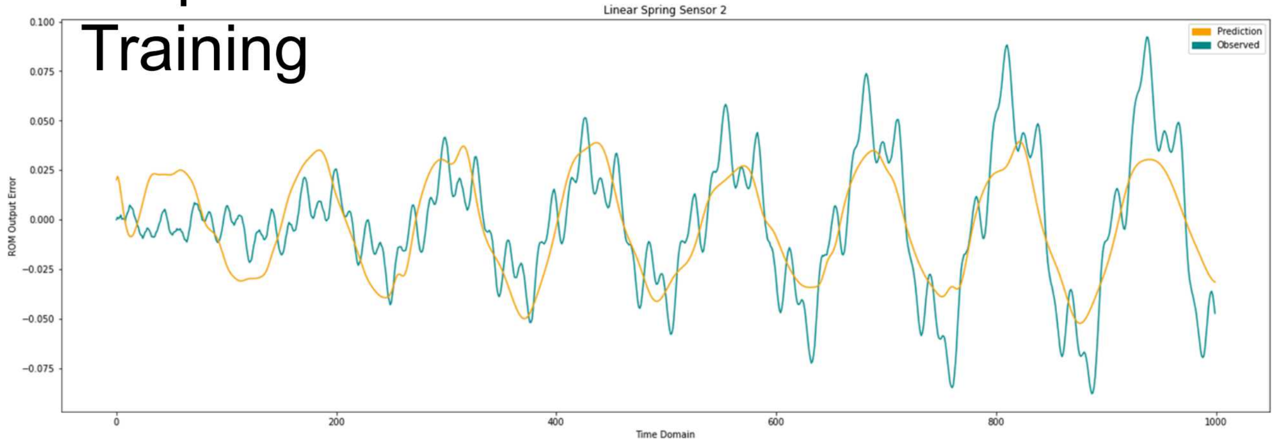

LSTM Results: Linear Spring

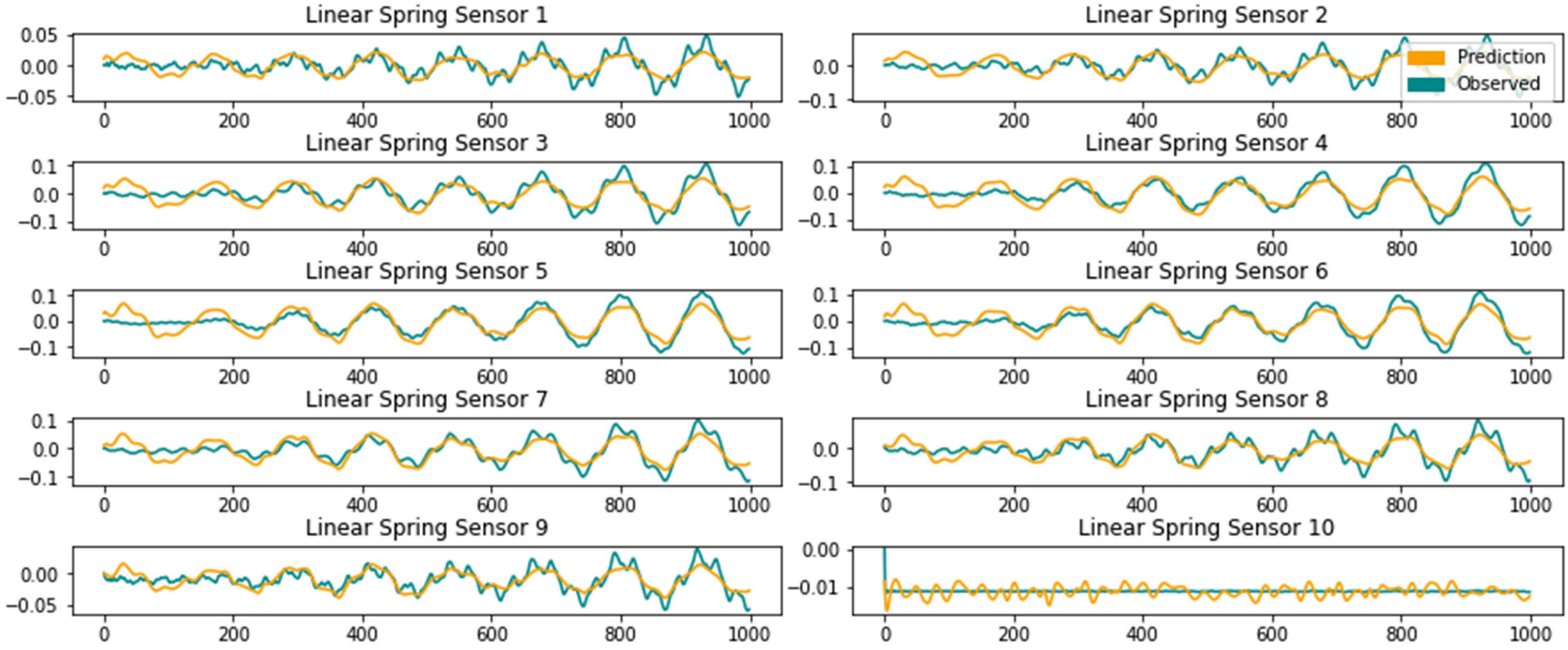

LSTM Results: Linear Spring; Varying k

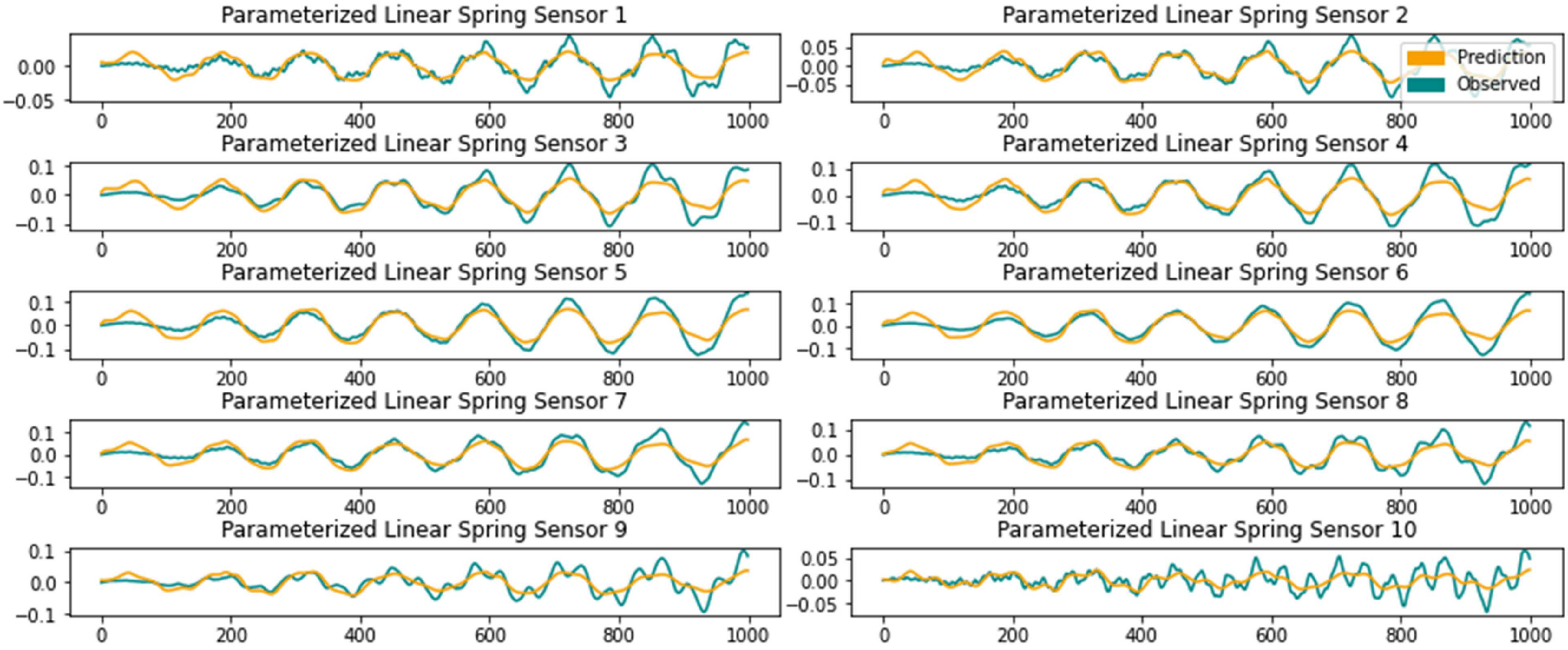

LSTM Results: Nonlinear Spring

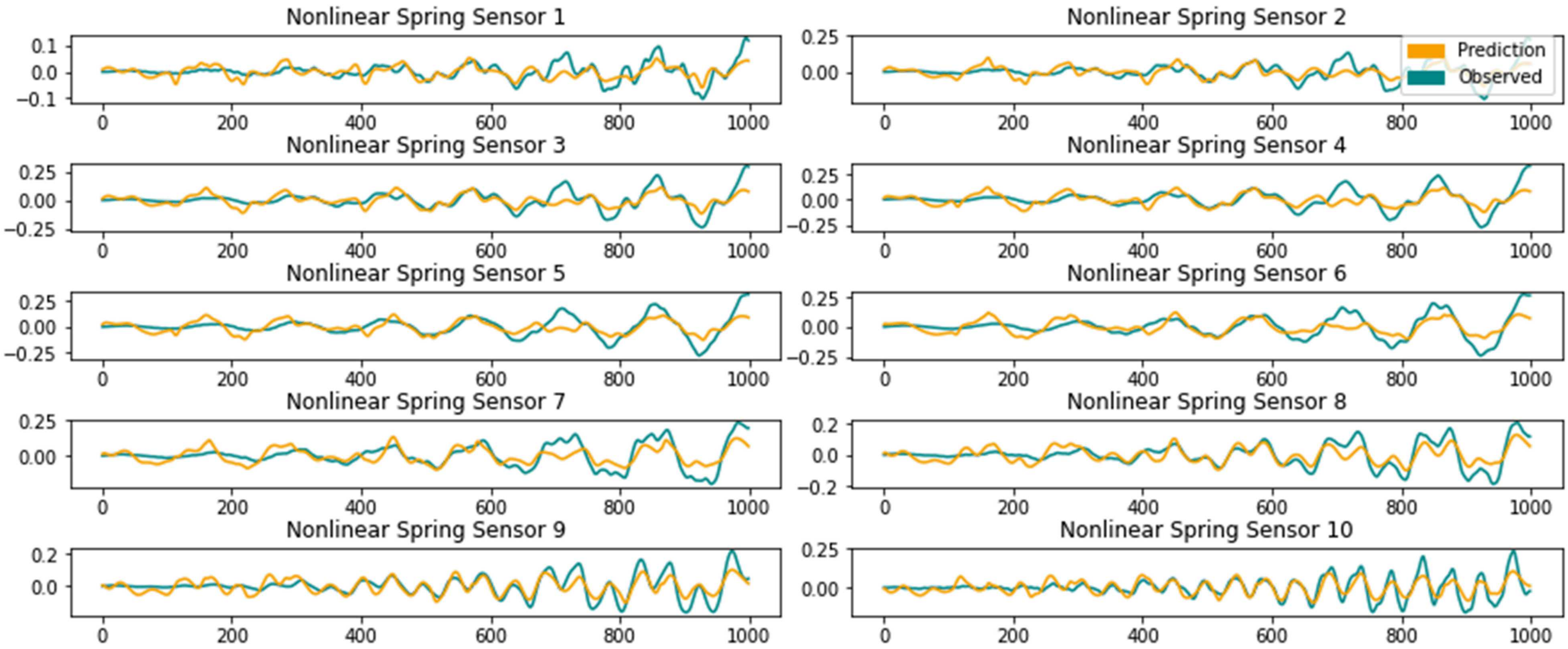

LSTM Results: Nonlinear Spring; Varying α

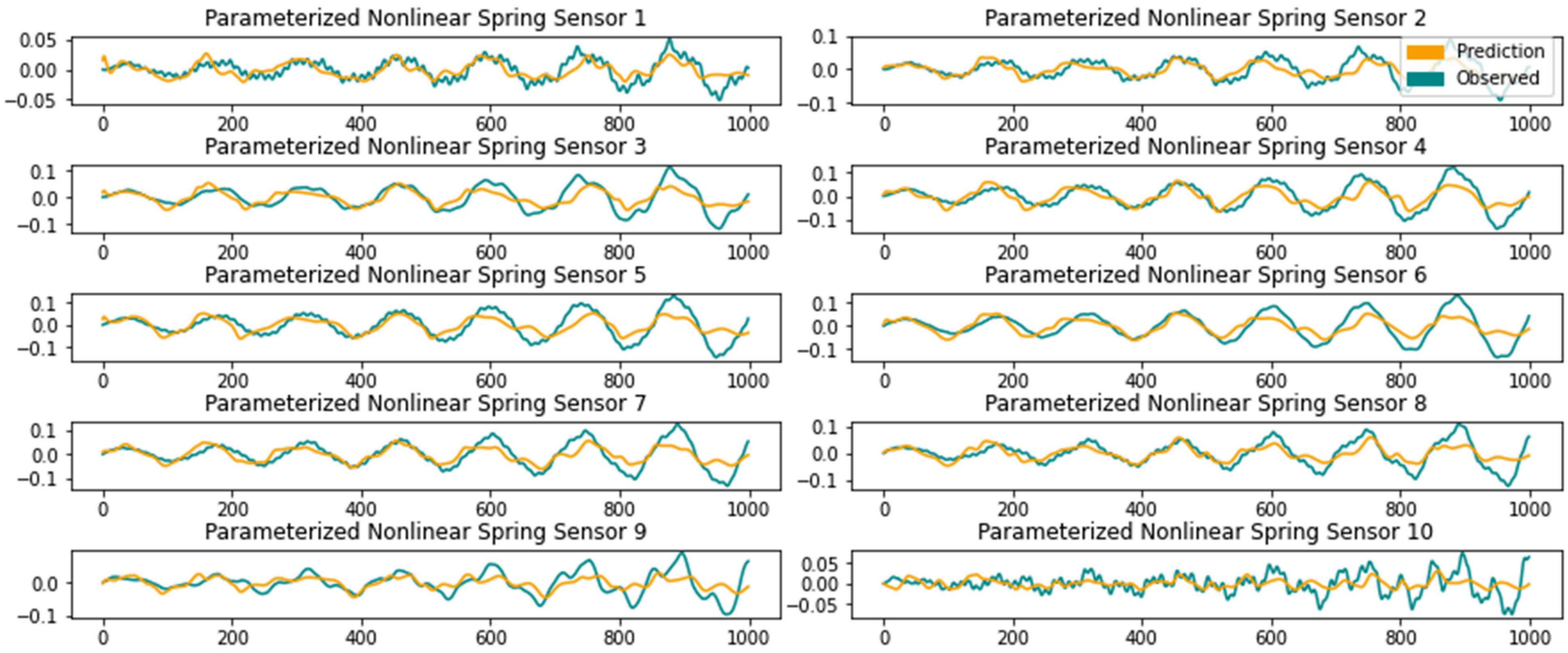

Koopman Results

- Preliminary training on smooth sinusoidal time series
- Downsampling required to increase training speed
- Extensive hyperparameter tuning required to train effectively
- Numerical stability issues

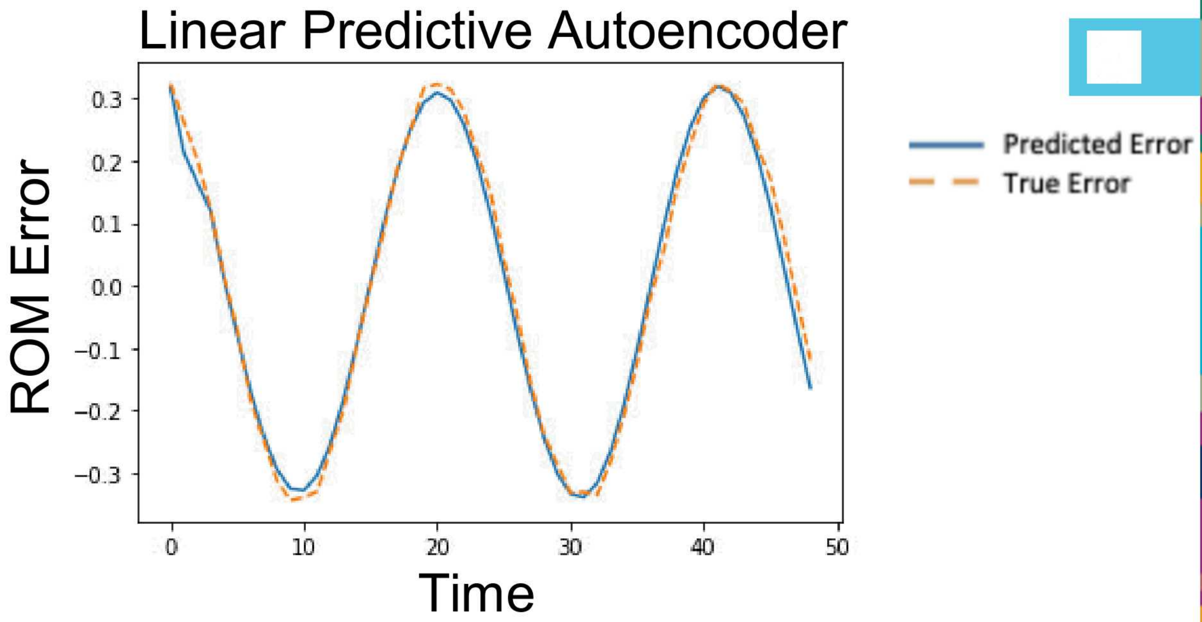

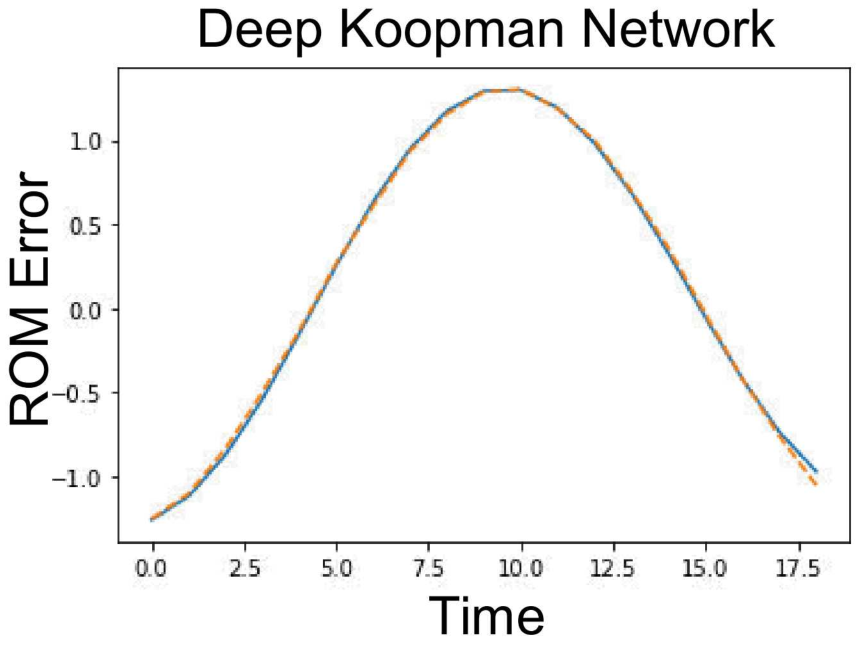

Koopman Results cont'd

- The network struggles to learn true ROM error
- Sequential network means we can't take advantage of parallelism
- All errors start near zero, so the model has trouble reconstructing unique trajectories from each IC

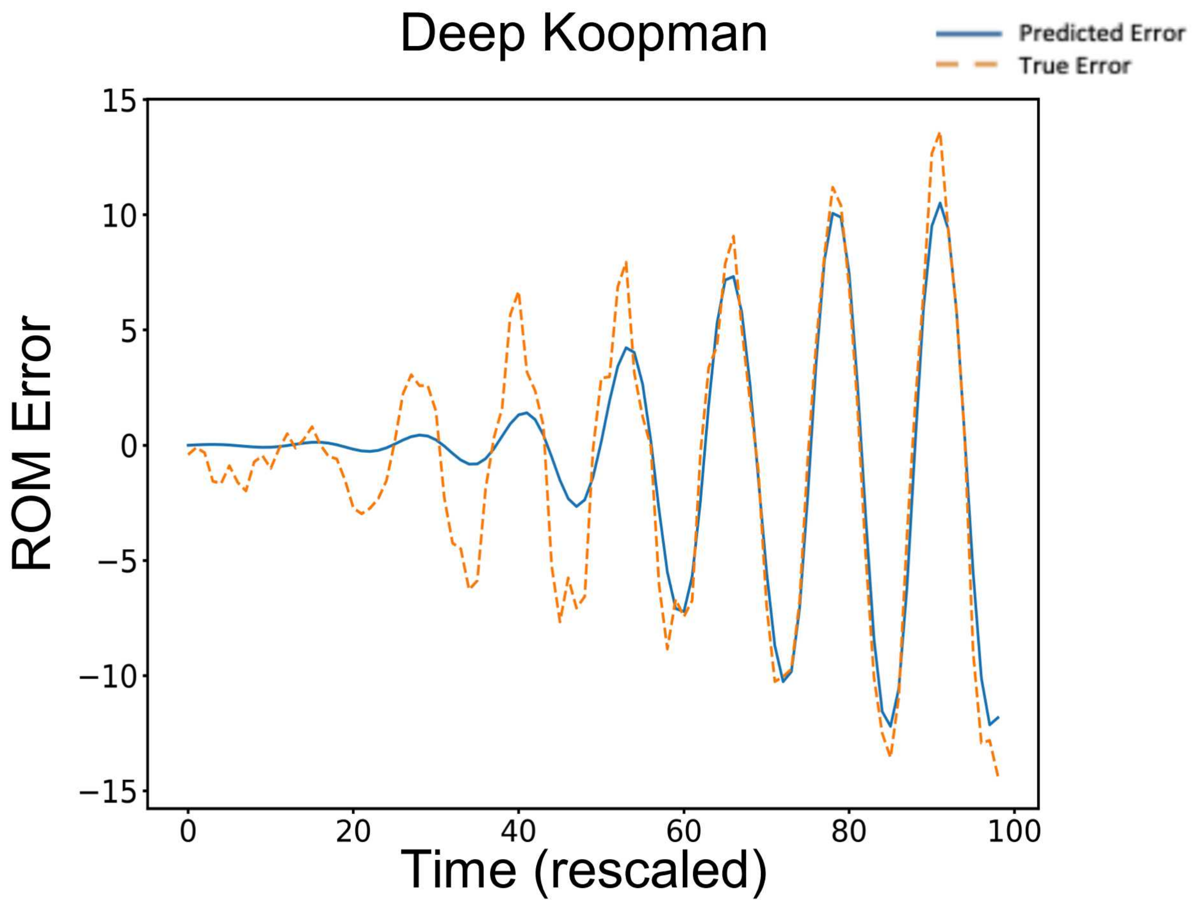

Conclusions

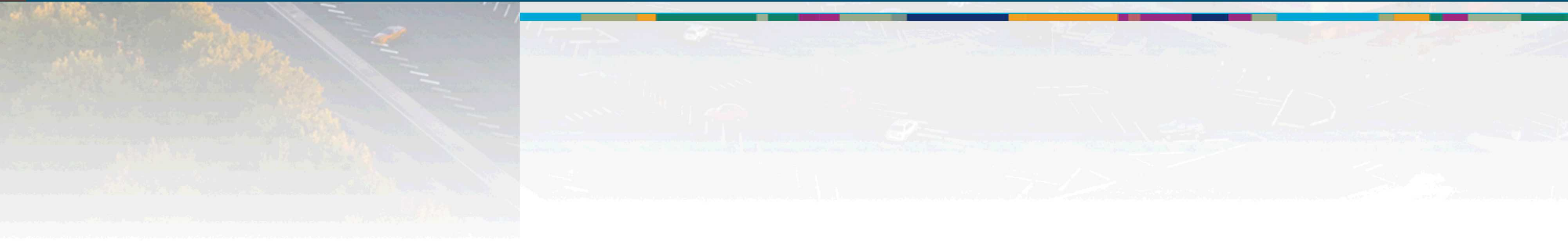

Conclusions

- Deep learning is an effective method for learning and predicting ROM error at coarse frequency scales
- Well-established architectures that maximize use of computational power often scale and train well
- Specialized architecture that aids in physical interpretability led to extreme sensitivity to hyperparameters and long train times

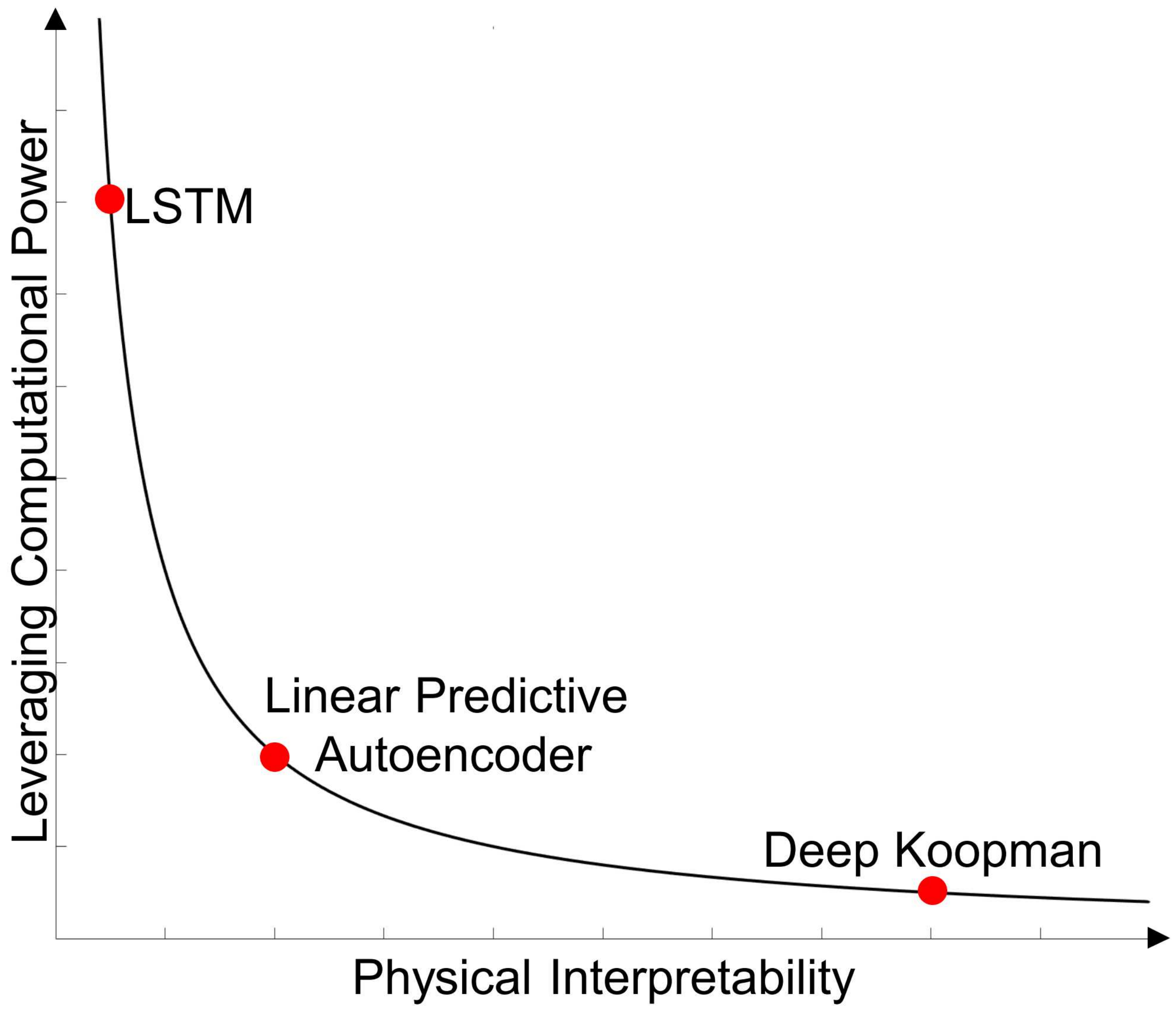

Future work

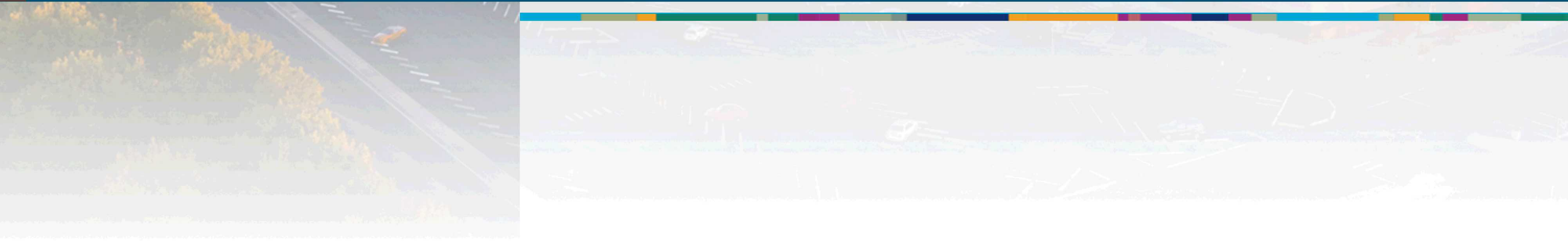

Future Work

- Investigate sensitivity of training to breadth vs. length of time series for use in experiment/simulation design
- Incorporation of ROM-specific features; i.e., dual-weighted residuals, into network
- Implementation with alternate modes of operation; i.e., control, data fusion, etc.
- Addition of statistical outputs or Bayesian training/prediction for real time uncertainty quantification and error statistics
- Determine how well error predictions enhance the ability of ROM predictions to account for extreme events

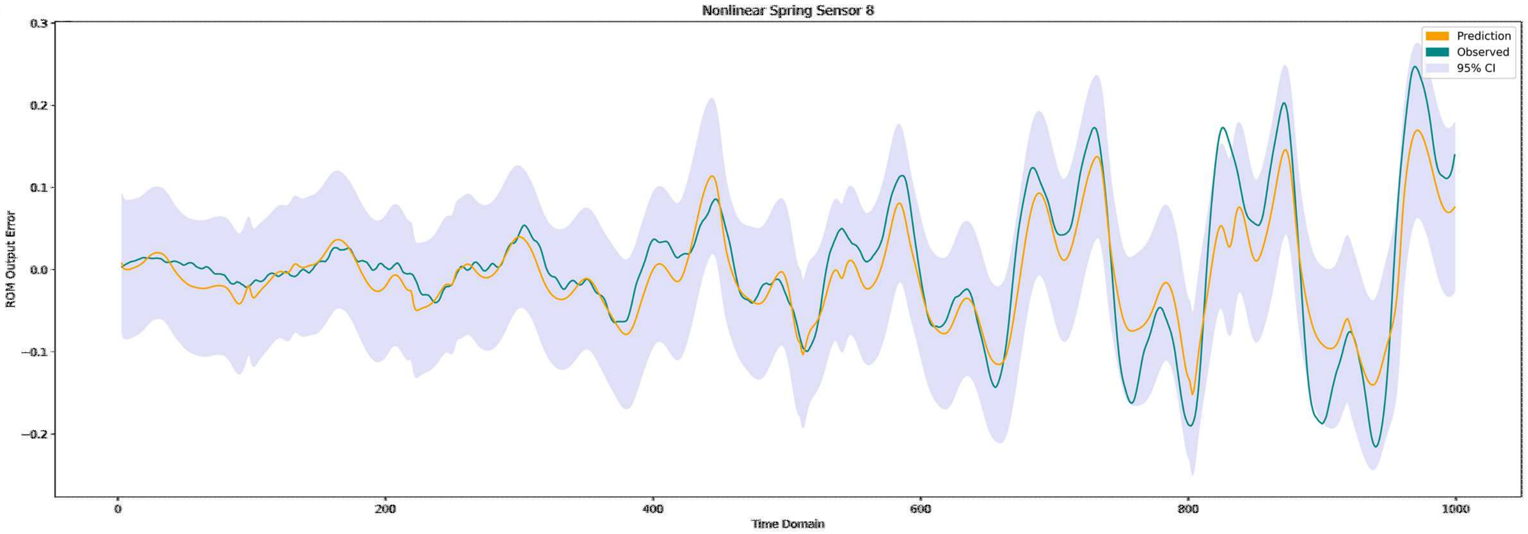

Acknowledgements

This research was conducted at the 2020 Nonlinear Mechanics and Dynamics Research Institute hosted by Sandia National Laboratories and the University of New Mexico.

Sandia National Laboratories is a multimission laboratory managed and operated by National Technology and Engineering Solutions of Sandia, LLC., a wholly owned subsidiary of Honeywell International, Inc., for the U.S. Department of Energy's National Nuclear Security Administration under contract DE-NA-0003525.

References

- M. Abadi et al, “TensorFlow: Large-scale machine learning on heterogeneous systems.” (2015). Software available from tensorflow.org.
- E. Chatzi, N. Dervilis, T. Simpson, “On the use of Nonlinear Normal Modes for Nonlinear Reduced Order Modelling.” (2020). arXiv preprint math.NA 2007.00466
- B. Lusch, J.N. Kutz & S.L Brunton, “Deep learning for universal linear embeddings of nonlinear dynamics.” Nat Commun 9, 4950 (2018). https://doi.org/10.1038/s41467-018-07210-0
- A. Mauroy and I. Mezić, "Global Stability Analysis Using the Eigenfunctions of the Koopman Operator," in IEEE Transactions on Automatic Control, vol. 61, no. 11, pp. 3356-3369, (2016). doi: 10.1109/TAC.2016.2518918.
- A. Pezke et al, “Automatic differentiation in PyTorch.” NIPS 2018
- P. Remy, “Stateful LSTM in Keras.” (2016) http://philipperemy.github.io/keras-stateful-lstm/